The dynamics of the piezo inkjet printhead operation

Article *in* Physics Reports · June 2010

DOI: 10.1016/j.physrep.2010.03.003

1 author:

Herman Wijshoff
Canon Global
33 PUBLICATIONS **486** CITATIONS

Physics Reports 491 (2010) 77–177

Contents lists available at ScienceDirect

Physics Reports

journal homepage: www.elsevier.com/locate/physrep

The dynamics of the piezo inkjet printhead operation☆

Herman Wijshoff

Océ Technologies B.V., P.O. Box 101, 5900 MA, Venlo, The Netherlands

ARTICLE INFO

Article history:
Accepted 11 March 2010
Available online 31 March 2010
editor: I. Procaccia

Keywords:
Inkjet
Piezoelectricity
Acoustics
Drop formation
Bubble dynamics
Wetting

ABSTRACT

The operation of a piezo inkjet printhead involves a chain of processes in many physical domains at different length scales. The final goal is the formation of droplets of all kinds of fluids with any desired volume, velocity, and a reliability as high as possible. The physics behind the chain of processes comprise the two-way coupling from the electrical to the mechanical domain through the piezoelectric actuator, where an electrical signal is transformed into a mechanical deformation of the printhead structure. The next two steps are the coupling to the acoustic domain inside the ink channels, and the coupling to the fluid dynamic domain, i.e. the drop formation process. The dynamics of the printhead structure are coupled via the acoustics to the drop formation process in the nozzle. Furthermore, wetting of the nozzle plate and air bubbles can have a negative influence on the printhead performance. The five topics (actuation, channel acoustics, drop formation, wetting, and air bubbles) are reviewed in this paper. This research connects the product developments for many emerging new industrial applications of the inkjet technology to the fundamental physical phenomena underlying the printhead operation.

Contents

☆ This research is performed in close cooperation with the Physics of Fluids group of Prof. Dr. Detlef Lohse of the University of Twente.

E-mail address: herman.wijshoff@oce.com.

0370-1573/$ – see front matter © 2010 Elsevier B.V. All rights reserved.
doi:10.1016/j.physrep.2010.03.003

1. Introduction

In this section an overview is presented of the main inkjet developments to clarify the importance of inkjet technology as a key technology for today's industry. Besides printing onto paper, many other applications have emerged in the last few years. The requirements to meet the needs in many areas justify an intensive research program. The basic printing principles are outlined and the main printhead operation issues are presented. Finally a guide through the next sections is given.

1.1. Historical overview on inkjet technology

Inkjet printing is an important technology in color document production [1]. The rapid development of inkjet technology started off around the late 1950s. Since then, many inkjet devices have seen the light of day. In this overview, the attention is mainly restricted to the development towards the most important inkjet concepts of today, namely continuous, piezoelectric, and thermal inkjet.

The first inkjet-like recording device, using electrostatic forces, was invented in 1858 by William Thomson, later Lord Kelvin. This was the Siphon recorder as shown in Fig. 1. The apparatus was used for automatic recordings of telegraph messages and was patented in 1867 (UK Patent 2147/1867). A siphon produces a continuous stream of ink onto a moving web of paper and a driving signal moves the siphon horizontally back and forth. The first experiments on manipulating a stream of droplets even goes back to 1749. That year, Abbé Nollet published his investigations on the effects of static electricity on a drop stream [2,3].

In 1822 the equations to describe the motion of fluids were formulated by the French engineer and physicist Claude Navier [4], seventy years after Euler had published his equation for ideal liquids without viscosity [5]. Navier also formulated the general theory of elasticity in a mathematically usable form in 1821 [6]. Hooke published his law on linear elasticity in 1678. George Stokes introduced his equations for the motion of liquids in 1845 [7]. Hence the name Navier–Stokes equations for the application of classical mechanics to a continuum under the assumption of a stress that is linear with the strain rate.

The foundation of modern inkjet technology is attributed to the Belgian physicist Joseph Plateau and the English physicist Lord Rayleigh. Plateau was the very first to publish on this field in 1843 with his experiments on the decay of a liquid column in a density-matched surrounding, the so-called Plateau tank [8]. He noticed that perturbations become unstable when their wavelength is long enough [9]. Only after Hagen published his wrong result [10], did he formulate the right criterion, the Plateau argument [11]. He derived the relationship of jet diameter to drop size in 1865 and described his work in detail in 1873 [12]. Lord Rayleigh published a series of founding papers starting with "Instability of jets" in 1878 [13–15]. He added the flow dynamics to the linear analysis of the decay of liquid jets, and found the right over-stretching of the most unstable breakup mode. His results were in good agreement with the measurements of Savart in 1833 [16], which was in fact the experimental foundation of the work of Plateau and Rayleigh. Savart was the first one who recognized that the break-up of liquid jets is governed by laws, independent of the circumstance under which the jet is produced. He used acoustic energy to form uniform drops.

What was missing in the studies on the behavior of jets was the realization that the surface tension is the driving force behind drop break-up. In the studies on dripping drops, gravity does play a central role in the formation of drops [17]. In the oldest reported observations of the behavior of liquid jets by Leonardo da Vinci in 1508 [18], the cohesion of a liquid, which results in the surface tension, was assumed to have only a contribution in holding the liquid together. Gravity was assumed to be the force leading to breakup of a liquid jet, as more quantitatively derived in 1686 by Mariotte [19], at about the same time as Newton published his famous "Philosophi Naturalis Principia Mathematica", with Newton's second law and the definition of Newtonian viscosity. The groundwork for the description of the role of surface tension forces as the driving force behind breakup was laid by Young in 1804 [20] and Laplace in 1805 [21]. They finally recognized that the same force, which holds the liquid together, is also the driving force behind the break-up of a liquid jet.

Other important events for the development of inkjet technology were in 1861 and 1865, when Maxwell published his equations, describing the electromagnetic forces [22,23]. The next event was the discovery of the piezoelectric effect (electricity from an applied mechanical stress) by Pierre and Jacques Curie in 1880 [24]. Their experimental demonstration consisted of a conclusive measurement of surface charges appearing on specially prepared crystals, which were subjected to mechanical stress. In 1881, Lippmann deduced mathematically the inverse piezoelectric effect (stress in response to an applied electric field). The Curie brothers immediately confirmed the existence of this property [25]. In the following years,

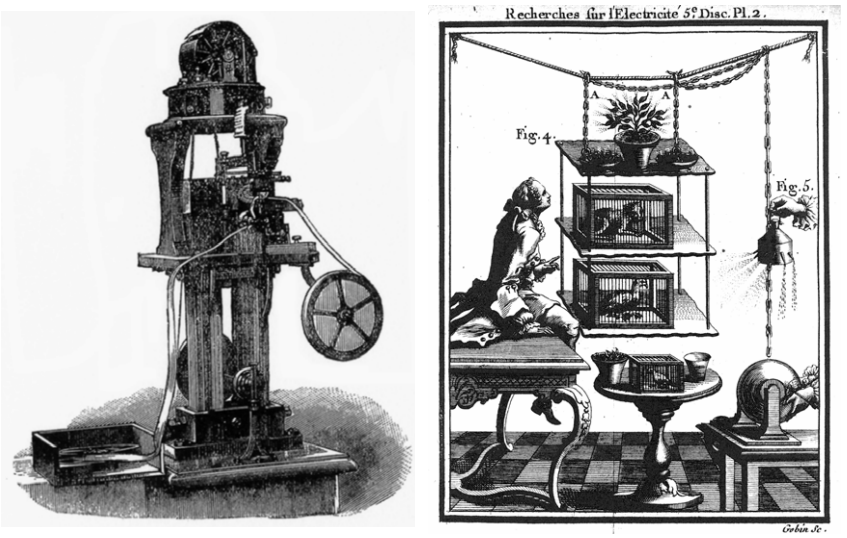

Fig. 1. (a) The Siphon recorder is the first practical continuous inkjet device. It was used for automatic recordings of telegraph messages and invented by William Thomson in 1858 (UK Patent 2147/1867). (b) An illustration from Abbé Nollet showing the first experiments on the effect of static electricity on a drop stream, published in 1749 [2].

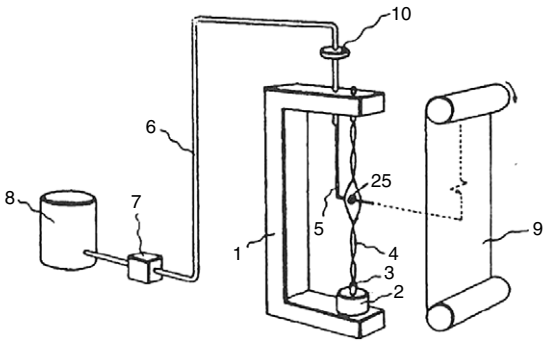

Fig. 2. Drawing of the first continuous inkjet recording device, which was patented in 1952 (US Patent 2566,443). This was the forerunner to the modern inkjet printing mechanisms.

the twenty natural crystal classes in which piezoelectric effects occur and all possible macroscopic piezoelectric coefficients were defined [26].

During the 19th century increasingly sophisticated experiments revealed the non-linear dynamics of jet breakup [27–29], from which for example the surface tension could be deduced [30,31]. The similar shapes were rediscovered several times [32,33]. Weber added viscosity to the analysis of jet decay [34]. So the main ingredients for nowadays inkjet devices were known. In 1931, the use of a piezoelectric material as actuator was reported [35]. Still, it took many decades before applications of the physical principles of drop formation were used in commercial working devices. In 1951, Elmqvist of the Siemens-Elema company patented the first practical inkjet device (US Patent 2566,433), which was based on the Rayleigh breakup. Instead of a continuous stream of ink, as with the Siphon recorder, now a continuous stream of droplets was jetted onto the paper, Fig. 2. This resulted in Elema's Mingograph [36]. Instead of being an inkjet printer, it was merely a medical voltage recorder (e.g. for ECG and EEG). The deflection of the drops was driven through analog voltages from a sensor, quite similar to current seismic apparatus. The dot positioning varied continuously, perpendicular to the paper transport direction. The jet was formed from a glass capillary with a length of 3 cm and a diameter of 100 μm, ending with a 15 μm nozzle opening. The breakup of the liquid jet was not synchronized. The Mingograph was capable of recording signals with a frequency up to 1.25 kHz. This was in fact the first inkjet printing principle coming to the market.

A continuous inkjet emerged in the 1960s [37,38]. In the early 1960s, R.G. Sweet of Stanford University demonstrated that by applying a pressure wave pattern to an orifice, the ink stream could be broken into droplets of uniform size and spacing up to frequencies of 120 kHz [39]. With a controlled jet break-up mechanism, the drops could be charged selectively and reliably as they emerged out of the continuous jet. Electrically conducting ink can be charged inductively. The charged drops were deflected towards several positions, when passing through an electric field, to form an image on the substrate. The

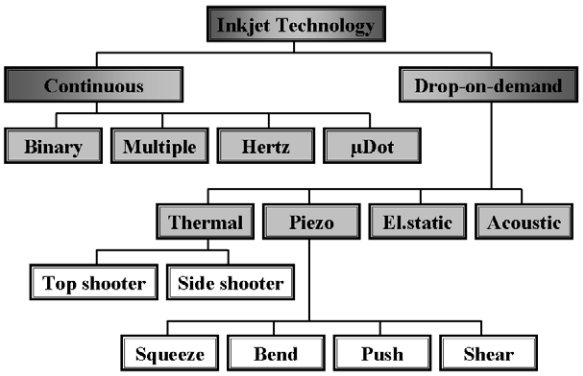

Fig. 3. Classification of inkjet printing technologies, adapted from [41].

uncharged drops were captured by the gutter and re-circulated in the system. This printing process is known as Continuous Inkjet (CIJ) printing (US Patent 3596,275), with the Inkjet Oscillograph as the first device. This device was elaborated for use by the Stanford Research Institute (SRI) for inkjet bar coding work for Recognition Equipment Incorporated (REI).

The A.B. Dick Company elaborated Sweet's invention. With the Lewis–Brown patent in 1964 (US 3298,030), character printing was enabled. This resulted in 1968 in the Videojet 9600, the first commercial CIJ printing product. A single jet with a drop frequency of 66 kHz was deflected to 11 raster positions. These activities were later continued in the VideoJet Technology company. Another company, that was involved in the further development of the multiple drop deflection technology, was Sharp. They released their Jetpoint printer in 1973. The developments were boosted by the huge research efforts of IBM in the 1970s, which licensed the technology from A.B. Dick and the Mead company. This resulted in 1976 in the IBM 6640 [40], a hardcopy-output peripheral application, which printed by deflecting a jet with a drop frequency of 117 kHz to 40 raster positions.

Honeywell filed in 1968 the Sweet–Cummings patent for multi-jet printing (US 3373,437). In this approach, the drops are not deflected to be deposited on different positions on the paper, but the deflected drop are captured. The patterns are printed with un-deflected drops from multiple orifices, the binary CIJ principle. The drops are now deflected in the direction of the paper transport, and not perpendicular as with the multiple CIJ, and only one deflection level is used. In Fig. 3, an overview is given of the main modern inkjet printing technologies.

The binary deflection was further developed, not only for bar code printing, but also for advertising purposes, with the so-called DIJIT printer, introduced in 1973 by the Mead company, which purchased the Cummings interests. The DIJIT head used 512 jets at a spacing of 100 npi with a drop repetition rate of 12 kHz. In 1983, the Mead company became Diconix, after being purchased by the Eastman Kodak company. In 1988, Diconix merged with Kodak to become Kodak Dayton Operations and this part was sold in 1993 to Scitex.

In the 1970s, Hertz of the Lund University of Technology in Sweden developed several continuous inkjet techniques, which enabled gray-scale printing by varying the number of drops per pixel [42]. In 1977, Applicon introduced the first color inkjet printer, based on the principles of Hertz. His methods were also adopted by Iris Graphics and Stork to produce high-quality color images for the prepress color hardcopy market [43]. The Scitex Iris Graphics proofer imaged up to 32 drops on a single dot at a resolution of 300 dpi.

Instead of continuously firing drops it is also possible to create drops only when an actuation pulse is provided: drop-on-demand. Major advantages of drop-on-demand (DOD) printers over CIJ printers include the fact that there is no need for complicated hardware for break-off synchronization, charging electrodes, deflection electrodes, guttering, and re-circulation systems, high pressure ink supplies and complex electronic circuitry. The first pioneering work in that direction was performed in the late 1940s by Hansell of the Radio Corporation of America (RCA), who invented the first drop-on-demand device as shown in Fig. 4. By means of a piezoelectric disc, coaxially arranged with an ink-filled conical nozzle, pressure waves could be generated that caused a spray of ink drops. However, this invention, intended for use as a writing mechanism in a pioneering RCA facsimile concept, was never developed into a commercial product [1].

The first DOD technique, that really emerged, was the electrostatic pull inkjet in the 1960s. The principle was known for a long time [44]. The first patent was filed in 1962 by Winston (US 3060,429). The basic working principle comprises the following. Conductive ink is held in a nozzle by negative pressure. By application of a high voltage pulse to an electrode located outside the nozzle, a droplet of ink is pulled out [45–47]. By application of the appropriate deflection fields, the droplet can be located on the substrate as with CIJ. However, now only one droplet at a time could be between the plates, otherwise the next drops would follow identical paths. With CIJ, multiple selectively charged drops can follow different paths through the constant homogeneous electric field. Companies developing electrostatic pull inkjet devices were the Casio, the Teletype, and the Paillard companies. The Inktronic Teletype machine in the late 1960s was marketed by the Teletype company. With the model 500 Typuter, the Casio company released a printer of this type in 1971, which was based on a Paillard prototype. Paillard had already stopped his development. In the 1970s, the DOD electrostatic pull principle was

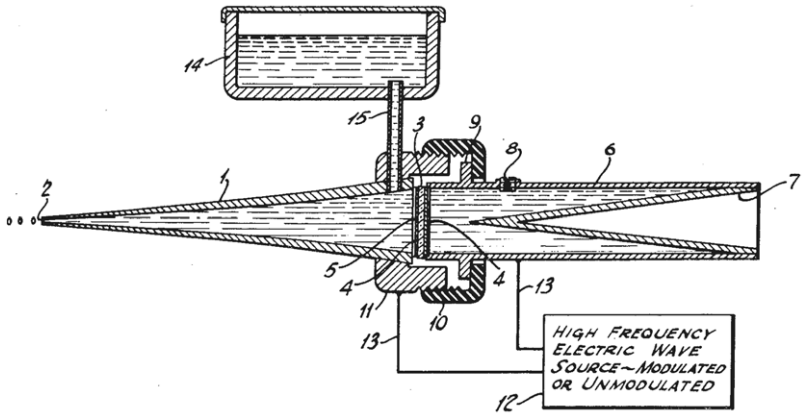

Fig. 4. Drawing of the first drop-on-demand piezo inkjet device, which was patented in 1950 but not further developed into a commercial product (US Patent 2512,743). A piezoelectric disc (5) generates pressure waves in the solid cone (1), which cause a spray of ink drops from the nozzle (2).

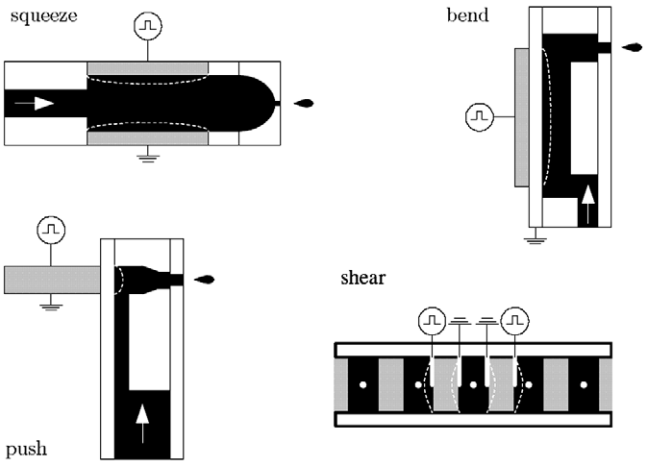

Fig. 5. Classification of piezo inkjet (PIJ) printhead technologies by the deformation mode used to generate the drops.

abandoned due to poor printing quality and reliability, although research activities for other applications continue until today [48–50], with many other applications than printing onto paper [51].

Generally, the basis of piezoelectric inkjet (PIJ) printers is attributed to three patents in the 1970s [52]. The common denominator of these three patents is, as in the first pioneering patent of 1950, the use of a piezoelectrical unit to convert an electrical driving voltage into a mechanical deformation of a ink chamber, which generates the pressure required for the drop formation from a nozzle. The first one is that of Zoltan of the Clevite company in 1972 (US Patent 3683,212), proposing a squeeze mode of operation [53]. In this mode, a hollow tube of piezoelectric material is used. When a voltage is applied on the piezoelectric material, the ink chamber is squeezed and a drop is forced out of a nozzle.

The second patent of Stemme of Chalmers University in 1973 (US Patent 3747,120) utilizes the bend mode of piezoelectric operation. In this mode, the bending of a wall of the ink chamber is used to eject a drop [54]. Therefore, the wall is made of a diaphragm with a piezo ceramic bonded onto it. The bend mode is also referred to as bimorph or unimorph mode. The third patent of Kyser and Sears of the Silonics company in 1976 (US Patent 3946,398) also used the bend mode operation [55]. Both bend-mode patents were filed in the same year. The minor difference between the two is that Stemme used a flat disc of piezoelectric material to deform a rear wall of an ink chamber and that Kyser and Sears used a rectangular plate to deform the roof of an ink chamber. Silonics was the second company to introduce a piezoelectric DOD printer, namely the Quietype in 1978, which used the bend mode of the Kyser patent. The printhead, which required 150 V driving amplitude, fired drops with a maximum repetition rate of 3 kHz. The electrical field is applied in the polarization direction of the piezo material. The deformation in the poling direction is not used, but the deformation perpendicular to the poling direction. Since the piezo ceramic is bonded onto a passive membrane, the actuator will bend. Obviously, the main discriminator between the PIJ patents is the dominating deformation mode used of the piezoelectric material, together with the geometry of the ink channels, Fig. 5.

The patent of Stuart Howkins (US Patent 4459,601) of the Exxon company in 1984, describes the push-mode version. With the push mode, also referred to as bump mode, a piezoelectric element pushes against an ink chamber wall to deform the ink

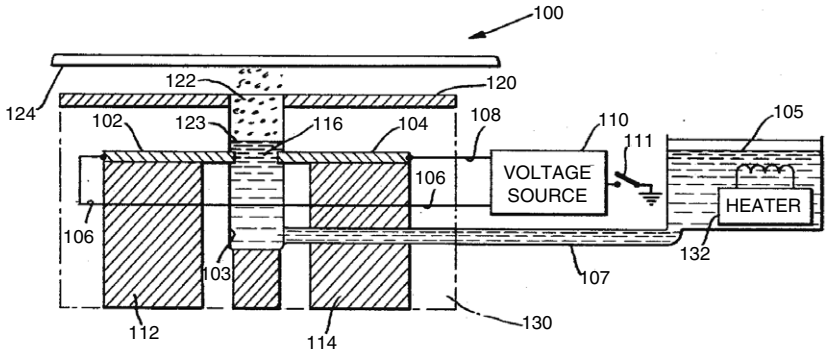

Fig. 6. Sudden steam printing, the first drop-on-demand thermal inkjet device, which was patented in 1965, but not further developed into a commercial product (US Patent 3179,042). An electric current from the electrodes (102 and 104) passes through a portion of the ink (116). The ink is preheated (132) nearly to its boiling temperature and the extra heat from electric current generates the steam that ejects the drops from the nozzle.

chamber. The electrical field is applied in the poling direction and the deformation is in the same direction or perpendicular to the poling direction. Finally, the patent of Fischbeck (US Patent 4584,590) proposed the shear-mode. In the shear mode the strong shear deformation component in piezoelectric materials is used to deform a ink chamber wall. The electric field is perpendicular to the polarization direction of the piezo ceramic. These modes complete the now commonly adapted categorization of the piezo inkjet printhead configurations: the squeeze, push, bend, and shear mode, Fig. 5. In this figure, a special version of the shear-mode inkjet is shown, the shared-wall principle, where the piezo ceramic is also the channel plate.

With sudden steam printing, Fig. 6, Naiman from the Sperry Rand Company basically invented another DOD technique, thermal inkjet printing, in the 1960s. By boiling aqueous ink at certain time instances, a drop of ink could be generated. The strength of this design clearly was not immediately acknowledged, since the company did not elaborate this idea into a commercial product. The idea was abandoned until the late 1970s when Canon and Hewlett Packard (HP) picked it up.

In 1979, Ichiro Endo and Toshitami Hara of the Canon company re-invented the drop-on-demand printhead, which is actuated by a water vapor bubble, called bubblejet. They were both working on a piezo-based drop-on-demand printhead. Accidentally, Endo watched a spray of ink from a needle, after touching the needle with a hot soldering iron. The first BubbleJet printer was launched in 1981 and was the first side-shooter device. The droplet was ejected in a perpendicular direction away from the evaporating bubble. In the same period also HP developed their thermal inkjet technology. John Vaught and Dave Donald, working on a squeeze mode piezo printhead, both got inspired by the working principle of a coffee percolator. This led to the first successful low-cost inkjet printer in 1984. The jetting direction was in line with the evaporating bubble, the so-called top-shooter design. The ThinkJet fired 180 pl drops from 12 nozzles at a maximum repetition rate of 1.3 kHz. In 1985, Canon introduced the BJ-80, which contained a printhead with 24 nozzles.

The invention of the thermal inkjet (TIJ) fundamentally changed inkjet research. By the replacement of the piezoelectric by a thermal transducer, the main bottleneck concerning miniaturization was resolved. The thermal transducer became a simple, small, and cheap resistor. Canon and HP joined their forces and protected themselves with a wall of patents. The real inkjet revolution started in 1988 with HP's DeskJet, which fired 85 pl drops at a repetition rate of 3.6 kHz. Canon caught up in 1990 with their BJ10, which had 64 nozzles at a resolution of 360 npi, and in 1992 with the BJ200. In 1991, HP launched the first full color TIJ. Their PainJet, introduced in 1986, was a three-color printer. Lexmark, spun off from IBM in 1991, joined the top three of thermal inkjet vendors in 1993 with the ExecJet IJ 4076.

TIJ can be manufactured using mass-production based on IC manufacturing technologies. This made the cost per nozzle much lower than the cost per nozzle of a piezoelectric printhead. Both the fact that inkjet printers now could be miniaturized and its low cost of manufacturing made TIJ the superior inkjet technology at that time. HP solved the reliability problem of the thermal drop-on-demand printheads by the concept of disposable heads and increased the performance of their thermal printheads continuously as shown in Fig. 7. HP claims that TIJ jets everything that nucleates like toluene, silver suspensions, and even functional proteins. Currently thermal inkjet, with top-shooters of HP, Canon, Lexmark and Olivetti (with a Canon-based technology) and side-shooters of Canon (the first series) and Xerox, dominates the low-end home/office color printer market. Xerox started within a few months after the demo of Canon in 1981 of their TIJ research and this became three years later their only inkjet technology. Océ also applies thermal drop-on-demand inkjet in its wide format color printing systems with printheads of various manufacturers.

After the introduction and immense success of TIJ, PIJ research efforts were largely diminished. However, critical in TIJ is the spreading and intercolor bleeding of water based inks. This requires special coatings on the media surface. At high productivity, cockling and drying of the media is another problem. Therefore, solid inks (hot-melt or phase-change ink), which require piezo actuation, remained important.

Only a few companies continued their research into PIJ. New initiatives with a bump-mode design were taken in 1983 by Howtek and Exxon, which were later acquired by Dataproducts. The 965 printer had printheads with 32 nozzles, but the product, although being technologically very impressive, was not a success. Epson emerged as the PIJ leader with the

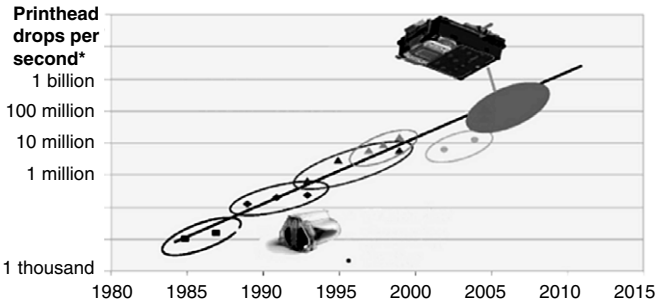

Fig. 7. HP Moore's law: inkjet printhead performance as printhead drops per second (the number of nozzles times the maximum drop-on-demand frequency) doubles every 18 months for the past 20 years. It started with 12 nozzles in a single color glass chip in 1984. Via different printer series (the different markers), this evolved into the 3900 nozzles in a six color single silicon chip in 2006, the Scalable Printhead Technology (SPT) [56].

introduction of the 12 nozzle SQ-2000 in 1984 and the big success of the Stylus 800, introduced in 1993. The printhead had 4×12 nozzles at a resolution of 90 npi each. Now the bump mode actuation is still used by Epson in their MLP heads. The bump mode is also used by Hitachi (which acquired Dataproducts) and applied in Ricoh printers like the IPSiO and the G707, by Trident in their PixelJet and the 780Jet, which have the unique capability that the heads can be re-assembled again, and by Brother in their HS5000 printer.

The bend mode is used by Tektronix (acquired by Xerox) in their pagewide heads in the Phaser printer series, by Brother/Kyocera in their new pagewide array and by Epson in their MLChips heads, introduced in 1997 for the low-end Stylus color printers. Epson uses water based inks, but Mimaki, Mutoh and Roland use oil based and solvent inks with Epson heads. Also Brother used the bend mode in their MCF580 printer.

The shear mode design came into the field in 1984 with Spectra, a Xerox licenses' formed company, in their Galaxy and Nova heads. Spectra was acquired by Markem, later by Dimatix and finally by FujiFilm. A special version of the shear mode is the shared wall design of Xaar. This company started in 1990 for commercializing the work of the Cambridge researchers and licensed its technology to the Swedish MIT, an IBM spin-off. In 1999, Xaar acquired MIT from Pelikan to become XAARJet, by then, IBM had sold all its printing activities. Other companies, which use the shared-wall concept, are Brother/Kodak in their Kodak5260 printer, ToshibaTEC, Konica, Sharp, and MicroFab.

The squeeze mode design never evolved further towards a multi-nozzle printhead for the graphical printing markets. Single nozzle devices or heads with only a few operating nozzles were developed at several laboratories. Also at Philips Laboratories in Hamburg [57,58]. In 1981, the P2131 printhead was developed for the Philips P2000T microcomputer. These activities were later continued as a spin-off company Microdrop Technologies [59]. The printhead is used for several specialized applications, for example the production of lenses [60].

At present, both TIJ and PIJ printing have evolved into the two most important technologies when it comes to printing. The initial advantages of TIJ over PIJ have been leveled over the years by further development of the PIJ technology. Thousands of nozzles can fire drops at several tens kHz with drop volumes down to 1 pl. Epson, which has put in more effort to increase the number of nozzles in their PIJ printhead, focused on print quality. HP focuses more on productivity. Canon is moving also towards high quality printing with very small drops. Lexmark, the number four, is somewhat behind, mainly because of the less R&D the company has spend on inkjet development.

A fundamental strength of the PIJ technology is its ability to deposit a wide variety of materials on various substrates in well-defined patterns. Recently many other applications than printing onto paper emerged [61–68]. In the display market, inkjet technology is used to manufacture Flat Panel Displays (FDP), Liquid Crystal Displays (LCD), color filters [69] (a part of LCDs), Polymer Light Emitting Diodes (PLED) [70], and flexible displays. The accompanying performance criteria are among the major driving forces behind much research and development efforts [71,72]. Within the chemical market, the inkjet technology is mainly used as a tool for research purposes. The unique capacity of the technology for dispensing small doses of liquids makes it very useful for this market. Applications include material and substrate development as well as coating purposes [73–75].

In the electronic market, inkjet printheads are used to create functional electrical traces using conductive fluids on both rigid and flexible substrates. One of the first applications of inkjet technology within this field was that for the production of Printed Circuit Boards (PCB) [76,77]. Other applications include the fabrication of electric components and circuits such as Radio Frequency Identification (RFID) tags, wearable electronics, solar cells [78], fuel cells, and batteries. Challenges for the inkjet technology within this field include the spreading of the ink and the required guarantees of continuity of the jetted lines and interconnections [79–85].

Three-dimensional mechanical printing claims the inkjet technology as a tool for rapid prototyping, small volume production, and the production of small sensors [86–88]. Jetting of UV-curable optical polymers is a key technology for the cost-effective production of micro-lenses. These tiny lenses are used in devices from fiber optic collimators to medical systems. The ability of inkjet technology to precisely jet spheres in variable, but consistent, drop sizes provides opportunities for the cost reduction of existing optical components and innovative new designs [89–91].

The life science market is rapidly expanding with new requirements for precise dispensing of DNA and protein substances [92]. The high costs of these fluids make inkjet technology with its precision placement and tight flow control an excellent dispensing tool. Applications include the use for DNA research, various medical purposes such as dosing of drugs, and food science. A quite futuristic application is the use of inkjet printing for the fabrication of living tissue [93–97].

1.2. Printing principles

The graphic printing applications require certain performance criteria to be met. For an inkjet printhead, an important set of requirements is related to the resulting drop properties, namely:

- Drop-speed: the resulting droplets are required to have a certain speed, typically several m/s. A high drop speed results in a short time of flight. The sensitivity for disturbing influences like variations in the printhead–substrate distance will be less, thus the dot position errors will be smaller.
- Drop-volume: depending on the application under consideration, the performance requirement concerning volume typically varies now from 2 to 32 pl. For some applications, it is required that the drop-size can be varied during operation. For example, for large areas that need to be covered large drops are desired, whereas for high resolution printing small drops are desirable. This is referred to as drop-size modulation.
- Drop speed and volume consistency: the variations in drop volume and speed must stay within a certain percentage band, typically around 2%. This is to avoid irregularities in the printed object.
- Drop shape: the shape of the dots on a substrate is negatively influenced by the formation of tails or satellite drops. These are highly undesirable for the quality of the print.
- Jet straightness: the droplets have to be deposed in a straight line towards the substrate, typically within 10 mrad accuracy.

Productivity and stability are important requirements, which are closely related to the jetting process. The productivity of an inkjet printhead is mainly determined by the jetting frequency, defined as the number of drops that a channel jets within a certain time f_{dod}, and by the number of nozzles N_{noz}, defined by the integration density or nozzles per inch and the printhead width. A high integration density has a lot of consequences for the functionality and the producibility. For the productivity of an inkjet printer, the firing power P_{jet} of the printheads is the key number. The productivity in m^2/s is given by:

$$P_{\mathrm{jet}} = \frac{N_{\mathrm{noz}} f_{\mathrm{dod}}}{\mathrm{dpi}^2} \times (24.4 \cdot 10^{-3})^2 \tag{1}$$

with dpi the number of dots per inch [98]. This results in a print time t_{print} for an area A_{print} of a printer of:

$$t_{\mathrm{print}} = \frac{A_{\mathrm{print}}}{\eta P_{\mathrm{jet}}} \tag{2}$$

with η the efficiency of the printer, which plays a very important role in a scanning system. Most inkjet printers use a carriage with several printheads which moves over the full width of the paper. Between the strokes of the carriage, or print swaths, the paper is transported over a certain distance to cover the full area. At higher frequencies, the carriage turn-time and the paper step give more and more limitations. These limitations result in an optimum DOD frequency for the productivity of scanning printer systems [99]. An expression for the optimum DOD frequency f_m, below which print duration dominates and above turning duration, is derived with a model which includes many parameters such as carriage driving force F_c, carriage mass m_c and width x_c, print width x_p and resolution r_x, and multi passing p_x in the swath direction, i.e. the number of strokes to print one line:

$$f_m = \frac{r_x}{p_x} \sqrt{\frac{F_c (x_p + x_c)}{2 m_c}}. \tag{3}$$

For productivity the maximum applicable DOD frequency for 600 dpi prints in most scanning printer concepts is 30–40 kHz. High productivity single pass printing requires a page-wide array with thousands of nozzles as explored by Spectra [100, 101] and Brother-Kyocera [102], and used by Xerox/Tektronix in their Phaser printer series. Another way to increase the number of nozzles is to use multiple nozzles per channel as explored by Trident [103].

The number of dots per inch is important for print cost and print quality. Print cost is directly related to the thickness of the ink layer or amount of ink/m^2. As a first order approximation, the required drop volume for a 600 dpi dot is about 32 pl and for a 1200 dpi dot about 4 pl, since volume scales as the third power of the spatial resolution. The total volume for a 600 dpi dot with four 1200 dpi drops becomes 16 pl instead of 32 pl with a single 600 dpi drop. Print quality is better with smaller dots at a high resolution. Finer details can be represented and also the graininess of the print is much less with small dots. For water based inks the lower amount of ink with smaller drops results in shorter drying time, another drive to move towards smaller drops. So there is a trade-off between productivity and print quality/cost. Drop size modulation is a way to meet both requirements. The small drops are used for achieving a high print quality and the large drops for productivity.

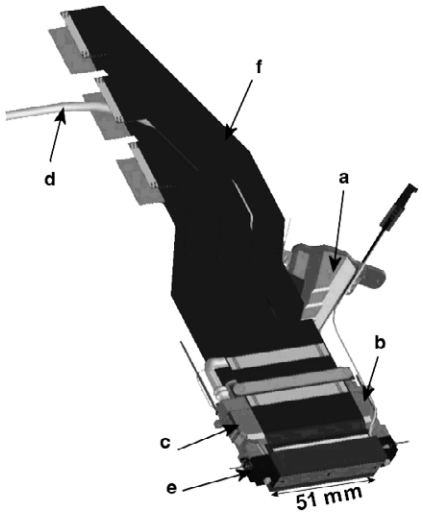

Fig. 8. 3D CAD drawing of a printheadprototype, developed at Océ, showing (a) the melting unit, (b) the filter units, (c) the reservoir, (d) the static pressure hose, (e) the central part, and (f) the electronic driving supply.

The stability of the jetting process is one of the most important performance requirements for inkjet printheads. Typically, it is required that at most one failure occurs per certain number of jetted drops. For printing onto paper this is typical one billion, but in some industrial applications no failure at all is allowed. Additional, more general, requirements include the lifespan of the printhead (typically more than ten billion actuations per channel, a fundamental strength of PIJ over TIJ), the materials compatibility (a wide variety of inks must be depositable, again a strength of PIJ over TIJ), the maintainability, and the cost of production and manufacturability of the printhead (a weakness of PIJ).

1.3. Printhead operation

1.3.1. Working principle

The starting point for the review is a printhead, developed at the R&D department of Océ, This printhead is referred to as the reference printhead. The final goal of the printhead operation is firing billions of drops. Before a drop is fired, a lot of processes must take place. In the case of hotmelt inks, it starts with the melting of the ink in the melting unit (a), Fig. 8. This unit must have enough capacity. A good heat transfer and draining of the melted ink at a given maximum temperature like 135 °C is necessary, taking into account some overshoot and time delay. Another task is filtering (b) the ink. The next unit is the reservoir (c), which must have enough volume, while keeping the total printhead dimensions within certain limits. Important aspects concerning the reservoir are:

- filtering with non-woven filters with high dirt holding capacity
- removal of air bubbles
- temperature control
- closing static pressure, for example supplied with hose (d)
- ink-level sensing.

The lower part of the printhead is the central part (e) where drop formation takes place. This part is the subject, which forms the basis of the discussion in this review and is shown in more detail in Fig. 9. The main components in the central part are:

- a last filter (k), to remove the dirt particles from the ink
- the channel block (h), in which the ink channels (l) are made
- the nozzle plate (g), where the drops are formed
- the actuator foil (i), which covers the ink channels in the channel block. The foil is also connected to:
- the actuator plate with piezo elements and substrate (j). Here the driving force for the drop formation process is generated. The required electric voltage is supplied by the electronic flex (f), Fig. 8.

The ink path from the reservoir and last filter to the nozzle can be divided into a supply channel, a pressure channel and a connection channel. The actuation takes place in the pressure channel, which is shown in Fig. 9 in a front view of a channel. When a voltage is applied on a piezo element, this element will change its shape. This deforms the ink channel, which generates the pressure waves to fire a drop. The reaction force is supplied by the substrate, which is connected to the channel block via passive piezo elements.

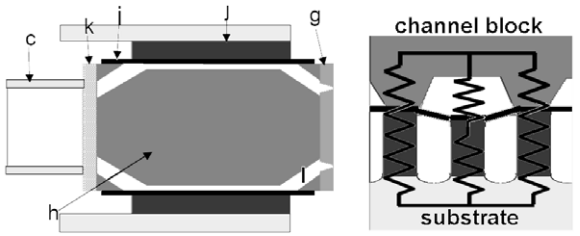

Fig. 9. Side view of channel structure of the reference printhead and front view with actuation principle as explained in Section 2.2.1, with (c) the reservoir, (g) the nozzle plate, (h) the channel block, (i) the actuator foil, (j) the actuator with piezo elements and the substrate, (k) a last filter, and (l) the ink channel.

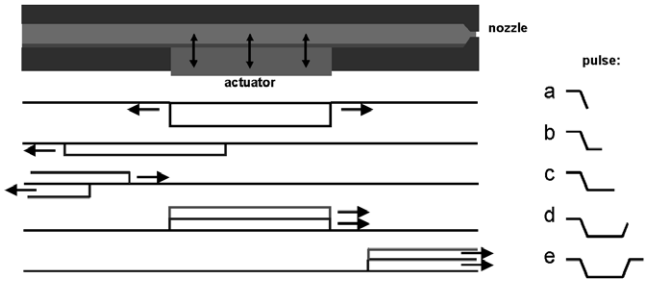

Fig. 10. Schematic drawing of the actuation principle. An electric voltage on a piezo element enlarges the channel and a negative pressure is generated. After reflection at the reservoir this becomes a positive pressure wave (only the part of the wave, which drives out a droplet, is shown). The positive pressure wave is amplified by the second slope of the driving waveform to get a large positive pressure peak at the nozzle, which fires a drop.

Typical dimensions are length 5–20 mm for the total ink channel with a cross-section of 0.01–0.05 mm^2. The channel block material is graphite with shaped channels, or a metal like brass or silicon with etched channels. The actuator foil has a thickness of 5–50 μm and we use poly-imide, metal, glass, or silicon as the material. The actuator plate is a piezo-ceramic material with a height of typical 500 μm with diced elements. In most cases we use a substrate to support the element structure. The substrate is several millimeters longer than the piezo elements, to enable the connection of the electronic flex. The nozzle plate thickness ranges from 30–125 μm and nozzle diameters from 18–50 μm. Different nozzle shapes are made in nozzle plates of nickel, tantalum, poly-imide or silicon.

A long ink channel with a nozzle at the right side and a large reservoir at the left side is the simplified geometry of the inkjet device like in [104], Fig. 10. A piezo actuator element drives each channel. To fire a droplet, an electric voltage is applied and the channel cross-section will be deformed by the inverse piezoelectric effect. This results in pressure waves inside the channel. The pressure waves propagate in the channel direction and will be reflected when the characteristic acoustic impedance Z of the channel changes. The acoustic impedance of the channel depends on the size of the channel cross-section A and the speed of sound c as:

$$Z = \frac{\rho c}{A} \tag{4}$$

with ρ the density of the ink. The speed of sound is influenced by the compliance of the channel cross-section, see Section 3.1.3. The reflection and transmission coefficients at the interface between domain 1 and domain 2 are:

$$R = \frac{Z_2 - Z_1}{Z_1 + Z_2} \qquad T = \frac{2Z_2}{Z_1 + Z_2}. \tag{5}$$

When the compliance does not change, the following relationship holds:

$$R = \frac{A_1 - A_2}{A_1 + A_2} \qquad T = \frac{2A_1}{A_1 + A_2} \tag{6}$$

At the large reservoir ($A_2 \gg A_1$) the transmission coefficient is zero and the reflection coefficient equals -1. This means that the pressure wave will be completely reflected and the amplitude of the wave will change.

The charging of the piezo element (a) enlarges the channel cross-section and the resulting negative pressure wave will be reflected at the reservoir at the left (b). The large reservoir acts as an open-end and the acoustic wave returns as a positive pressure wave (c). The de-charging of the piezo element reduces the channel cross-section to its original size. This will amplify the positive pressure wave when tuned to the travel time of this acoustic wave (d). The channel structure and driving pulse are designed to get a large incoming positive pressure peak at the nozzle (e), which drives the ink through the nozzle. Acceleration of the ink movement in the small cross-section of the nozzle (conservation of mass and incompressibility) results in drop formation.

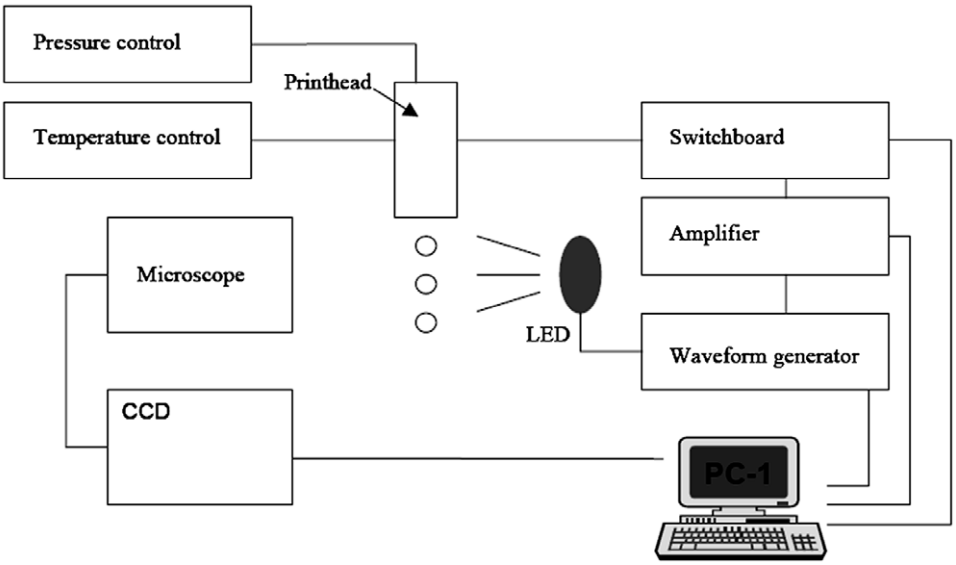

Fig. 11. Outline of experimental setup with printhead control, driving electronics and optical recording equipment.

1.3.2. Printhead testing

Droplets are measured by means of optical methods [105,106]. Especially the instabilities of a liquid jet are difficult to measure [107–109] and a number of optical techniques are used for quantitative measurements [110–112]. In our research we used stroboscopic illumination at drop formation rate and high-speed camera recordings up to 160,000 images/s with a Phantom V7 camera from Vision Research or up to one million images/s with a Shimadzu HPV-1 camera. The basic setup for the optical measurements is outlined in Fig. 11. The setup can be divided into a part which controls the printhead and a part to visualize the droplets.

The required reference temperature is reached by a PID controller (Eurotherm 2408), which measures the temperature of the printhead with thermocouples and controls the input voltages for the heating elements. The printhead is mounted in a vertical direction with the nozzles face down, similar to its position in an inkjet printer. To avoid that the ink simply flows out of the nozzles under the influence of gravity, an air pressure unit (TS 9150G) makes sure that the pressure in the ink reservoir remains 8 mbar below the ambient pressure. The setup is connected to a personal computer that is equipped with National Instruments IMAQ PCI 1409 and PCI GPIB cards for image capturing and processing and for communication, respectively. A Newport MM3000 motion controller is used for automatic positioning of the printheads in the measuring positions with Newport xy-tables.

We use Labview software to control the measurements and the measuring results can be directly exported to for example Excel for further analysis. After defining the actuation signal, it is sent to an arbitrary waveform generator (Philips PM 5150/Wavetek 75A). The waveform generator sends the signal to an amplifier (Krohn-Hite 7602). From the amplifier, the signal is fed to a so-called switch-board. The switch-board is controlled by the personal computer and determines which channels are provided with the appropriate actuation signals.

We use a standard CCD camera (for example Sony SSC-M370CE or Watek LCL902K) to capture the images from an Olympus SZH-10 microscope of the drop formation with a frame rate of 25 images/s. A LED produces flashes of 100 ns and the strobe frequency is the same as the drop repetition rate or DOD frequency. We will only see the reproducible part of the drop formation, because the images are integrated over many (depending on the DOD frequency up to several hundred) droplets, recorded at a certain time interval after the start of the actuation [113,114]. Drop properties can be derived very easily from these images. The drop speed is calculated from the distance of adjacent drops and the known repetition time. The drop size is calculated from the number of pixels, or by weighting a certain number of captured drops. Drop direction is calculated from the centers of mass. To capture non-reproducible phenomena we use the stroboscopic illumination at camera rate or a high-speed camera recording [115]. With the first option every 40 ms one drop is visualized at a certain time after the start of the actuation with a progressive scan camera. With a high-speed camera all drops are recorded with 1–10 μs time intervals, in a certain time frame (up to typical 1 s), using a trigger signal to read back the relevant time frame.

Another option is the use of laser-Doppler interferometry (Ono Sokki laser vibrometer LV1500) to record the meniscus movements without drop formation. The measuring principle is based on mixing an undisturbed and a Doppler-shifted laser beam. The Doppler effect, the frequency shift Δf, of the reflected beam is given by:

$$\Delta f = \frac{2v}{c} f_0 = \frac{2v}{\lambda} \tag{7}$$

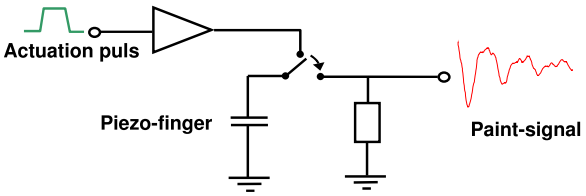

Fig. 12. Outline of Paint measurement. Switching the piezo elements between an electronic driving circuit and a measuring circuit enables both the actuation of the channels and the measurement of the pressure variation inside the channels.

with f_0 the frequency of the undisturbed laser beam, λ the wavelength of the laser beam, c the speed of light, and v the normal speed of the surface which reflects the laser beam. The meniscus speed is derived from the interference pattern of the reflected beam with the reference beam and the frequency characteristics are recorded with an HP 3585A spectrum analyzer. With laser-Doppler it is also possible to measure actuator displacements with an accuracy of 20 nm [116]. Another setup for the latter is a speckle interferometer. The speed of a non-jetting meniscus can also be derived from the stroboscopic CCD-camera recordings, when zooming on the nozzle exit area [117]. Another alternative is the built-in measurement method of the meniscus position, which also allows measurements in the jetting situation. This is offered by a sensing nozzleplate with a capacitive layer inside the nozzle [118,119].

All these measurements give details on the ink flow outside the printhead and the deformations of the exterior of the printhead. The phenomena inside the channels are difficult to measure. Only when using special transparent printheads, e.g. channels in or covered by a glass plate, and flow tracing particles can the flow inside be measured [120]. The only suitable method for the opaque heads uses the actuator also as a sensor. As is generally known, a piezo can be used as an actuator or as sensor, see e.g. [121]. For that, one uses the piezo's inverse (actuator) and direct (sensor) piezoelectric effect. The former comprises the following. If an electrical voltage V is applied to the piezo unit, a displacement y of the piezo unit results. The latter refers to the following phenomenon. If a force F is applied to a piezo's surface, an electric charge Q results. Together, this behavior can be described as:

$$\begin{bmatrix} y \\ Q \end{bmatrix} = \begin{bmatrix} d & 1/k \\ C & d \end{bmatrix} \begin{bmatrix} V \\ F \end{bmatrix} \tag{8}$$

with C the capacity, d the piezoelectric charge constant, and k the stiffness of the piezo, see Section 2 for more details.

Switching the piezo elements from the electronic driving circuit to a measuring circuit gives an accurate recording of the average pressure inside the ink channel, which we from now on call the "Paint" signal (Piezo-Acoustic sensing of INk channels in the Time domain), Fig. 12. First the driving waveform is applied, which takes 5–20 μs. After that, the current from the piezo element can be measured until the next actuation cycle starts. The main problem for this setup is that the amplitude of the Paint signal is only 50–100 μA while the current for charging the piezo is about 10 mA. The big discharge current from the piezo can disturb the measurement, so the piezo must be completely de-charged before the acoustic measurement starts.

However, with a reference a Paint measurement during actuation is even possible. One option is to calculate the contribution of the direct path to the Paint signal and subtract this from the measurement [122]. The main drawback of the computational compensation is related to the required accuracy of the piezo model. The non-linear behavior of the piezo elements is very difficult to model accurately.

The acoustic measurement also enables monitoring of jetting stability [123], see Section 6 and feed-forward control of the driving waveform. For most designs, the input waveform is manually shaped, based on physical insight into the working of a printhead. Normally, the actuation pulse is tuned to the first eigenfrequency of the ink channel. Additionally, somewhat more complex waveforms are designed for purposes like smaller droplets and damping of the residual vibrations. A control framework enables the systematic exploration of better driving waveforms to enhance the performance of the printhead, without having to perform a redesign of the printheads. Iterative Learning Control (ILC) as feed-forward control is very effective in improving the performance of a process that performs repetitive tasks [124–126]. So more specifically, given the highly repetitive character of the jetting process, ILC was a logical choice as control strategy for our printheads [122]. Calculations of feed-forward signals require a good understanding of the complete system dynamics.

With measurements we have only limited access to the interior of the printhead. We need not only for control purposes more information on the phenomena preceding the drop formation for a better understanding of the operating principles of the piezo printhead. Details on ink flow and acoustic pressure waves are only available through modeling [127]. Therefore, the modeling of the physical phenomena with available commercial codes and the development of dedicated special models are an essential part in the development of a new inkjet technology. Added to the measurements, the modeling reveals the chain of processes, which lead to drop formation. This enables a faster and better development of new printheads [128].

When modeling inkjet printheads, we have to face many challenges, like with the modeling of all Micro Electro-Mechanical Systems (MEMS) [129]. The modeling comprises a multi-scale simulation from nanometers to meters of multi-physics: solid mechanics, fluid dynamics, electromagnetism, materials science, electronic circuit design, mechatronics etc. Most of the models used in our research are derived from continuum mechanics, although in some cases the continuum mechanics are pushed to its limits. The continuum theory requires that the variables like density, pressure and velocity

are defined by some averaging process and be determined as the solution to some system of equations. We must keep this in mind when going to the smallest length scales. The domains of interest in our research are the structural dynamics, including piezoelectricity and acousto-elastic interaction, and the fluid dynamics [130]. The management of small-scale flows is a common denominator in micro-electromechanical systems (MEMS) [131].

1.4. Guide through the sections

The aim of the research is to explore the processes which lead to the final goal, the stable and reproducible formation of billions of drops. The first step is the actuation. The transformation of an electric voltage to a deformation of the ink channels is described in Section 2. The deformations inside the printhead cannot be measured and modeling with the commercial finite element code Ansys plays an important role. The deformation of the channel cross-section results in pressure waves. The acoustic properties of the ink channels are the subject of Section 3. The pressure waves play a central role in the printhead operation. They connect the electrical/mechanical domain of the actuator to the fluid dynamic domain inside and outside the nozzles. Measurements are done with the laser-Doppler setup and the acoustic Paint measurement. Details on ink flow and acoustic pressure waves inside the ink channel are available through modeling. The acousto-elastic interaction plays an important role in the "narrow-channel" model. Acoustic modeling with Ansys gives the details of the interactions with the structure dynamics of the printhead. A finite volume method, based on traveling plane waves, provides an efficient model for the refill of the nozzle and the influence of residual vibrations. A lumped parameter model provides an efficient method for modeling the acoustic properties of small MEMS-based inkjet printheads.

Another approach, modeling the complete printhead operation with one model in a multi-physics approach [132], leads to a very long calculation time, even when for example the structural part is modeled with lumped elements [133], and is not further considered in this review.

The drop formation is the final goal of the printhead operation. The pressure waves in the ink channels are the driving force behind the drop formation process. In Section 4, the details of the drop formation process are described. Optical measurements and modeling provide the information we need. For the modeling of the free surface flow with surface tension, and its impact on channel acoustics, we use the commercial volume of fluid code Flow3D [134]. The main drop properties can also be derived with a simple model based on a balance of energies and empirical relationships. The pinch-off process itself can be described with scaling laws.

Also the flow phenomena on the nozzle plate are important. Wetting of the nozzle plate can influence the drop formation process. The material interactions, which determine the wetting properties, are not known in detail. Therefore, an experimental study of the wetting phenomena is performed. This is described in Section 5. Simple analytical formulas can describe some aspects, but real material interactions can only be resolved through molecular modeling, which still has to be done yet. Wetting can also result in air entrainment. Air bubbles play an important role in the jetting stability. The theoretical and experimental research on the generation and the behavior of air bubbles and their impact on the printhead performance is the subject of Section 6. The acoustic measurement is an indirect measuring tool for the existence of air bubbles. Transparent heads are developed for direct visual measurements. Modeling is done with different numerical models.

In the last section the results are summarized, conclusions are drawn and an outlook on further developments is presented. The experiments are done with printheads developed at Océ Technologies B.V. For the research, a transparent test ink is used as reference fluid, which has a viscosity of about 10 mPa.s at the jetting temperature of 130 °C, a surface tension of 30 mN/m, a density of 1000 kg/m^2 and a speed of sound of 1250 m/s.

2. Structure dynamics

In this section the driving force in piezoelectric printheads is discussed. The actuator design for the reference printhead will be presented, which is based on the bump mode actuation, but also the alternatives, the bend mode and the shear mode actuation, will be discussed. The deformation of the channels to generate the pressure waves for firing droplets from the nozzles can also result in local cross-talk effects, like the direct and the pressure induced cross-talk effect, as will be shown with numerical simulations. Exciting many channels at the same time excites also resonances in the printhead structure.

2.1. Piezoelectricity

The driving force to fire a droplet with a piezo inkjet printhead is generated by the actuator, which deforms the structure through the inverse piezoelectric effect. Barium titanate ($BaTiO_3$), the first piezoelectric ceramic with a perovskite structure (a tetragonal/rhombohedral structure very close to cubic), was found around 1943. Roberts detected the piezoelectric effect in $BaTiO_3$ in 1947. In 1954, the discovery of the piezoelectric ceramic $Pb(Zr_xTi_{1-x})O_3$, lead zirconate titanate (PZT), was reported by Jaffe (US Patent 2708,244). In the following years, PZT became the main industrial product in piezoelectric ceramic materials [135]. Many actuator applications have emerged for the use of PZT [136,137].

Ceramic perovskites have a cubic structure that is stable at temperatures above their Curie temperature, as seen in Fig. 13. When the temperature decreases and falls below the Curie temperature, the structure changes. The cubic structure becomes

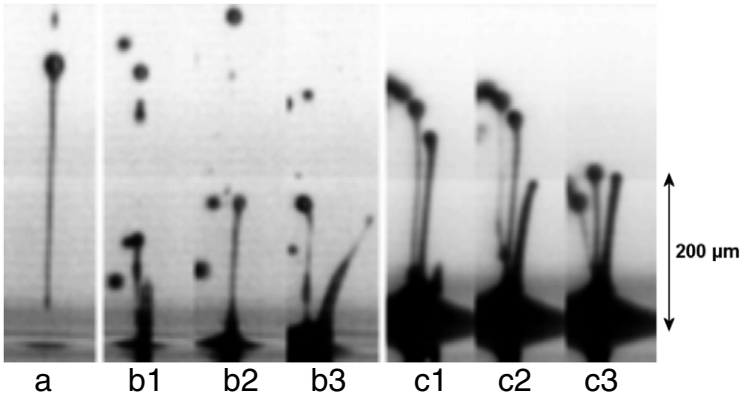

Fig. 84. High speed camera recordings with (a) the undisturbed drop formation in the left picture. The drop formation with partial blocked nozzles are shown in the other pictures, (b) with drops still jetted away and (c) without jetted drop. The recordings are made with a Phantom V7 high speed camera at 60 μs after the start of the actuation.

The drop formation is even blocked when the ink layer becomes more than 20 μm. A jetting nozzle induces several flow patterns in the ink layer. The continuous jetting of drops induces an air flow towards the nozzle. This air flow drags the outer part of the ink layer always towards the nozzle. As a consequence a strong sink flow can be visible or a Couette type of flow, when the overfilling of the nozzle adds ink to the inner part of the ink layer. Also an actuated, but non-jetting, nozzle induces all kind of flow phenomena. Dipole, source and sink flow patterns complete the observed phase diagram of possible flow patterns in the ink layer around an actuated nozzle.

The nickel nozzle plate and the ink are in a complete wetting regime. Older ink on the nozzle plate has other properties which results in a partial wetting regime. This older ink accumulates in the middle of the nozzle plate. The dynamic movement of the ink in an actuated nozzle results also in an increase of the surface tension. The precursor film of fresh ink, which was measured to be 13 nm in thickness, provides a way of communication between the nozzles and the central band of ink. A trunk flow drives the ink from the middle of the nozzle plate towards actuated nozzles. Marangoni flow is the driving mechanism behind this flow pattern.

An ink layer can also have a negative impact on the jetting stability. This will be discussed in the next section.

6. Bubble dynamics

In this section, the main factors which determine the jetting stability are discussed. Even after removing large dirt particles and air bubbles from the ink, there are sometimes air bubbles generated during the drop formation process. We will see that because of the relative low acoustic pressures in the printheads, air entrainment is the only mechanism for the generation of air bubbles. Wetting and small dirt particles play a crucial role in this process. There is a critical ink layer thickness, which results directly in air entrainment. Dirt particles with a size of 20 μm disturb the drop formation and can also induce the generation of air bubbles. Air bubbles can be measured directly in special transparent heads. The effect of air bubbles on the channel acoustics can be measured by using the piezo actuator also as a sensor. Then it will be discussed that a small air bubble oscillates at its natural frequency after the collapse. The influence of the confined space, i.e. the ink channel with nozzle, is that the collapse and the after-bounce are suppressed. If an air bubble can dissolve or be jetted out, no problem is generated. However, at the end of this section, we will see that an air bubble can also grow in an acoustic field by rectified diffusion. The air bubbles grow to a size comparable to the displacement by the acoustic pressure waves. A large air bubble will then counteract the pressure build-up and the drop formation process ceases completely.

6.1. Stability

6.1.1. Dirt and air entrapment

A very important requirement for todays productive drop-on-demand inkjet printers is the stability of the jetting process. Large dirt particles with a radius more than 15 μm can block a nozzle opening completely and there will be no drop formation at all. A nozzle can also be partially blocked by a large dirt particle. This results in severe deviations of the drop speed and size, the jetting angles and the drop shape, see Fig. 84. Big dirt particles can originate from the head itself (e.g. graphite particles), dragged along with the ink (e.g. not good enough filtering or non-compatible ink components), or can come from outside (e.g. paper fibres and common dust). The large dirt particles have to be removed during normal operating conditions. The most common cause of instabilities which remains are air bubbles.

Air bubbles will influence the acoustics and the drop formation process and can result in nozzle failure [478,479]. The ink can contain a lot of air bubbles before the drop formation starts. This air can originate from the ink manufacturing process

or from failures in the ink supply system. For a normal printhead operation, these sources have to be eliminated and further research is therefore concentrated on the generation of air bubbles during normal printhead operation. The removal of air is also very important in experiments with dripping drops [262,480].

Two possible sources for the generation of air bubbles during normal printhead operation are cavitation [481] and air entrainment at the nozzle. Cavitation takes place when the negative acoustic pressure exceeds the Blake threshold at the cavitation nuclei. Cavitation will take place somewhere inside the ink channel where the negative acoustic pressure amplitude has its largest value. Cavitation can take place at small air bubbles, at non-wetted channel/nozzle walls, at non-wetted dirt particles, or at inclusions by surfactant [482]. So, for a stable drop formation, the ink must be free of air and dirt, the channel walls must have good wetting properties, and when using surfactant, the concentration must stay below the critical micelle concentration. Then, the acoustic design of our printheads can be made such that the acoustic negative pressure remains always above the threshold for cavitation, see also Section 3. Then, air entrainment at the nozzle during printhead operation remains as the only possible source for the generation of air bubbles.

6.1.2. Acoustic detection of air bubbles

The disturbance or the failure of the drop formation process itself is not suitable for a quantitative measurement of the behavior of the bubble itself. The printheads developed for application in a printer are opaque. A direct observation of air bubbles in these printheads is not possible. Only in a special transparent head is a direct observation of air bubbles possible [483–485]. A way to measure the effect of air bubbles in the opaque heads is to use the piezo actuator also as a sensor. This is the Paint measurement, see Section 1.3.2. With the Paint measurement, the electric current from the piezo elements is measured. The Paint current I_p from a piezo element with area A_p is given by the equation:

$$I_p = \frac{\mathrm{d}Q}{\mathrm{d}t} = A_p \frac{\mathrm{d}D_3}{\mathrm{d}t} \tag{130}$$

with D_3 the electric displacement or charge density in the polarization and actuation direction of the piezo element, see Section 2.2. The electric field is in the actuation direction $E_3 = V/h_p$, with h_p the height of the piezo element. With Eq. (13) we get:

$$I_p = d_{33} A_p \frac{\mathrm{d}T_3}{\mathrm{d}t} + \epsilon_3 A_p \frac{\mathrm{d}E_3}{\mathrm{d}t}. \tag{131}$$

The normal stress component T_3 is generated by the pressure P in the ink channel. With V the voltage on the electrodes, this equation becomes:

$$I_p = d_{33} A_p \frac{\mathrm{d}P}{\mathrm{d}t} + \frac{\epsilon_3 A_p}{h_p} \frac{\mathrm{d}V}{\mathrm{d}t}. \tag{132}$$

The capacitance of the piezo element is given by $C_p = \epsilon_3 A_p/h_p$. After integrating the pressure, which can show local variations, over the length l_p of the piezo element we get:

$$I_p = C_p \frac{\mathrm{d}V}{\mathrm{d}t} + d_{33} b_p \int_0^{l_p} \frac{\mathrm{d}P}{\mathrm{d}t} \mathrm{d}z \tag{133}$$

with b_p the width of the piezo element. The Paint current is now known in terms of the actuator voltage and the channel pressure. With the general homogeneous solution for the acoustic channel pressure and the particular solution, which is the pressure due to the actuator, in the frequency domain per frequency according to d'Alemberts solution:

$$P(z,t) = P_r \mathrm{e}^{\mathrm{i}(\omega t - kz)} + P_l \mathrm{e}^{\mathrm{i}(\omega t + kz)} - \alpha \rho c_{\mathrm{eff}}^2 V \tag{134}$$

we can express the Paint current or signal in terms of propagating waves towards the nozzle and coming from the nozzle with wave number k and frequency ω. Inserting this equation in Eq. (133) results in:

$$I_p = \mathrm{i}\omega (C_p - \alpha d_{33} A_p \rho c_{\mathrm{eff}}^2) V + d_{33} b_p \frac{\omega}{k} \left(P_l \mathrm{e}^{\mathrm{i}kl_p} - P_r \mathrm{e}^{-\mathrm{i}kl_p} \right). \tag{135}$$

Not only the drop formation, the refill and the wetting of the nozzle plate changes the reflection of the acoustic pressure wave, but also an air bubble has a large influence on the pressure waves P_l coming from the nozzle.

6.2. Air entrainment

6.2.1. Wetting layer

Air entrainment is directly linked to the presence of an ink layer on the nozzle plate [352,279,485,419]. An ink layer around the nozzle results in a lower drop speed, Section 5.4. The drop speed decreases with ink layer thickness up to 20 μm and the nozzle ceases to fire drops with an ink layer thickness more than 20 μm. The experiment with adding a layer of ink through the neighboring channels demonstrated this impact on the drop formation. The same experiment also shows

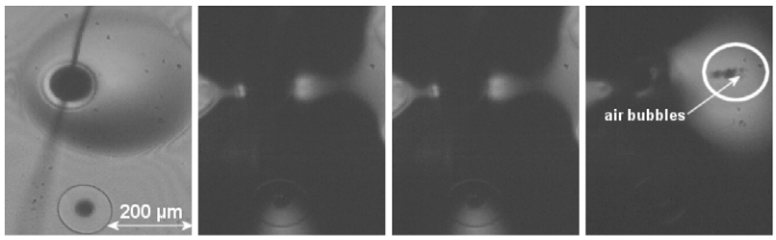

Fig. 85. Top view of an experiment where ink is supplied at $t = 0$ ms through the neighboring nozzles via a static pressure. The pictures are taken with a high-speed camera with 10 kfps. The first frame shows the regular jetting. The second frame is taken at the moment when the ink layer reaches the jetting nozzle. The third frame shows the moment when jetting stops. The last frame shows the air bubbles, which are created. These bubbles are inside the white circle.
Source: Adapted from [279].

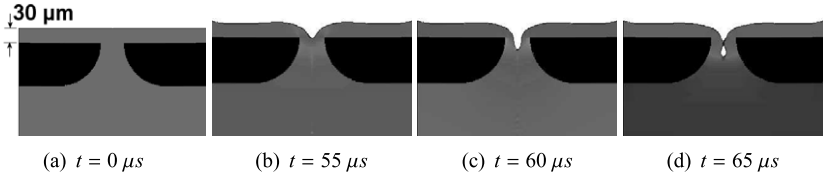

Fig. 86. (a) Flow3D simulation with an ink layer of 30 µm on the nozzle plate. (b–d) During the second actuation cycle, which started 50 µs after the first cycle, an air bubble is entrapped.
Source: Taken from [279].

the formation of air bubbles. Four stages of this experiment are shown in a top view in Fig. 85a–d. First the normal jetting situation is depicted. In the second frame the supply of an ink layer through neighboring channels is shown. The stopping of the drop formation is shown in the third frame. Finally, the creation of air bubbles is depicted. After the drop formation has failed, small air bubbles are visible in the ink layer as indicated.

The ink layer is applied during 1 s. The ink layer covers a large part of the nozzle plate and increases continuously in thickness until it is very thick. The drop formation fails, but the actuation continues at a repetition rate of 20 kHz. Air bubbles are visible in the ink layer after 0.2 s. After 1 s, the ink supply stops and the ink layer thickness decreases. After 1.5 s, jetting starts again. It turns out that an air bubble is also entrapped in the jetting nozzle [279].

Flow3D simulations are used for a qualitative check whether air entrainment can be induced by the ink layer itself. With an ink layer thickness of 0–20 µm, only the drop speed is lowered. With an ink layer thickness of more than 20 µm, no drops are generated anymore. In a simulation with an ink layer thickness of 30 µm on the nozzle plate, air entrainment is visible as shown in Fig. 86a–d. With this simulation it is assumed that the influence of the ink layer on the pressure waves inside the printhead is negligible. Two actuation cycles at a repetition rate of 20 kHz are simulated. During the first cycle, which started with no fluid movement at all, no air is entrained. Air is entrained during the second cycle. The actual air entrainment occurs when the meniscus is pulling back and ink is already flowing into the nozzle. The void is then closed at the top, because a lot of ink flows in from the layer around the nozzle. At an ink layer thickness of more than 40 µm, only a net inflow of ink is visible without a large deflection of the free surface.

The experiment with an ink layer supplied through the neighboring channels shows the formation of multiple bubbles in the ink layer. Because the ink layer thickness varies slowly on a seconds time scale, the critical ink layer is present during multiple drop actuation cycles. Each cycle, air can be entrained. To determine the critical layer thickness, experiments are performed with additional nickel plates to create a well defined ink layer thickness around the jetting nozzle [279]. Different thicknesses of the additional nozzle plate are used to vary the ink layer thickness. By firing only three drops in one sequence, the amount of ink around the nozzle is not changed significantly. The critical layer thickness turned out to be between 30 µm and 40 µm, in agreement with the simulations. Below this critical layer thickness, the impact on drop formation is not strong enough and above the drop formation process is hindered too much. Another source for the distortion of the drop formation process are small dirt particles, which will be discussed in the next section.

6.2.2. Small dirt particles

With a wetted nozzle plate, a flow towards the nozzle is observed in most cases during jetting, Section 5.2.1. Relatively small dirt particles, caught in the ink layer, are likely to reach the jetting nozzle and this can result in a distortion of the drop formation. This distortion also influences the Paint signal. Therefore the acoustics inside the ink channels are continuously monitored with the Paint signal [279]. At a repetition rate of 20 kHz, a time interval of only 30 µs between the actuation pulses is taken for further analysis of the Paint signal. The amplitude of the current from the piezo element $I(t)$ during that

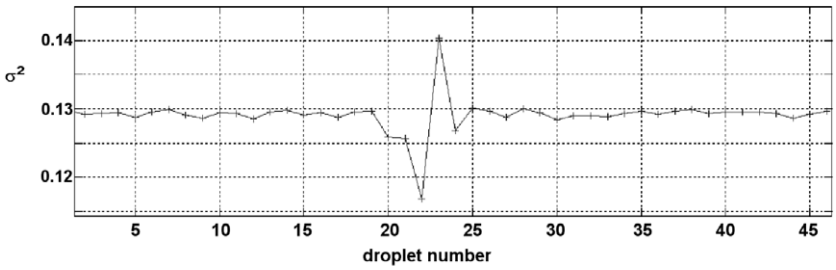

Fig. 87. The amplitude of the Paint signal. During 25 drop formation cycles before and after a distortion the variance varies less than 0.5%, the distortion leads to a deviation of 5%–10%.

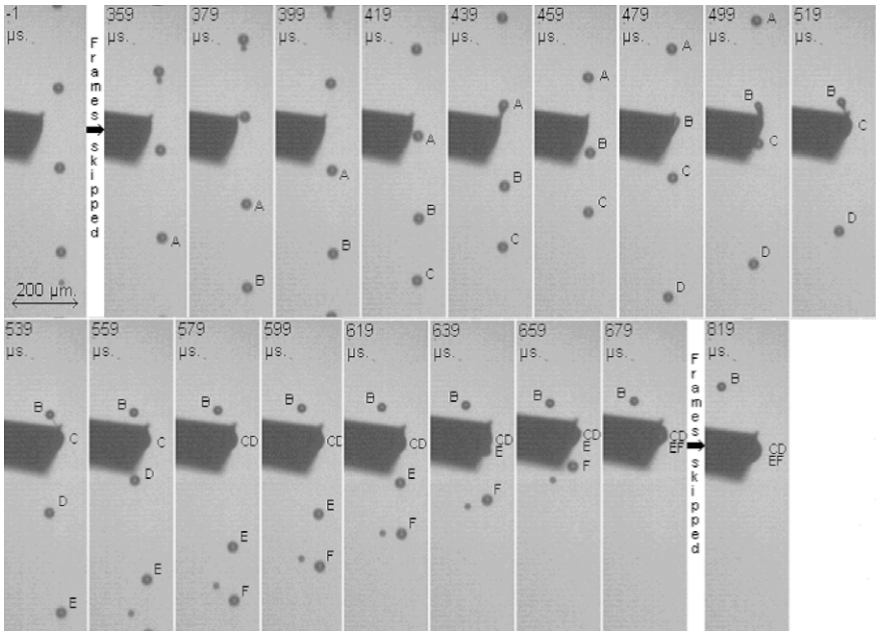

Fig. 88. High-speed camera recording of the capture of the last jetted drops after a disturbance triggered the piezoelectric device. A piezo element with a tiny metal chisel is visible at the left of the drop stream. After the trigger signal, the piezoelectric device moves into the stream of drops. The times are given relative to the trigger moment. Four droplets, indicated with C, D, E and F, are caught. Jetting was stopped after droplet F.

time interval T is calculated:

$$\sigma^2 = \frac{1}{T}\int_0^T [I(t)]^2\,\mathrm{d}t. \tag{136}$$

The amplitude of the Paint signal varies by 5%–10% during a distortion, Fig. 87. The amplitude of the Paint signal over 25 drop formation cycles before and after the distortion varies by less than 0.5%.

The influence of the distortion on the Paint signal is used to trigger a high-speed camera to record the drop formation when the distortion takes place [486]. The correlation between the distorted drop formation and the variation in the Paint signal is published in more detail in [279]. The deviation of the amplitude can not only trigger a high-speed camera but also a piezoelectric device that can move 60 µm within 1 ms. This device, with a tiny metal chisel attached to it, was placed under the nozzle plate at a distance of a few micrometers from the stream of jetted drops. When triggered, this device moves into the stream of drops to capture them, see Fig. 88. At the same trigger signal also the actuation is stopped, and only the last few drops are captured for further analysis. It turns out that the captured droplets contain relatively large particles with a diameter of about 20 µm. These particles are not found in captured drops where no distortion occurred. The minimum in the Paint signal always corresponds to the drop which is transporting the particle. At that moment, the nozzle is (partially) blocked, which results in lower acoustic amplitudes inside the ink channel.

A variation of a few micrometers in the position of the meniscus results in a comparable variation of the Paint signal, see also Section 3.4.1. To explain that the Paint amplitude is first several percent lower and then several percent larger, the meniscus must first be protruded out of the nozzle and second the meniscus must be retracted. Also a variation in the drop speed is observed during a distortion. The first droplet is 0.1–0.2 m/s faster and the second droplet up to 0.4 m/s slower, with often a deviating shape and jetting angle [279]. The variation in the drop speed, as a result of the different meniscus

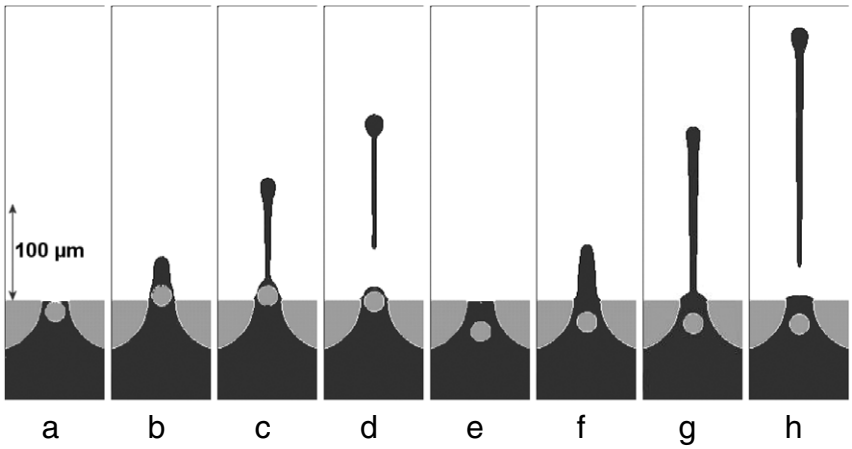

Fig. 89. Simulation of the effect of a spherical particle with a diameter of 20 µm on the drop formation. The pressure in the channel is kept the same and the starting position of the meniscus is also at its original position. The drop formation is shown at 0, 15, 30 and 45 µs after start of the actuation. First with the particle at 10 µm under the meniscus surface (a,b,c,d) and second with the particle at 30 µm under the surface (e,f,g,h).

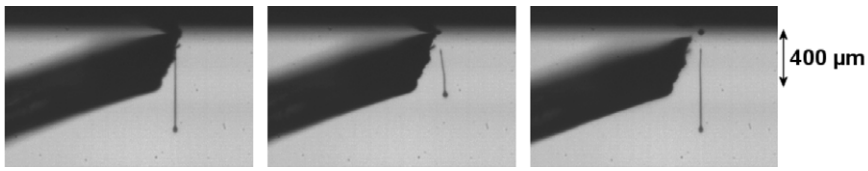

Fig. 90. High-speed camera recording of the effect of a partial covering of the nozzle opening with a teflon wiper. Shown are the drop formation before, during (the wiper moves away from the camera), and after the covering. The drop formation during the partial coverage is distorted a lot. After the distortion, the drop formation is normal again.

positions (because of a variation in the refill level, Section 3.4.1), corresponds to the observed variations during the distortion of the Paint signal.

The dirt particles itself can also be the source of the observed variations in drop speed. For a qualitative check, the drop formation is simulated with dirt particles at different positions. In Fig. 89 two examples are shown with a spherical particle at 10 µm and at 30 µm under the meniscus surface. The drop speed varies with the particle at different positions under the surface. With respect to the undisturbed drop speed, the variations are:

- at 5 µm, 1.9 m/s slower and the particle is jetted away
- at 7.5 µm, 2.8 m/s slower and the particle is jetted away
- at 10 µm, 1.3 m/s faster and the particle remains inside the nozzle
- at 10 µm, 0.9 m/s faster and the particle remains inside the nozzle
- at 30 µm, 0.4 m/s slower and the particle remains inside the nozzle
- at 40 µm, 0.5 m/s faster and the particle remains inside the nozzle.

From the capturing of the drops, visually and with the piezoelectric element, we know that the last drop in the distortion drags along the dirt particle. In the simulation this happens when the dirt particles are very close to the surface.

The variation of the amplitude of the Paint signal, shown in Fig. 87, is the most common example of a distortion. After the disturbance occurred, jetting keeps going on as usual. But sometimes after a disturbance, an air bubble is entrapped, which becomes later visible as a larger deviation of the Paint signal. Then, there is also a disturbance of the drop formation visible, which finally even can lead to the complete breakdown of the drop formation process. This will be shown in the next sections. The entrainment of an air bubble is always preceded by a distortion. No air bubbles are detected without a distortion preceding it. So the described distortion is a necessary but not sufficient condition for air entrainment [279].

The exact mechanism of how air is entrained is still not known. In reality, the dirt particles have irregular shapes, mostly in the shape of flakes. The drop formation model is a 2D model rotational symmetric model. To simulate irregular shapes a full 3D model is required, which leads to a very long calculation time. The particles are relatively large. The particle size is typically 20 µm, the nozzle diameter is 30 µm. Partial blocking of the nozzle opening could be the origin of the air entrainment process. To check this, experiments are done with a 400 µm thick teflon wiper. During the jetting of a single nozzle, the 1 mm wide wiper partially moves over the nozzle with a speed of 3 µm/µs. So the nozzle is partially blocked for several actuation cycles. The drop formation is distorted a lot during this period, Fig. 90. If partial blocking of the nozzle is the mechanism behind air entrainment, the experiment should lead to a deterministic generation of air bubbles. However, this is not the case.

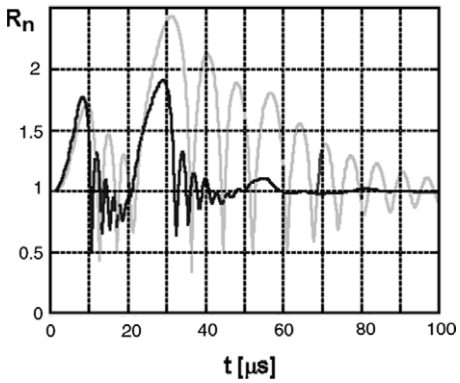

Fig. 91. The change in bubble size (as normalized radius $R_n = R(t)/R_0$) of bubbles with a diameter of 20 μm (black) and 40 μm (grey). The calculations are done with the Rayleigh–Plesset equation and the pressure from the narrow channel model. The imposed pressure variation is large enough to generate a collapse with an oscillation after the collapse [492].

This is also qualitatively confirmed with Flow3D simulations with a 3D drop formation model with a partially covered nozzle opening. In all the simulations the drop formation is also distorted a lot, with a large deviation of the jetting directions, but air entrainment is not seen. The asymmetric retraction of the meniscus does not give any clues on a larger chance to entrain air.

6.3. The oscillating bubble

6.3.1. Size dynamics

The radius, position and size of an air bubble changes in an acoustic field [487–489]. For a bubble in an infinitely large volume, the change of the bubble radius R of a bubble with radius R_0 at ambient pressure is given by the Rayleigh–Plesset equation [490]:

$$R\ddot{R} + \frac{3}{2}\dot{R}^2 = \frac{1}{\rho}\left(p_g - p_0 + p_v - \frac{2\gamma_l}{R} - \frac{4\eta\dot{R}}{R} - p_\infty(t)\right). \tag{137}$$

The right term represents the forces generated through the pressure difference between the gas pressure inside the bubble p_g with respect to the ambient pressure, with corrections for the vapor pressure p_v, the Laplace pressure, and the pressure from viscous stresses. The last term, p_∞, is the imposed acoustic pressure at a distance where the pressure due to the inertia of the radial flow field around the bubble is negligible with respect to the imposed pressure fluctuations. The polytropic equation is used as the equation of state:

$$pV^\Gamma = \text{constant} \tag{138}$$

with Γ the polytropic index, which is 1.0 for isothermal behavior and 1.4 for adiabatic behavior. For the gas pressure in the Rayleigh–Plesset equation, the following expression can now be used:

$$p_g = \left(p_0 + \frac{2\gamma_l}{R_0} - p_v\right)\left(\frac{R_0}{R}\right)^{3\Gamma}. \tag{139}$$

The Rayleigh–Plesset equation is the basis for the explanation of the net displacements and the mass exchange of air bubbles in an acoustic field.

It is assumed that the bubble oscillates isothermally, so that the polytropic index $\Gamma = 1$ [491]. The imposed pressure fluctuation p_∞ is calculated with the narrow channel model of the reference printhead, see Section 3.1. The resulting dynamic changes in bubble size for bubbles with a radius of 10 μm and a 20 μm are shown in Fig. 91.

In Fig. 91 we can see that the bubble radius increases twice, at 9 μs and at 30 μs. This corresponds to the negative pressure peaks in the pressure at the entrance of the nozzle, see also Fig. 32. When the imposed pressure becomes higher than the ambient pressure, the bubbles collapses. After the collapse the bubble resonates with its natural frequency. The collapse and resonance of a bubble occurs when the frequency of the imposed pressure field is much lower than the natural frequency of the bubble [493]. The channel frequency of the 8 mm long pressure channel is 50 kHz and the natural frequencies of the bubbles are 150 and 300 kHz for the 40 μm and the 20 μm bubbles, respectively.

The collapse of the bubble is an important effect and can generate many effects such as cavitation damage from the jet formed with the asymmetric collapse near a solid wall [494,495] and can even excite sonoluminescence [496]. The jetting effect can be used for a micro-pump [497,498] and the dynamic behavior of air bubbles is also used in an actuator [499]. In our case, the oscillating bubble is a disturbing effect, which influences the channel acoustics and the drop formation.

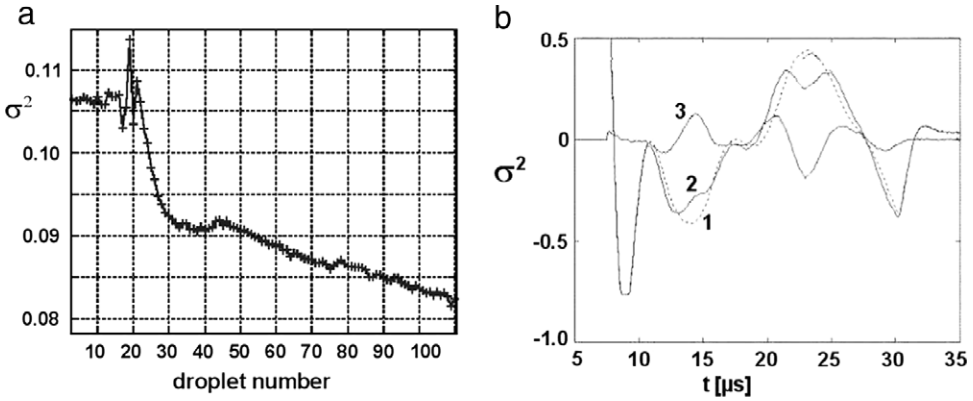

Fig. 92. (a) The amplitude of the Paint signal when a distortion occurs before cycle 20 and air is entrained. The amplitude of the Paint signal deviates more than 10 % within 100 drop formation cycles at a repetition rate of 20 kHz. The actuation amplitude is the nominal driving amplitude for a drop speed of 7 m/s. (b) The shape of the Paint signal without an air bubble (dotted line 1), with an air bubble (continuous line 2), and the difference between the two signals (continuous line 3). This shows a 170 kHz distortion after 100 drop formation cycles.

6.3.2. Impact on channel acoustics

With acoustic transmitters and receivers in an acoustic pipe, several acoustic signals could be used for the exact detection of air bubbles [500]. With our Paint measurement, only the global acoustic response can be measured. When air is entrained, the amplitude of the Paint signal will show an increasing deviation after the distortion, instead of remaining at the same value as shown in Fig. 87. At a repetition rate of 20 kHz, the variance will deviate more than 10% within 100 drop formation cycles, Fig. 92a. It turns out that the deviation is caused by a typical pattern. This pattern becomes more clear when we look at the difference between disturbed Paint signal and the signal without an entrained air bubble, the reference signal. When looking at the shape of the Paint signal, Fig. 92b, it turns out that the deviation is caused by a distortion with a frequency of 170 kHz [279].

The question is what causes the 170 kHz distortion. It could be the afterbounce as shown in Fig. 91. After the collapse, the bubble oscillates at its natural frequency. The natural frequency f_0 of a free bubble, neglecting surface tension, viscosity, vapor pressure and advection, is called the Minnaert frequency [482]:

$$f_0^M = \frac{1}{2\pi R_0}\sqrt{\frac{3\Gamma p_0}{\rho}}. \tag{140}$$

The resonance frequency of 170 kHz corresponds to a bubble radius of 18 μm. However, the behavior of an air bubble in an infinite space is different from the behavior in a bounded liquid [501,502]. Now the pressure field is not three dimensional anymore. Between two plates it is two-dimensional [503] and in a long channel only one-dimensional [504,505]. The confined space, where the bubble is located, has a large effect on the dynamic behavior of the bubble [506–508]. In our case, the confined space is the semi-closed connection channel with a diameter of 250 μm and a small nozzle opening. Within these constraints, the resonance frequency will be reduced by 30%–50% for a bubble with a radius of 10–20 μm [509,510]. So the radius of the bubble causing a 170 kHz resonance is only 9–12 μm. The volume of such an air bubble is 2–8 pl, much smaller than the volume displacement by the acoustic pressure field.

The effect of the confined space can be taken into account by adding the pressure disturbance caused by an air bubble to the imposed pressure in the Rayleigh–Plesset equation. When a bubble shows a collapse in the response to the imposed pressure field, also thermal and acoustic damping should be taken into account [511,512] and in extreme cases even the minimum radius, which is determined by the excluded volume of the gas molecules [513]. This makes the description of the dynamical behavior of a bubble in an acoustic field rather complicated and is not taken into account in our analysis.

The imposed pressure is calculated with the narrow channel model. With an air bubble with a volume V_b between the channel and the nozzle, the continuity equation can be written as [485]:

$$\frac{\mathrm{d}V_b}{\mathrm{d}t} = 4\pi R^2\dot{R} = A_n u_n - A_{\mathrm{ch}} u_{\mathrm{ch}}. \tag{141}$$

With this equation added to the narrow channel equation and the Rayleigh–Plesset equation, the effect of the confined space can be calculated. The change of the bubble radius in the reference printhead driven at normal actuation amplitude as calculated with and without the effect of the confined space is shown in Fig. 93. The confined space dampens the collapse and afterbounce almost completely.

With regular printheads, we can only measure the distortion of the drop formation and the impact on channel acoustics through Paint. A direct measurement of air bubbles is only possible with an optical detection in special, transparent test printheads [483], see also Fig. 95. A transparent nozzle plate and a transparent connection channel are made with powder-blasting out of glass plates. The transparent connection channel has a length of 400 μm and a hourglass shaped cross-section

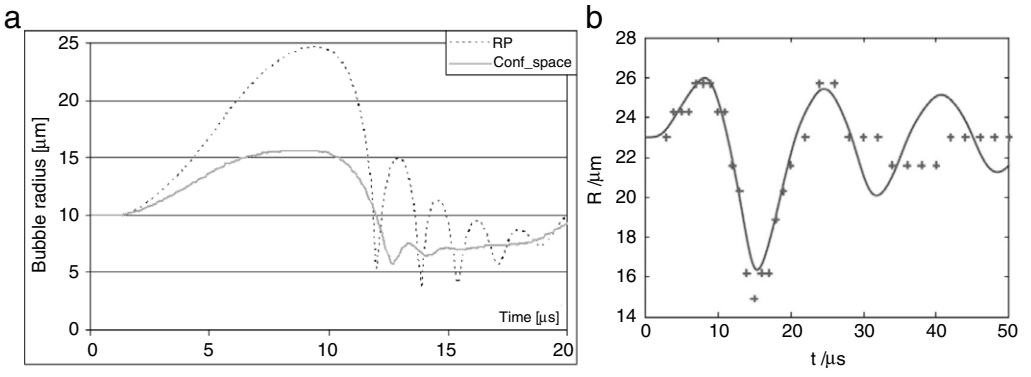

Fig. 93. (a) The calculated change of the radius of a bubble in a reference printhead at normal driving amplitude as calculated with the Rayleigh–Plesset equation without and with the effect of the limited space around the air bubble. (b) The measured (dots) and calculated (line) change of the bubble radius in a special transparent head, with comparable acoustic properties.
Source: (b) taken from [514].

with a diameter between 80 μm and 250 μm. The 70 μm long conical shaped nozzle has an entrance diameter of 50 μm and an outlet diameter of 30 μm. These two glass plates replace the nickel nozzle plate. The pressure channel of this head has a length of 5 mm and there is also the normal connection channel with a length of 1 mm. The acoustic properties of this printhead are still comparable with the opaque reference head. High speed camera recordings with a Phantom V7 camera at 40 kfps and a continuous light source behind the glass plates show the relation between the behavior of an entrained air bubble and the impact on channel acoustics and the drop formation.

Also in the optical recordings, there is no afterbounce visible, Fig. 93b and the measured data fits well with the calculated results. So the resonance at the natural bubble frequency after a collapse is not the cause of the 170 kHz distortion in the Paint signal.

The distortion is caused by the fact that the acoustic properties of the channel are changed. The reflection of the pressure wave will be altered by the presence of an air bubble as we will see in Section 6.5.3. We see the influence of a bubble as a 170 kHz distortion because this frequency is next to the basic channel resonance at 50 kHz the next strong peak in the frequency characteristics of this head. The frequency characteristics describe the relation between the electric activity in the actuator and the meniscus movement and acts also as a filter for the Paint measurements. The high frequency components are more sensitive to small changes in the reflection conditions of the pressure waves and therefore, the higher frequency components are altered more than the low frequency components.

6.3.3. Impact on drop formation

In the experiments with the transparent head, the oscillations of a bubble have an effect on the drop speed [485]. This is shown in Fig. 94a for a range of bubble radii between 11 and 19 μm. The driving amplitude is low, which results in a drop speed of only 1 m/s without an air bubble. In the experiment, the droplet velocity increases and reaches a maximum of 2.5 m/s. Then the droplet velocity gradually decreases to 1 m/s at 0.9 s. A small amplitude oscillation with $f = 50$ Hz is superimposed onto the droplet velocity, reflecting the AC frequency of the devices. This effect is negligible compared to the effect of the entrained air bubble on the drop speed.

The recorded images of the ejected droplets and oscillating bubbles are analyzed with a gray-level threshold to determine the location of the edges of the droplets and bubbles. The images of the bubbles only consist of some tens of pixels, limiting the accuracy of the size determination. Other sources of errors are the optical diffraction and the assumed sphericity of the bubbles in the digital image analysis. For the ejected drops and for the bubbles within the channel (away from the walls) we do not have any indication of deviations from sphericity. However, the air bubbles, when pushed against the glass nozzle plate, seem to be slightly non-spherical.

The scatter in the bubble radius is found to be quite large, due to the low contrast in the images and because multiple bubble radii are measured over one acoustic cycle, see also Fig. 93b. When we compensate for the latter by plotting the average radius (over 40 bubble radii), the bubble growth becomes more obvious. This is used in Fig. 94b where the two data sets are combined to get the drop speed as a function of bubble size. The measured drop speed increases to 2.5 m/s with increasing bubble size until a radius of 16.5 μm and than decreases very fast with increasing bubble size. Finally, jetting fails when the bubble radius becomes larger than 19 μm.

A resonance effect of the bubble oscillation with the meniscus movement results in the increase of the velocity. This can be verified with a simple model for a harmonic oscillator [515], which is based on the approach used in [509]. The dynamic behavior of the bubble is based on the polytropic relation $pV^{\Gamma} = constant$ between bubble volume and the pressure. The meniscus movement is based on Newton's second law. The viscous dissipation is taken into account with a Poiseuille flow profile in the nozzle to correct for the pressure loss between the pressure at the bubble and the ambient pressure. The

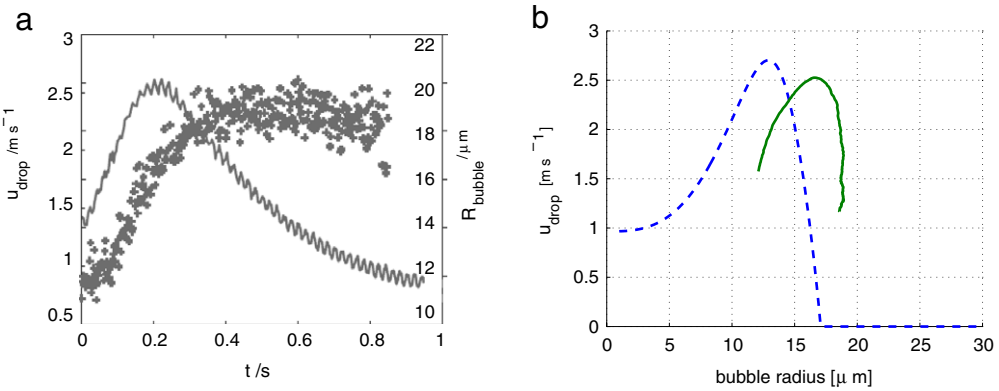

Fig. 94. (a) Simultaneously measured bubble radius and drop speed with the transparent head described in [485]. The actuation is started at $t = 0$ s. The bubble diameter increases from 22 to 38 μm and the drop speed increases from 1 to 2.5 m/s at 0.2 s and decreases again. (b) The resulting relationship between bubble diameter and drop speed as measured (solid line) and calculated with the simple harmonic oscillator model (dashed line). The measured drop speed shows a maximum at a bubble diameter of 33 μm. Jetting fails with a bubble diameter larger than 38 μm.

continuity equation completes the set of equations. After linearization around the equilibrium volume, a forced harmonic oscillator equation for the meniscus speed is obtained. A sinusoidal velocity with frequency f is imposed with the main channel resonance frequency, which is 50 kHz for the transparent head. The radius of the bubble where the resonance effect takes place reads according to this model [485]:

$$R_0^{res} = \left(\frac{3\Gamma \rho A_n^3 p_0}{16\pi^3 l_n (\rho^2 f^2 A_n^2 + 16\eta^2)} \right)^{\frac{1}{3}}. \tag{142}$$

In the model, the conical nozzle shape is replaced by a straight nozzle with the same outlet diameter as the conical shaped nozzle, i.e. 30 μm. The conical nozzle has an entrance diameter of 50 μm and a length of 70 μm. This is transformed to a straight nozzle with the same acoustic impedance, see Section 3.1.2 and Eq. (66). The length of the acoustic equivalent straight nozzle is 32 μm. The resulting drop speed is shown in Fig. 94b, together with the measured results. The drop speed is calculated with the energy balance as mentioned in Section 3.2.2. The results of the simple model agree reasonable with the experimental data. Only the bubble radius where the resonance effect takes place is a little smaller, 13 μm instead of 16.5 μm.

The eigenfrequency of a bubble with radius R_0 which acts as a harmonic oscillator with the meniscus movement of a nozzle is:

$$f_0^H = \sqrt{\frac{3\Gamma R_n^2}{4\pi \rho l_n R_0^3}}. \tag{143}$$

The eigenfrequency of a bubble with radius $D_0 = 16.5\ \mu m$ is 50 kHz, the same as the main channel resonance frequency.

6.4. The moving bubble

6.4.1. Balance of forces

Many forces are acting on a bubble in an acoustic pressure field. The movement of a bubble is determined by the competition between the acoustic and the hydrodynamic forces [516]. First there is the primary Bjerknes force. The force acts in the direction of the acoustic pressure gradient. A small bubble will be pushed towards the pressure node, i.e. the small bubble at the nozzle will move into the channel. A very large bubble will have a low natural resonance frequency and start to oscillate in anti-phase with the acoustic pressure field [517]. The primary Bjerknes will now act in the opposite direction towards the pressure anti-node, i.e. the bubble will move towards the nozzle plate.

The secondary Bjerknes forces are generated by the acoustic pressure field emitted by the oscillating bubble itself or by another bubble. The basis equation is the same as the equation for the primary Bjerknes force, but now the pressure field is generated by the bubble itself. Due to a mirror effect, this force will push bubbles against a rigid wall. The same mirror effect results in a repulsing force against a free surface, e.g. the meniscus [518]. Many expressions can be obtained for the secondary Bjerknes force.

The two Bjerknes forces can explain the main displacement characteristics of the only directly experimentally observed displacement of a bubble. This is the optical measurements with the transparent printhead, Fig. 95 [484]. A small bubble, which is generated near the nozzle, moves with a speed of 5 mm/s into the channel, because of the primary Bjerknes force, and is after 118 ms attracted against the (transparent) connection channel wall, because of the secondary Bjerknes force.

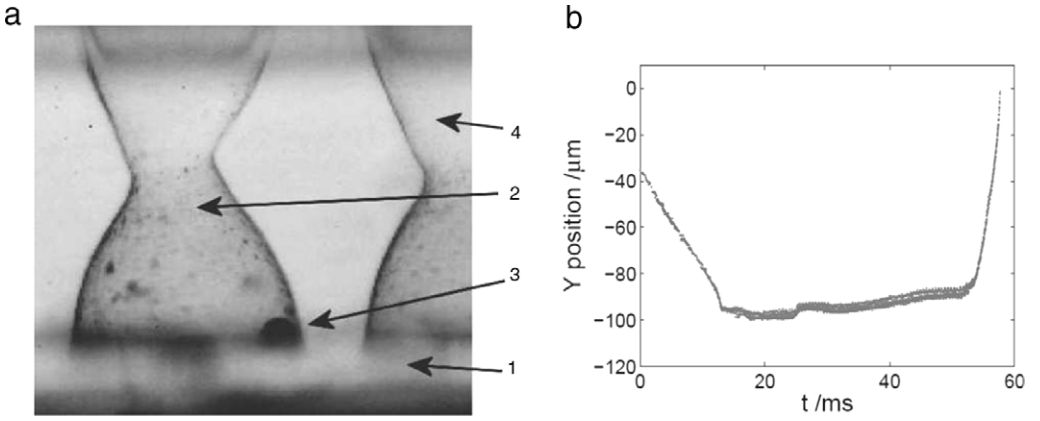

Fig. 95. (a) The transparent head, used for direct visual measurements of entrapped air bubbles with the nozzle plate 1, the connection channel 2, an air bubble 3, and a neighboring channel 4. (b) The y position of the air bubble as a function of the time after the air entrapment. The bubble first moves into the channel. At $t = 52$ ms the Bjerknes force reverses sign and the air bubble is pushed back towards the nozzle.
Source: Taken from [484].

After a while this bubble has grown in size to a diameter of 32 μm. The natural frequency of this bubble as harmonic oscillator, as described in the previous section, is reduced to 55 kHz and tends to become lower than the frequency of the main channel resonance. The bubble moves after 55 ms in the opposite direction towards the nozzle plate with a speed of 20 mm/s.

The drag force from the ink flow becomes important especially near the nozzle itself [519–521]. This force tends to drag the bubble along with the ink flow, thus along with the drop formation. Buoyancy or gravity forces play no role in our case. Other forces which could play a role are lift forces from the radial flow field [522,523], the added mass and inertia forces and finally the Basset history force which results from the absorbed momentum in the boundary layer around the bubble [524]. These acoustic and hydrodynamic forces will result in complicated movement patterns, which will be discussed in the next section.

6.4.2. Net displacements

The forces on the bubble result in a displacement pattern, which can only be resolved numerically for an opaque printhead. In Fig. 96a the net displacement after one drop formation cycle is shown. For a bubble with a diameter of 10 μm at different positions on the nozzle axis. The results are simulated with a 2D rotational symmetric drop formation model in Flow3D. So only bubbles at the nozzle axis can be simulated. The pressure inside the bubble is calculated with the polytropic equation. The initial pressure inside the bubble is equal to the ambient pressure, enlarged with the Laplace pressure $2\gamma/R_0$. The pressure in the connection channel at a position 300 μm in the channel in front of the nozzle is kept the same. There is only a one-way coupling between the channel acoustics and the flow phenomena in the nozzle. The bubble cannot influence the pressure waves in the channels in these simulations.

Depending on the axial position, the bubble is either moved inwards or outwards after one drop formation cycle. There are four positions where the net axial displacement becomes zero. Two positions are unstable because the bubble at locations around this point moves further away from these positions. Those are the position at 25 μm and 72.5 μm. But, the two axial positions at 62.5 μm and 105 μm are stable. The bubble at locations around points moves towards these positions, so these two positions can act as a bubble trap.

At axial positions between the meniscus and 20 μm behind the surface, the bubble is jetted out. Also experiments show that jetting out of an air bubble is a possible recovery mechanism. In Fig. 96b the measured amplitude of the Paint signal is shown. At drop formation cycle 70, a distortion occurs followed by air entrainment. At drop formation cycle 124, a second distortion is visible without any consequences. With drop formation cycle 155, the amplitude of the Paint signal returns in one cycle to its normal value, which can only be caused by jetting out of the bubble. The numerical simulation of the jetting out is shown in Fig. 97. The bubble moves along with the drop formation. The drop shape will be distorted, but after this drop formation cycle, no deviations will be found anymore.

Numerical simulations of complete movement patterns with Flow3D require a huge computational effort. For many starting positions, the net displacement has to be calculated over many drop formation cycles. Furthermore, in most cases off-axis positions have to be simulated to get a complete picture. This requires the use of a full 3D drop formation model in Flow3D. However, modeling off-axis bubbles results in extreme long CPU times with Flow3D because of the very fine grid size needed over a large area. An alternative numerical option is to use a boundary element method for the simulations of bubble dynamics [525–528] or to use a lumped parameter approach [529], where the equations for the individual forces are added to a Navier–Stokes solver for the flow in the nozzle.

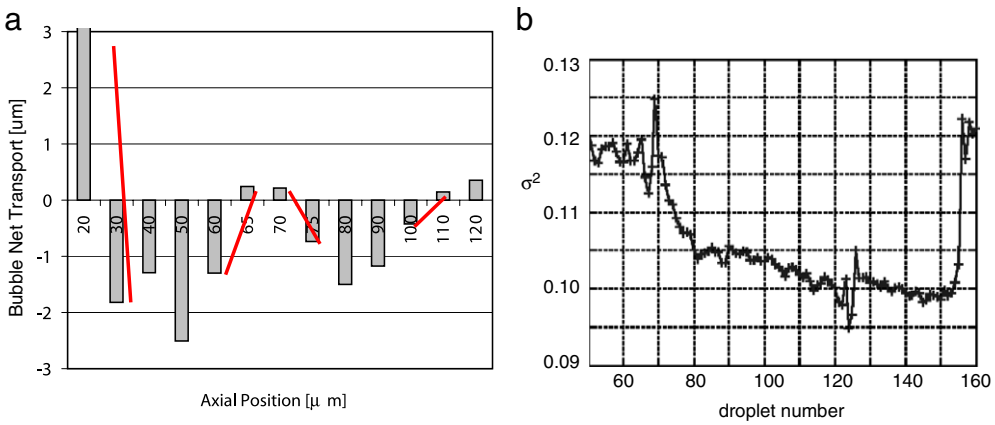

Fig. 96. (a) Simulation of the net bubble displacement after one drop formation cycle. Depending on the axial position the bubble with a diameter of 10 μm is moved outward or inward. At axial positions around 62.5 μm and 105 μm the bubble can be trapped. At axial positions between 0 μm and 20 μm the bubble is jetted out. (b) Measured amplitude of the Paint signal with distortions at drop formation cycles 70 and 124, air entrainment after drop formation cycle 70. The jetting out of a bubble is visible at drop formation cycle 155. This is a fast recovery mechanism, generated by the net displacement pattern inside the nozzle.

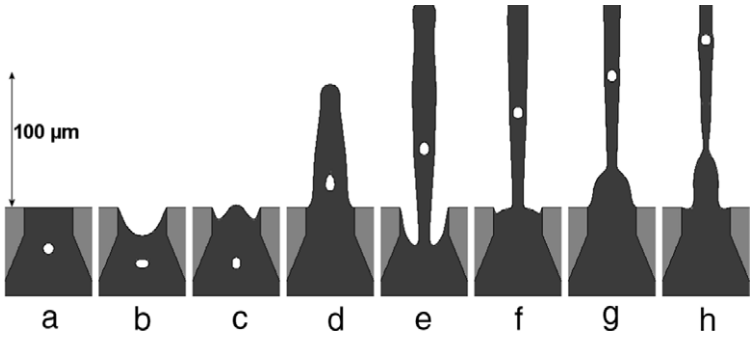

Fig. 97. Simulation with Flow3D of the jetting out of a bubble. The bubble has a diameter of 10 μm at an axial position 20 μm under the meniscus. The frames show the drop formation with the bubble at 0, 8, 16 . . . 56 μs after start of the actuation. The channel length is 8 mm and nozzle diameter is 32 μm.

6.5. The growing bubble

6.5.1. Rectified diffusion and dissolution

A bubble in an acoustic pressure field will grow by rectified diffusion when the acoustic pressure variations are strong enough [490,491,530,531]. At pressure maxima, air is squeezed out of the bubble, but this loss is overcompensated at the pressure minima when the bubble expands. This results in a net gas diffusion into the bubble. Rectified diffusion is a result of a surface effect and a shell effect, e.g. an expanded bubble can absorb more air because of its larger surface area and the higher concentration gradient of the dissolved air in the liquid around the bubble, which is compressed by the expanded bubble.

In the transparent head, the growth rates are optically measured. The measured net growth rate is 0.04 pl/ms when actuating at 10 kHz with a relative low driving amplitude for a drop speed of 1 m/s [485]. This is a net growth of 0.004 pl/cycle. With a very low non-jetting actuation amplitude at a repetition rate of 20 kHz, the net growth rate turns out to be much larger, 0.39 pl/ms or 0.02 pl/cycle [484]. This difference is an indication of an influence of the flow field around the bubble.

Just after the air entrainment, the bubble has a radius of 6 μm (0.9 pl) as measured visually with the transparent heads [484]. In the opaque reference printheads, the bubble size is estimated at 20 μm (4 pl) after 100 drop formation cycles at a repetition rate of 20 kHz with a nominal driving amplitude for a drop speed of 7 m/s, Section 6.3.2. With the assumption that the bubble size just after the air entrainment is the same as in the transparent heads, we get an estimation of the net growth rate of 0.62 pl/ms or 0.03 pl/cycle.

Without an acoustic pressure field, the bubble will dissolve. There is no net transport of ink and the ink around the bubble will saturate with dissolved air and the dissolution rate will be rather low. In the experiments without actuation with the transparent head [485], the dissolution rate of a 26 μm bubble is constant at 0.5 pl/s until the bubble is completely dissolved. This is shown in Fig. 98. The dissolution rate is 2 to 3 orders of magnitude slower than the growth by rectified diffusion. This can also be seen in the figure, where the bubble size increases much faster when the actuation is started.

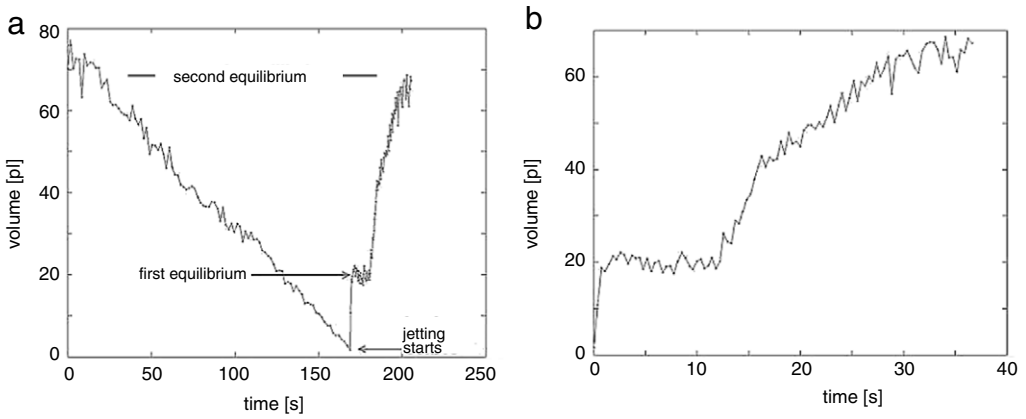

Fig. 98. Measured bubble size with actuation stopped at $t = 0$ s until $t = 165$ s. The dissolution rate is 0.46 pl/s. Then the actuator is turned on and droplets are jetted from the nozzle. The bubble size increases fast and saturates at an equilibrium size of 20 pl within a second. The equilibrium is broken after 12 s at the moment jetting breaks down. This is shown in the second figure, which shows only the first 40 s after the actuator is turned on again. Without drop formation the bubble size saturates at a much larger size of almost 70 pl.

The bubble size increases fast and saturates at an equilibrium size of 20 pl within a second. After 1000–5000 actuation cycles, the growth by rectified diffusion is compensated by the dissolution of the bubble. This equilibrium is broken at the moment when jetting breaks down. Without drop formation the bubble size saturates at a much larger size of almost 70 pl.

With jetting, the ink around the bubble will be continuously refreshed. The ink around the air bubble will be less saturated with dissolved air. This results in higher dissolution rates. The saturation size in the jetting situations will be smaller than in the non-jetting situations. Experimental data are only obtained with a transparent head. In the jetting situations the bubble size saturates always at a radius of 17–20 μm (20–33 pl) and in the non-jetting situations at a radius of 22–25 μm (50–70 pl) [484,485,483].

For very large bubbles, viscous forces and the surface tension forces are not strong enough anymore to limit the growth of bubble shape instabilities [492,532,533]. Shape instabilities will also limit the growth of bubbles, but are not likely to occur in the confined space of an ink channel and the observed bubbles sizes so far.

6.5.2. Influence of the actuation

When turning off the actuation for a specific time interval, the bubble will either be entirely dissolved or only partly. This can be seen in the Paint signal after the actuation is started again. If the time interval is long enough, the bubble will be dissolved completely, and the Paint signal is normal again. When the time interval is not long enough, the bubble is dissolved only partly. The bubble is still present and the modification of the Paint signal by the bubble will be still visible. The bubble will again grow by rectified diffusion until it saturates at its equilibrium size.

This is in fact what happens in the experiment with the regular head, where the growing and dissolution cannot be measured optically. A bubble is created during an actuation at a high drop repetition rate. Then the repetition rate is lowered stepwise and the Paint signal is monitored until a new equilibrium is established. By lowering the repetition rate the bubble will get more and more time to dissolve until it is dissolved completely before the next drop is jetted. The results of this experiment are shown in Fig. 99.

The analysis of the Paint signal is this figure is as follows. The current from the piezo element $I(t)$ during a time interval T is compared with a reference $I_0(t)$ (i.e. the signal without air bubbles) and the variance σ^2 of the difference is calculated:

$$\sigma^2 = \frac{1}{T}\int_0^T [I(t) - I_0(t)]^2 \, \mathrm{d}t. \tag{144}$$

At a low actuation amplitude, the rectified diffusion is slow and the bubble dissolves completely in a relatively short time. Lowering the repetition rate to 1–7 kHz is already sufficient at actuation amplitudes of 50%–80% of the nominal amplitude, which is 35 V for this printhead. At nominal actuation amplitude the repetition rate must be lowered to 200 Hz before the bubble dissolves completely.

Because of jetting out along with the drop, bubbles can disappear already at 400 Hz at the nominal driving amplitude. This is shown in Fig. 99b+c, where the variance of the difference between the Paint signal and the reference signal is depicted as a function of the decreasing repetition rate. In Fig. 99b, the decreasing deviation of the Paint signal is shown when a bubble dissolves completely between a repetition rate of 6 and 3.5 kHz. In the lower picture the decreasing deviation is shown when the bubble is jetted out at a repetition rate 285 Hz. The jetting out of the bubble is indicated by the stepwise decrease of the Paint signal to the normal value.

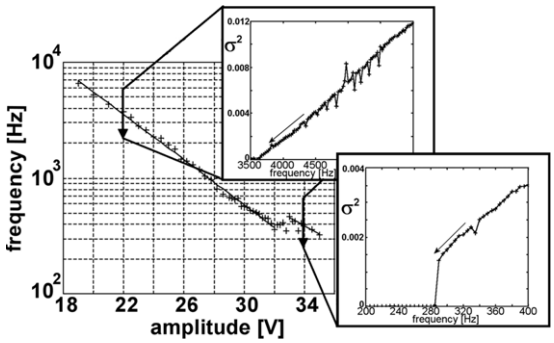

Fig. 99. (a) Measured drop repetition rate at which the air bubble, which is created at a repetition rate of 20 kHz, dissolves completely when lowering the repetition rate. At low driving amplitude the rectified diffusion is weak and the bubble dissolves already at a high repetition rate. At a high actuation amplitude, the repetition rate must be lower before the bubble disappears. (b) The decrease of the deviation of the Paint signal (as variance of the difference with the reference Paint signal). At 22 V the bubble dissolves and the deviation decreases gradually to zero (upper picture). (c) At 35 V the bubble can be jetted out and the deviation decreases stepwise to zero (lower picture).

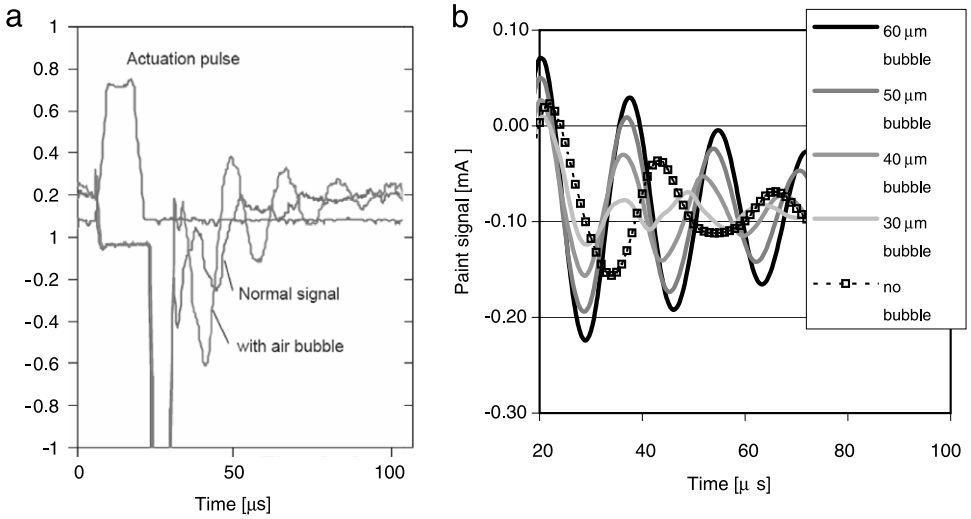

Fig. 100. Measured (a) and calculated (b) effect of a large air bubble on the Paint signal. A large air bubble acts as an open boundary condition for the pressure waves inside the channel. The acoustic properties of the channel shift to a $\frac{1}{2}\lambda$ resonator with a frequency of 65 kHz instead of 50 kHz. The frequency and also the amplitude of the acoustic pressure increase.

6.5.3. Impact on the actuation

At high repetition rates of 10–20 kHz and nominal actuation amplitudes, air bubbles grow during 1000–5000 actuation cycles to a bubble size of 50–70 pl. This volume is comparable to the total volume displacement by the acoustic pressure wave. The volume displacement of acoustic pressure field can be counteracted by the change in bubble size. This will change the acoustic properties of the channel completely.

Without an air bubble, the nozzle acts as a partial closed boundary condition for the pressure waves inside the ink channel, see Section 3.1.2. The channel will act almost as a $\frac{1}{4}\lambda$ resonator. A large bubble can counteract the pressure build-up. This results in a complete open reflection. The channel will act now as a $\frac{1}{2}\lambda$ resonator. The main resonance frequency will increase and also the amplitude of the pressure wave will increase. This is visible in the measured and in the calculated Paint signal, Fig. 100. The Paint signal is calculated with Flow3D and shows the same general trend. The simulations with the acoustic model can only show the effect of air bubbles with diameters of more then 30 μm, because the grid size in the nozzle is 3–4 μm.

To simulate the effect of a wide range of bubble sizes on the pressure waves inside an ink channel, the narrow-channel model is extended [514]. To keep the calculation time as low as possible, only cylindrical geometries are considered. The big advantage is that for the velocity profile in the frequency domain, see equation 3.22 for a rectangular cross-section, which has an open form, a much more efficient closed form equation can be used [534]:

$$B_{\mathrm{ch}} = 1 - 2\frac{J_1(kR_{\mathrm{ch}})}{kR_{\mathrm{ch}}J_0(kR_{\mathrm{ch}})} \tag{145}$$

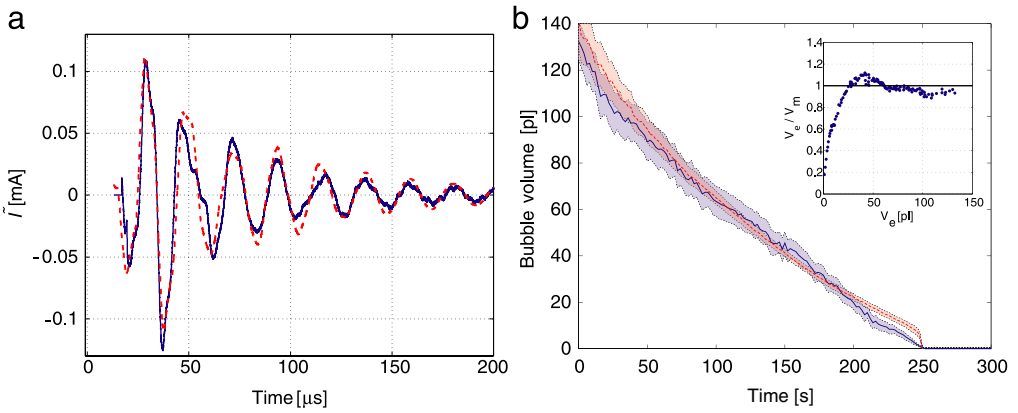

Fig. 101. (a) The measured and calculated Paint signal as difference between the disturbed and undisturbed signal from the new transparent head, measured after an actuation with a 454 driving waveform with an amplitude for a drop speed of 6 m/s with a bubble volume of 81 pl and 86 pl respectively. (b) The direct optically measured bubble volumes (blue) and the bubble volumes derived with the model from the acoustic Paint signal (dotted line). At small bubble volume, the difference becomes rather large, as shown in the insert.
Source: Taken from [535].

with J_n the n^{th} order Bessel function. A linear form of the Rayleigh–Plesset equation without acoustic and thermal damping in the frequency domain with only harmonic perturbations around the radius R_0 at ambient pressure is used:

$$-\omega^2 r = \frac{1}{\rho R_0}\left(-r\left(p_0 + \frac{2\gamma_l}{R_0} - p_v\right)\left(\frac{3\Gamma}{R_0}\right) + r\frac{2\gamma_l}{R_0^2} - \mathrm{i}\omega r\frac{4\eta}{R_0} - p_\infty\right) \tag{146}$$

with p_∞ the pressure at a large distance. Together with the continuity Eq. (141), the impact of an air bubble on the channel acoustics can be calculated accurately.

With a second printhead setup with a transparent section, but now with a regular electroformed 100 µm nickel nozzle plate, the dissolution of an air bubble is recorded optically, and during this process, the Paint signal is recorded by actuating and listening with a repetition rate of only 1 Hz [535]. This means there is practically no influence of the actuation on the dissolution of the air bubble. The next step was to match the measured Paint signals with calculated Paint signals. In Fig. 101a, an example of a measured and a calculated Paint signal is shown.

With the corresponding calculated Paint signal, the bubble size can also be determined theoretically. The result is shown in Fig. 101b. The acoustically derived bubble volumes deviate less than 12% from the directly optically measured bubble volumes, except for very small bubble volume, where the non-linear behavior of an air bubble starts to play a role [529].

When a distortion leads to air entrainment, the bubble radius is 10 µm after hundred drop formation cycles. The drop speed remains the same during the first 100 drop formation cycles in reference printhead. The bubble continues to grow and the drop speed starts to decrease with 1 m/s during the next 300 drop formation cycles [279].

In the experiments with the transparent head [485], jetting breaks down at a bubble radius of 19 µm. The bubble size is then of the same order as the volume displacement by the acoustic pressure field. The bubble counteracts the acoustic pressure variation. There is no driving force left for the ink movement in the nozzle and the drop formation comes to an end, as validated with acoustic simulations in Flow3D [130].

Bubbles can also disturb the drop formation directly. During the meniscus movement, the capillary pressure changes because of the changing curvature of the meniscus. The decreasing capillary pressure when a drop starts to neck results in a larger bubble size and thus in an increasing flow rate back into the nozzle with more increasing necking and more decreasing capillary pressure etc. [480]. However, in our fast drop formation process, the capillary pressure is too small with respect to the total pressures involved to see any influence of this effect.

6.6. Concluding remarks

In Section 5 the wetting of the nozzle plate was discussed. The wetting of the nozzle plate is also a source for jetting instability, the subject of this section. There is a critical layer thickness, which directly leads to air entrainment. The generation of air bubbles is the mechanism, which can lead to nozzle failure. The wetting layer plays also a role in combination with 20 µm small dirt particles, caught in the ink layer and transported towards the nozzle. The distortion by a dirt particle can be detected with an acoustic measurement, which uses the piezo elements also as sensors.

An entrapped air bubble will oscillate in the acoustic pressure field. The acoustic properties of the ink channel act as a filter for this measurement. Therefore the influence of small air bubbles is recorded as a signal with a frequency of 170 kHz. Primary and secondary Bjerknes forces, drag forces and many other forces result in movement patterns of the air bubble. The movement of an air bubble can result in jetting out, thus in a fast recovery. The movement of air bubbles can be visualized

with a special transparent head. Small air bubbles do not have a negative effect on the drop formation process. However, in the pressure field the bubbles will grow by rectified diffusion. The growth rate is much faster than the dissolution rate, the other recovery mechanism. The air bubbles grow in the pressure field to a size comparable with the drop size and the displacement by the acoustic pressure waves. The large air bubble will then counteract the pressure build-up and the drop formation process ceases completely.

7. Conclusions and outlook

In the past decades, inkjet technology has evolved into a technology which plays an important role in the graphical printing industry and in many emerging new industrial and medical applications. The piezo inkjet technology has unique capabilities due to its ability to deposit a wide variety of materials on various substrates in well defined patterns. To comply with the increasing and diverging requirements for today's inkjet technology, a fundamental understanding of the underlying processes is very important.

The physics behind the chain of processes comprise the two-way coupling from the electrical to the mechanical domain through the piezoelectric actuator, the coupling to the acoustic domain inside the ink channels, and the coupling to the fluid dynamic domain, the drop formation process. Furthermore, wetting of the nozzle plate and air bubbles can have a negative influence on the printhead performance. The five topics (actuation, channel acoustics, drop formation, wetting, and air bubbles) are the sections of this article.

The first step is the actuation, which implies the transformation of an electric voltage to a deformation of the ink channels. With a piezoelectric actuator design, an efficient transformation of electric potential to mechanical deformations can be realized. However, mechanical constraints can result in cross-talk effects, and resonances in the printhead structure can be excited. The deformations inside the printhead cannot be measured. Modeling with a commercial finite element code is a way to resolve this. The numerical modeling provides the design rules for an efficient actuation, without generating cross-talk effects. The drive towards smaller printheads with more nozzles will push the balance between the operational demands and the manufacturability to its limits. A printhead design is a compromise between the two aspects, the functional requirements and the cost of production. The numerical modeling is the tool to match the often conflicting requirements for the different parts in the printhead. This leads to an optimal printhead design within known constraints. New actuation principles can also be explored, before starting the expensive and time consuming manufacture of a new printhead design.

The deformation of the channel cross-section results in pressure waves. The pressure waves in the ink channels play a central role in the printhead operation, Section 3. They connect the electrical–mechanical domain of the actuator to the fluid dynamic domain in and outside of the nozzles. The traveling wave provides an efficient acoustic mechanism to generate the required pressure for the drop formation process, when the acoustic impedance of the nozzle matches the impedance of the ink channel. Also refill, the filling of the nozzle for the next drop formation cycle, is driven by the acoustic pressure waves. However, residual vibrations in the ink channel must be as low as possible before the next drop formation cycle starts. Another disturbing effect is acoustic cross-talk, which is the traveling of pressure waves through the reservoir towards neighboring channels. This can be avoided with a thin foil on the ink supply. Measurements are done with the laser-Doppler setup and an acoustic measurement, which uses the piezo elements also as sensors. Details of the phenomena inside the ink channels, such as local pressure variations, are available through modeling. The acousto-elastic interaction plays an important role in the "narrow-channel" model and acoustic modeling with Ansys provides the details of the interactions with the structure dynamics of the printhead. With fundamental knowledge of the acoustic properties, new printhead concepts can be developed successfully into an operating printhead that can fire billions of drops with constant size and velocity and a reliability as high as possible. The flow and pressure at the nozzle sets the boundary condition in the acoustic modeling. The pressure at the entrance of the nozzle is the coupling to the final stage of the printhead operation, the drop formation.

The application of the traveling wave principle leads to the drop formation process, which takes several tens of microseconds. The drop formation process is the subject of Section 4. Optical measurements and modeling provide the information, which leads to its better understanding. The tail break-off process is not affected by the actuation. Up to four satellite drop formation mechanisms can generate extra drops, which have a negative impact on the printing result. An important application is drop size modulation. With the knowledge of the drop formation process, eight drop size modulation techniques are identified. For the modeling of the free surface flow with surface tension and its impact on channel acoustics we use the commercial volume of fluid code Flow3D. The calculations provide also information on the meniscus retraction, the internal distribution of the speed of the ink, and the impact of the drop formation process on the pressure waves inside the ink channels. The Flow3D software is adapted to incorporate flexible walls, which was until recently not feasible in the standard code. We can predict the resulting drop properties accurately. This will be used to investigate the jetting behavior of many new liquids, which are used in different new applications. The critical material properties can be defined and this will be used as a guide for the development of new jetting materials. The jetting of smaller drops is more sensitive to the influence of the surrounding air. This is a new challenge for the modeling of the drop formation, requiring the development of new models.

The flow of ink on the nozzle plate is important. Wetting of the nozzle plate can influence the drop formation and the pressure waves inside the ink channels. The material interactions, which determine the wetting properties, are not known in detail for many materials. Therefore, an experimental study of the wetting phenomena is performed with a nickel nozzle

plate, Section 5. An actuated nozzle induces several flow patterns in an ink layer around the nozzle opening. When jetting, an induced air flow also influences the flow pattern around a nozzle. The nickel nozzle plate and the ink are in the complete wetting regime, except for a central band of (older) ink in the middle of the nozzle plate, which is in the partial wetting regime. The precursor film provides a means of communication between the central band of ink and the nozzles. Differences in surface tension of the ink result in Marangoni flow over the entire nozzle plate. The experimental observations can be understood with theories described in the literature. A numerical model, which can predict the wetting properties, is not available. The molecular interactions have to be taken into account. However, molecular modeling will only provide the interaction parameters. The parameters must be translated into a macroscopic flow pattern with additional models. This is closely related to the research on the interactions of ink with the media. The impact, spreading, and solidification of drops onto a solid surface is the final stage of the printing process. New applications require the depositions of various kinds of liquids on different types of substrates. Numerical modeling of the wetting phenomena, which can take into account the material interactions, would be a very powerful tool in the development of new inkjet applications. The final goal is to control the wetting properties of the nozzle plate. Either a uniform thin layer of ink or no ink layer at all will improve the jetting behavior of the printhead.

Wetting, without or with dirt particles, can also result in air entrainment. Air bubbles play an important role in the jetting stability. The theoretical and experimental research on the generation and the behavior of air bubbles and their impact on the printhead performance is the subject of Section 6. The resulting drop properties, the Paint measurement and visualization with a special transparent head are the experimental tools. Various aspects of the generation and the behavior of air bubbles are clarified. An air bubble oscillates in the acoustic pressure field. The oscillations can result in an enhanced drop speed and also the acoustic pressure waves are altered, as measured with Paint. Many forces act on an air bubble, which results in complicated movement patterns. The air bubble grows in the acoustic pressure field by rectified diffusion, with a growth rate much faster than the dissolution rate. Large air bubbles disturb the drop formation. The ultimate goal is to prevent the generation of air bubbles, or to control the behavior of air bubbles. Small air bubbles, which do not have a negative influence on the drop formation, can be manipulated with acoustic pressure waves. Either a controlled jetting out or a fast dissolution would remove an air bubble before the drop formation is disturbed. The air bubble also influences the acoustic properties of the ink channels. Therefore, a numerical model will have to incorporate a full two-way coupling between the dynamic behavior of an air bubble and the pressure waves inside the ink channels. Only with numerical modeling, the results of the acoustic measurements can be translated into bubble properties such as bubble radius, position, velocity, etc.

The requirements for the inkjet printing technology will increase. The near future demands for smaller drops, higher drop velocities, higher drop repetition rates, smaller printhead designs, a maximum jetting stability, complex fluids, etc. To meet these challenges, inkjet research will continue towards high integration densities in the printhead, zero cross-talk levels, zero variation of the resulting drop properties, and the elimination of nozzle failure. Also many new jetting materials will be explored, even the jetting of molten pure metals is one of the new applications. Material interactions will play an important role, which pushes the modeling to bridge the gap between continuum theories of our macro world and the molecular, particle based, theories of the micro- and nano-world. This makes the development of new inkjet technologies an exciting environment, where scientific research and industrial development can reinforce each other for many years to come.

Acknowledgements

The research, described in this thesis, is done at the R&D Department of Océ Technologies B.V., in close cooperation with the Physics of Fluids research group of the University of Twente. I want to thank all the people who have contributed to this research, especially my Océ colleagues, Hans Reinten, Marc van den Berg, and Wim de Zeeuw and from the University of Twente especially Prof.Dr. Detlef Lohse and PhD students Jos de Jong, Roger Jeurissen and Arjan van der Bos.

References

[1] J.F. Pond, Inkjet Technology and Product Development Strategies, Torrey Pines Research, 2000.
[2] J.A. Nollet, Recherches sur les causes particulieres des phenomenes electriques, Les Freres Guerin, Paris, 1749.
[3] J.A. Nollet, Mr. Watson, An examination of certain phenomena in electricity, Phil. Trans. 46 (1749) 368.
[4] C.L.M.H. Navier, Memoires sur les lois du movement des fluides, Mem. Acad. Sci. Inst. France 6 (1822) 389.
[5] L. Euler, Principes géneraux du mouvementdes fluides, Mem. Acad. Sci. Berlin 11 (1755) 274.
[6] C.L.M.H. Navier, Memoire sur les lois de l'áquilibre et du mouvement des corps solides élastiques, abstract presented to the Acadámie des Sciences on May 14, (1821). Bulletin des sciences par la Socitété Philomatique de Paris, 177, (1823). Published in Mémoires de l'Institut National 7, 375 (1827).
[7] G.G. Stokes, On the theories of the internal friction of fluids in motion, and of the equilibrium and motion of elastic solids, Trans. Cambr. Phil. Soc. IIX (1849) 287.
[8] J.A.F. Plateau, Mémoire sur les phénomenes que présente une masse liquide sans pesanteur, Mém. Acad. Sci. Bruxelles 16 (1843) 3.
[9] J.A.F. Plateau, Recherches expérimentales et théoriques sur les figures d'équilibre d'une mass liquide sans pesanteur, Mém. Acad. Sci. Bruxelles 23 (1849) 5.
[10] G. Hagen, Über die Auflösung flüssiger Cylinder in Tropfen, Verh. Preuss. Akad. Wissenschaften 281 (1849).
[11] J.A.F. Plateau, On the recent theories of the constitution of jets of liquid issuing from circular orifices, Phil. Mag. 12 (1856) 286.
[12] J.A.F. Plateau, Statique expérimentale et theorique des liquides soumis aux seules forces moléculaires, Gauthier Villars, 1873.
[13] Lord Rayleigh, On the instability of jets, Proc. Lond. Math. Soc. 10 (1878) 4.
[14] Lord Rayleigh, On the instability of a cylinder of viscous liquid under capillary force, Philosophical Magazine 34 (1892) 145.
[15] Lord Rayleigh, On the instability of cylindrical fluid surfaces, Philosophical Magazine 34 (207) (1892) 177.
[16] F. Savart, Memoire sur la constitution des veines liquides lancees par des orifices circulaires en mince parol, Ann. Chim. 53 (1833) 337.

[17] T. Tate, On the magnitude of a drop of liquid formed under different circumstances, Phil. Mag. 27 (1864) 176.
[18] L. da Vinci, Codex Leicester, Christie's London, 1508.
[19] E. Mariotte, Traité du mouvement des eaux et des autres corps fluides, E. Michallet, Paris, 1686.
[20] T. Young, Cohesion of fluids, Philos. Trans. R. Soc. Lond. 95 (1804) 65.
[21] P.S. Laplace, Mechanique celeste, supplement au X libre, Courier, Paris, 1805.
[22] J.C. Maxwell, On physical lines of forces, Phil. Mag. 25 (1861) 161.
[23] J.C. Maxwell, A dynamical theory of the electromagnetic field, Phil. Trans. 155 (1865) 459.
[24] J. Curie, P. Curie, Development, par pression, de l'electricite polarise dans les crystaux hemiednes et fares inclines, Comp. Rend. 91 (1880) 294.
[25] J. Brünahl, Physics of piezoelectric shear mode inkjet actuators, Ph.D. Thesis Royal Institute of Technology Stockholm, 2003.
[26] A. Ballato, Piezoelectricity: old effect, new thrust, IEEE Trans. Ultrason. Ferroelectr. Freq. Control 42 (1995) 916.
[27] G. Magnus, Hydraulische Untersuchungen, Ann. Phys. Chem. 106 (1859) 1.
[28] C.V. Boys, Soap-bubbles and the forces which mould them, Phil. Mag. 30 (1890) 248.
[29] Lord Rayleigh, Some applications of photography, Nature 44 (1891) 249.
[30] P. Lenard, Ueber die Schwingungen fallender Tropfen, Ann. Phys. Chem. 30 (1887) 209.
[31] Lord Rayleigh, Investigations in capillarity: the size of drops, Phil. Mag. 48 (1899) 321.
[32] E.A. Hauser, H.E. Edgerton, B.M. Holt, J.T. Cox, The application of the high-speed motion picture camera to research on the surface tension of liquids, J. Phys. Chem. 40 (1936) 972.
[33] H.E. Edgerton, E.A. Hauser, W.B. Tucker, Studies in drop formation as revealed by the high-speed motion camera, J. Phys. Chem. 41 (1937) 1029.
[34] C. Weber, Zum Zerfall eines Flüssigkeitsstrahles, Z. Angew. Math. Mech. 11 (1931) 11.
[35] C. Baldwin Sawyer, The use of rochelle salt crystals for electrical reproducers and microphones, Proc. R.E. 19 (11) (1931) 2020.
[36] F.J. Kampfhoefner, Ink jet printing, IEEE Trans. Electron Devices 19 (1972) 584.
[37] J.M. Schneider, C.D. Hendricks, Source of uniform-sized liquid droplets, Rev. Sci. Instrum. 35 (1964) 1349.
[38] M.R. Keeling, Ink jet printing, Phys. Technol. 12 (1981) 196.
[39] R.G. Sweet, High frequency recording with electrostatically deflected ink-jets, Rev. Sci. Instrum. 36 (1965) 131.
[40] W.L. Buehner, J.D. Hill, T.H. Williams, J.W. Woods, Application of ink-jet technology to a word processing output printer, IBM J. Res. Dev. 21 (1977) 1968.
[41] H.P. Le, Progress and trends in ink-jet printing technology, J. Imaging Sci. Technol. 42 (1998) 49.
[42] C.H. Hertz, S.I. Simonsson, Intensity modulation of ink-jet oscillographs, Med. Biol. Eng. 7 (1969) 337.
[43] J. Heinzl, Printing with ink droplets from a multi-nozzle device, in: Joseph Gaynor (Ed.), Advances in Non-Impact Printing Technologies for Computer Abd Office Applications, 1981, p. 1191.
[44] J. Zeleny, The electrical discharge from liquid points, and a hydrostatic method of measuring the electric intensity at their surfaces, Phys. Rev. 3 (1914) 69.
[45] G. Taylor, Disintegration of water drops in an electric field, Proc. R. Soc. Lond. A 280 (1964) 383.
[46] J.D. Jackson, Classical Electrodynamics, Wiley, New York, 1975.
[47] H. Li, T.C. Halsey, A.E. Lobkovsky, Singular shape of a fluid drop in an electric or magnetic field, Europhys. Lett. 27 (1994) 575.
[48] M. Clopeau, B. Prunet-Foch, Electrostatic spraying of liquids in cone-jet mode, J. Electrost. 22 (1989) 135.
[49] J. Fernández de la Mora, J. Navascués, F. Fernández, J. Rosell-Llompart, Generation of submicron monodisperse aerosols in electrosprays, J. Aerosol Sci. 21 (1990) S673.
[50] H. Kawamoto, S. Umezu, R. Koizumi, Fundamental investigation on electrostatic inkjet phenomena in pin-to-plate discharge systems, J. Imaging Sci. Technol. 49 (1) (2005) 19.
[51] A.G. Bailey, Electrostatic Spraying of Liquids, Wiley, New York, 1988.
[52] R.D. Carnahan, S.L. Hou, Ink jet technologies, IEEE Trans. Ind. Appl. 1A-13 (1977) 95.
[53] N. Bugdayci, D.B. Bogy, F.E. Talke, Axisymmetric motion of radially polarized piezoelectric cylinders used in ink jet printing, IBM J. Res. Dev. 27 (1983) 171.
[54] E. Stemme, S.G. Larsson, A piezoelectric capillary injector, IEEE Trans. Electron Devices 20 (1973) 14.
[55] E.L. Kyser, L.F. Collins, N. Herbert, Design of an impulse ink jet, J. Appl. Photogr. Eng. 7 (1981) 73.
[56] R. Beesom, The ABCs of HP's SPT (Scalable Printhead Technology), in: IMI 13th Annual European Inkjet Conference, 2005.
[57] M. Döring, Ink jet printing, Philips Tech. Rev. 40 (1982) 192.
[58] J. van Randeraat, R.E. Setterington, Piezoelectric Ceramics, Mullard Ltd, London, 1974.
[59] J. Perelaer, Microstructures prepared via inkjet printing and embossing techniques, Ph.D. Thesis, Eindhoven university of technology ISBN 978-90-386-1529-5, 2009.
[60] J.Y. Kim, V. Fakhfouri, C. Ingrosso, M. Striccol, M.L. Curri, J. Brugger, Drop on demand ink jet printing of functional materials: case stude of SU8 and NC based polymer nanocomposites, in: Proc. IS&T's NIP24 and DF2008, 2008, p. 269.
[61] J.C. Yang, W. Chien, M. King, W.L. Grosshandler, A simple piezo-electric droplet generator, Exp. Fluids 23 (1997) 445.
[62] C.Y. Lung, M.D. Barnes, N. Lermer, W.B. Whitten, J.M. Ramsey, Single-molecule analysis of ultradilute solutions with guided streams of 1-μm water droplets, Appl. Opt. 38 (1999) 1481.
[63] W.T. Berggren, M.S. Westphall, L.M. Smith, Single-pulse nano- electrospray ionization, Anal. Chem. 74 (2002) 3443.
[64] D.Y. Shin, P. Grassia, B. Derby, Oscillatory limited compressible fluid flow induced by the radialmotion of a thick-walled piezoelectric tube, J. Acoust. Soc. Am. 114 (2003) 1314.
[65] A.L. Brady, M. McDonald, S.N. Theriault, B. Smith, The impact of Silicon MEMS on the future of ink jet printhead design and performance, in: Proc. IS&T's NIP21, 2005, p. 264.
[66] J.M. Meacham, M.J. Varady, F.L. Degertekin, A.G. Fedorov, Droplet formation and ejection from a micromachined ultrasonic droplet generator: visualization and scaling, Phys. Fluids 17 (2005) 100605.
[67] M. Schoeppler, Diverging ink jet technologies and applications, in: Proc. IS&T's NIP22, 2006, p. 1.
[68] Chr. Williams, Ink-jet printers go beyond paper, Phys. World 19 (2006) 24.
[69] F.K. Chen, J.P. Lu, P.J. Su, C.F. Sung, Y.Z. Lee, J.W. Shiu, K. Cheng, Mask-free fabrication of color filter by an all ink-jet printing process, in: Proc. IS&T's NIP23, 2007, p. 852.
[70] J.F. Dijksman, P.C. Duineveld, M.J.J. Hack, A. Pierik, J. Rensen, J.E. Rubingh, I. Schram, M.M. Vernhout, Precision inkjet printing of polymer light emitting displays, J. Mater. Chem. 17 (2007) 511.
[71] R. Bennett, Precision industrial ink-jet printing technology for full color PLED display and TFT-LCD manufacturing, in: Proc. of the 3rd International Display Manufacturing Conference, Japan, 2003.
[72] E.I. Haskal, M. Buechel, J.F. Dijksman, Ink jet printing of passive matrix polymer light emitting displays, Proc. Int. Symp. Soc. Inf. Disp. 33 (2002) 776.
[73] T. Nakanishi, I. Ohtsu, M. Furuta, E. Ando, O. Nishimura, Direct MS/MS analysis of proteins blotted on membranes by a matrix-assisted laser desorption/ionization-quadrupole ion trap-time-of-flight tandem mass spectrometer, J. Proteome Research 4 (2005) 743.
[74] I. Ohtsu, T. Nakanisi, M. Furuta, E. Ando, O. Nishimura, Direct matrix-assisted laser desorption/ionization time-of-flight mass spectrometric identification of proteins on membrane detected by western blotting and lectin blotting, J. Proteome Research 4 (2005) 1391.
[75] H.S. Koo, M. Chen, P.C. Pan, LCD-based color filter films fabricated by a pigment-based photo resist inks and printing technology, Thin Solid Films 515 (2006) 896.
[76] C.W. Wang, W.C. Chen, K. Cheng, Y.Z. Lee, Inkjet patterning of UV-curable etching resist for flexible conductive circuit electrodes, in: Proc. IS&T's NIP23, 2007, p. 855.

[77] W. Voit, W. Zapka, A. Menzel, F. Mezger, T. Sutter, Inkjet printing of phase-change materials, in: Proc. IS&T's NIP24 and DF2008, 2008, p. 678.
[78] A. Lennon, R. Utama, A.H. Batillie, M. Lenio, N. Kuepper, S. Wenham, Inkjet method for forming openings to buried semiconductor layers of silicon solar cells, in: Proc. IS&T's NIP23, 2007, p. 882.
[79] J. Heilmann, The applications of inkjet for the printing of PDLC display cells, in: Proc. IS&T's NIP21, 2005, p. 48.
[80] A. Knobloch, Printed RFID labels based on polymer electronics, in: Proc. DF2005, 2005, p. 121.
[81] H.H. Lee, K.S. Chou, K.C. Huang, Inkjet printing of nanosized silver colloids, Nanotechnology 16 (10) (2005) 2436.
[82] J. Szczech, J. Zhang, K. Kalyan, P. Brazis, D. Gamota, Printed electronic using traditional graphic arts printing technologies, in: Proc. DF2005, 2005, p. 213.
[83] K.A. Bertness, C.M. Dodson, P.T. Blanchard, N.A. Sanford, R.S. Mills, Nanowire placement with ink jet heads, in: Proc. IS&T's NIP23, 2007, p. 836.
[84] S. Maekawa, T. Yoshida, S. Kinpara, H. Eguchi, Y. Ohta, Wide print-head with high-stiffness and control method drive, in: Proc. IS&T's NIP23, 2007, p. 310.
[85] V. Sanchez-Romaquera, Inkjet printing of metal-dielectric crossovers, in: Proc. IS&T's NIP23, 2007, p. 818.
[86] D.B. Wallace, W.R. Cox, D.J. Hayes, Direct write using inkjet techniques, in: Direct-Write Technologies for Rapid Prototyping Applications — Sensors, Electronics, and Integrated Power Sources, Academic Press, San Diego, 2002, pp. 177–227.
[87] W. Voit, W. Zapka, L. Belova, K.V. Rao, Application of inkjet technology for the deposition of magnetic nanoparticles to form micronscale structures, IEEE Proc. 150 (5) (2003) 252.
[88] W.Y. Yeong, C.K. Chua, K.F. Leong, M. Chandrasekaran, 3D inkjet printing for rapid prototyping: development of a physical model, in: Proc. Int. Conf. Materials Processing for Properties and Performance, 2004, p. 379.
[89] W.R. Cox, T. Chen, D. Ussery, D.J. Hayes, J.A. Tatum, D.L. MacFarlane, Microjetted lenslet triplet fibers, Opt. Commun. 123 (1996) 492.
[90] T. Chen, W.R. Cox, D. Lenhard, D.J. Hayes, Microjet printing of high precision microlens array for packaging of fiber-optic components, Proc. SPIE Optoelectronic Interconnects, Integr. Circuits Packag. 4652 (2002) 136.
[91] A. Bietsch, J. Zhang, M. Hegner, H.P. Lang, C. Gerber, Rapid functionalization of cantilever array sensors by inkjet printing, Nanotechnology 15 (8) (2004) 873.
[92] O.A. Basaran, Small-scale free surface flows with breakup: Drop formation and emerging applications, AIChE J. 48 (2002) 1842.
[93] M. Chee, R. Yang, E. Hubbell, A. Berno, X.C. Huang, D. Stern, J. Winkler, D.J. Lockhart, M.S. Morris, S.P.A. Fodor, Accessing genetic information with high-density DNA arrays, Science 274 (1996) 610.
[94] P. James, R. Papen, Nanolitre dispensing: a new innovation in robotic liquid handling, Drug Discov. Today 3 (9) (1998) 429.
[95] P.W. Cooley, D.B. Wallace, B.V. Antohe, Application of inkjet printing technology to biomems and microfluidic systems, Proc. SPIE Conference Microfluidics BioMEMS 4560 (2001) 177.
[96] D. Radulescu, et al., 3d printing of biological materials for drug delivery and tissue engineering applications, in: Proc. DF2005, 2005, p. 96.
[97] J.C. Charter, R.M. Alvis, S.B. Brown, K.C. Langry, T.S. Wilson, M.T. McBride, M.L. Myrick, W.R. Cox, M.E. Grove, B.W. Colston, Fabricating optical fiber imaging sensors using inkjet printing technology: A pH sensor proof-of-concept, Biosens. Bioelectron. 21 (7) (2006) 1359.
[98] R.R. Allen, Inkjet printing with large pagewide arrays: issues and challenges, in: Proc. IS&T's NIP12, 1996, p. 43.
[99] D. Bruijnen, R. van de Molengraft, A. Draad, T. Heeren, Productivity analysis of a scanning inkjet printer, in: Proc. IS&T's NIP21, 2005, p. 129.
[100] Y. Zhou, The application of piezo ink jet technology to high-speed dod single pass printing, in: Proc. IS&T's NIP16, 2000, p. 28.
[101] C. Tracy, D. Grose, The quality plan for the manufacture of an ink jet print assembly with 1536 jets, in: Proc. IS&T's NIP18, 2002, p. 157.
[102] A. Hirota, N. Aichi, S. Ishikura, Development of drop-on-demand piezoelectric line inkjet printhead, in: Proc. IS&T's NIP21, 2005, p. 257.
[103] Y. Zhou, Recent advances in highle durable piezoelectric inkjet print head technology, in: Proc. IS&T's NIP20, 2004, p. 855.
[104] D.B. Bogy, F.E. Talke, Experimental and theoretical study of wave propagation phenomena in drop-on-demand ink jet devices, IBM J. Res. Dev. 28 (1984) 314.
[105] S. Allaman, G. Desie, Improved ink jet in situ visualization strategies, in: Proc. IS&T's NIP20, 2004, p. 383.
[106] H. Dong, W.W. Carr, J.F. Morris, Visualization of drop-on-demand inkjet: drop formation and deposition, Rev. Sci. Instrum. 77 (2006) 085101.
[107] A. Kalaaji, B. Lopez, P. Attané, A. Soucemarianadin, Breakup length of forced liquid jets, Phys. Fluids 15 (2003) 2469.
[108] H. Gonzáles, F.J. Garcia, Comment on "Breakup length of forced liquid jets" [Phys. Fluids 15, 2469 (2003)], Phys. Fluids 18 (2006) 019101.
[109] P. Attané, Response to "Comment on 'Breakup length of forced liquid jet'" [Phys. Fluids 18, 019101 (2006)], Phys. Fluids 18 (2006) 019102.
[110] R.C. Ritter, N.R. Zinner, A.M. Sterling, Analysis of drop intervals in jets modelling obstruction of the urinary tract, Phys. Med. Biol. 19 (1974) 161.
[111] S.X. Quian, J.B. Snow, H.M. Tzeng, R.K. Chang, Lasing droplets: highlighting the liquid–air interface by laser emission, Science 231 (1986) 486.
[112] N. Vágó, A. Spiegel, P. Couty, F.R. Wagner, B. Richerzhagen, New technique for high-speed microjet breakup analysis, Exp. Fluids 35 (2003) 303.
[113] M. Doring, Inkjet printing, Philips Tech. Rev. 40 (1982) 192.
[114] G.D. Martin, S.D. Hoath, I.M. Hutchings, Inkjet printing — the physics of manipulating liquid jets and drops, J. Phys. Conf. Series 105 (2008) 012001.
[115] C. Rembe, S.A.D. Wiesche, M. Beuten, E.P. Hofer, Investigations of nonreproducible phenomena in thermal inkjets with high-speed cine photomicrography, J. Imaging Sci. Technol. 43 (1999) 325.
[116] Y. Zhou, Measurement of the displacement of a shear mode piezoelectric transducer using laser Doppler vibrometer, in: Proc. IS&T's NIP14, 1998, p. 23.
[117] K.S. Kwon, Inkjet status monitoring using meniscus measurement, in: Proc. IS&T's NIP24 and DF2008, 2008, p. 134.
[118] M. vd Velden, J.W. Spronck, R.H. Munnig Schmidt, J. Wei, P.M. Sarro, Characterization of a nozzle-integrated capacitive sensor for microfluidic jet systems, in: Proc. IEEE Sensors2007, 2007, p. 1241.
[119] J. Wei, M. vd Velden, P.M. Sarro, Fabrication of vertical electrodes on channel sidewall for picoliter liquid measurement, in: Proc. Transducers2007, 2007, p. 1613.
[120] C.D. Meinhart, H. Zhang, The flow structure inside a microfabricated inkjet printhead, J. MEMS Systems 9 (2000) 67.
[121] J.W. Waanders, Piezoelectric Ceramics. Properties and Applications, Philips Components, Eindhoven, 1991.
[122] M.B. Groot Wassink, Inkjet printhead performance enhancement by feedforward input design based on two-port modeling, Ph.D. Thesis, Delft University of Technology, 2007.
[123] J. de Jong, Air entrapment in piezo inkjet printing, Ph.D. Thesis, University of Twente, 2007.
[124] R.W. Longman, Iterative learning control and repetitive control for engineering practice, Int. J. Control 73 (2000) 930.
[125] S. Arimoto, S. Kawamura, F. Miyazaki, Bettering operation of robots by learning, J. Rob. Sys. 1 (1984) 123.
[126] K.L. Moore, Iterative learning control: an expository overview, Appl. Comp. Contr. Signal Proc. Circuits 1 (1998) 151.
[127] H.M.A. Wijshoff, Free surface flow and acousto-elastic interaction in piezo inkjet, in: Proc. NSTI Nanotech2004, 2, 2004, p. 215.
[128] H.M.A. Wijshoff, Better printheads via simulation: flow3D helped double the speed of a new wide-format printer without sacrificing quality, Desktop Engineering 13 (2) (2007) 46.
[129] J.A. Palesko, D.H. Bernstein, Modeling MEMS and NEMS, Chapman & Hall CRC Press, 2003.
[130] H.M.A. Wijshoff, Structure- and fluid-dynamics in piezo inkjet printheads, Ph.D. Thesis, University of Twente, 2008.
[131] M. Gad-el-Hak, The fluid mechanics of microdevices — the Freeman scholar lecture, J. Fluids Eng. 121 (1999) 5.
[132] Y. Zhou, A coupled field analysis of an ink jet printhead with shear mode piezo transducer, in: Proc. IS&T's NIP13, 1997, p. 809.
[133] H. Seitz, J. Heinzl, Modelling of a microfluidic device with piezoelectric actuators, J. MicroMech. & Microeng. 14 (2004) 1140.
[134] H. Wijshoff, Color flow through the years, in: P.J. Waterman (Ed.), First Pass CFD Analysis Part 2, Desktop Engineering, 2008, p. 1.
[135] B. Jaffe, W.R. Cook, H. Jaffe, Piezoelectric Ceramics, Academic Press, London, 1971.
[136] K. Uchino, Recent topics of ceramic actuators: how to develop new ceramic devices, Ferroelectrics 91 (1989) 281.
[137] K. Uchino, Piezoelectric Actuator and Ultrasonic Motors, Kluwer Academic Publishers, Boston, MA, 1997.
[138] R. Guo, L.E. Cross, S.E. Park, B. Noheda, D.E. Cox, S. Shirane, Origin of the high piezoelectric response in $PbZr_{1-x}Ti_xO_3$, Phys. Rev. Lett. 84 (2000) 5423.

[139] B. Noheda, J.A. Gonzalo, R. Guo, S.E. Park, L.E. Cross, D.E. Cox, G. Shirane, The monoclinic phase in PZT: new light on morphotropic phase boundaries, in: R. Cohen (Ed.), Fundamental Physics of Ferroelectrics, AIP, New York, 2000.
[140] B. Noheda, J.A. Gonzalo, L.E. Cross, R. Guo, S.E. Park, D.E. Cox, G. Shirane, A tetragonal-to-monoclinic phase transition in a ferroelectric perovskite: the structure of $PbZr_{1-x}Ti_xO_3$, Phys. Rev. B 61 (2000) 8687.
[141] B. Noheda, D.E. Cox, Bridging phases at the morphotropic boundaries of lead-oxide solid solutions, Phase Trans. 79 (2006) 5.
[142] K.D. Wolf, Electromechanical energy conversion in asymmetric piezoelectric bending actuators, Ph.D. Thesis, Technical University Darmstadt, 2000.
[143] B.A. Auld, Wave propagation and resonance in piezoelectric materials, J. Acoust. Soc. Am. 70 (6) (1981) 1577.
[144] G.A. Maugin, Continuum Mechanics of Electromagnetic Solids, Elsevier, New York, 1988.
[145] H. Reiss, Methods of Thermodynamics, Dover Publications, 1996.
[146] F. Jona, G. Shirane, Ferroelectric Crystals, Dover Publications, New York, 1993.
[147] D. Cibis, K. Krüger, Optimization of a DoD printhead signal for the ink-jetting of conductive circuits, in: Proc. IS&T's NIP24 and DF2008, 2008, p. 125.
[148] T. Takahashi, Adaptability of piezoelectric inkjet head, in: Proc. IS&T's NIP17, 2001, p. 323.
[149] T. Chen, Piezoelectric inkjet print head technology for Precision Dispensing Application, in: Proc. DF2006, 2006, 66.
[150] Q.M. Wang, L.E. Cross, Performance analysis of piezoelectric cantilever bending actuators, Ferroelectrics 215 (1998) 187.
[151] C. Germano, Flexure mode piezoelectric transducers, IEEE Trans. Audio Electroacoust. 19 (1) (1971) 6.
[152] K. Uchino, M. Yoshizaki, K. Kasai, H. Yamamura, N. Sakai, H. Asakura, Monomorph actuators using semiconductive ferroelectrics, Jap. J. App. Phys. 26 (7) (1987) 1046.
[153] R.J. Roark, W.C. Young, Formulas for Stress and Strain, McGraw-Hill, New York, 1975.
[154] H.T. Banks, R.C. Smith, Y. Wang, The modeling of piezoceramic path interactions with shells, plates and beams, Quartely Appl. Mech. 53 (2) (1995) 353.
[155] A. Donoso, O. Sigmund, Optimization of piezoelectric bimorph actuators with active damping for static and dynamic loads, Struct. Multidisc. Optim. 38 (2) (2008) 171.
[156] X. Li, W.Y. Shih, I.A. Aksay, Electromechanical behavior of PZT-brass unimorphs, J. Am. Ceram. Soc. 82 (7) (1999) 1733.
[157] S.A.N. Prasad, Two-port electroacoustic model of a piezoelectric composite circular plate, Ph.D. Thesis, University of Florida, 2002.
[158] Y. Ohba, M. Miyauchi, T. Tsurumi, M. Daimon, Analysis of bending displacement of lead zirconate titanate thin film synthesized by hydrothermal method, Jap. J. Appl. Phys. 32 (1993) 4095.
[159] D.E. Glumac, T.G. Cooney, L.F. Francis, W.P. Robbins, A theoretical examination of MEMS microactuators responses with an emphasis on materials and fabrication, Mat. Res. Soc. Symp. Proc. 360 (1995) 407.
[160] J.M. Torres, R.S. Dhariwal, Electric field breakdown at micrometer separations, Nanotechnology 10 (1999) 102.
[161] M. Usui, H. Hayashi, K. Hara, T. Kitahara, Development of the new MACH (MACH with MLCips, in: Proc. IS&T's NIP12, 1996, p. 50.
[162] T. Mimura, S. Sakai, Micro piezoelectric head technology of color inkjet printer, in: Proc. DPP2001, 2001, p. 230.
[163] J. Zhang, New developments in Epson's inkjet head technology, in: Proc. IS&T's NIP21, 2005, p. 269.
[164] M. Okumura, T. Takahashi, Novel micro piezo technology for ink jet printhead, in: Proc. IS&T's NIP23, 2007, p. 314.
[165] K. Ozawa, T. Usui, K. Ida, H. Takahashi, S. Sakai, Development of a femtoliter piezo ink-jet head for high resolution printing, in: Proc. IS&T's NIP23, 2007, p. 898.
[166] R.F. Burr, D.A. Tence, S.S. Berger, Multiple dot size fluidics for phase change piezoelectric ink jets, in: Proc. IS&T's NIP12, 1996, p. 12.
[167] S.S. Berger, R.F. Burr, J.D. Padgett, D.A. Tence, Ink manifold design of phase change piezoelectric ink jets, in: Proc. IS&T's NIP13, 1997, p. 703.
[168] Chr. Menzel, A. Bibl, P. Hoisington, MEMS solutions for precision micro-fluidic dispensing applications, in: Proc. IS&T's NIP20, 2004, p. 169.
[169] M. McDonald, Scaling of piezoelectric drop-on-demand jets for high resolution applications, in: Proc. IS&T's NIP12, 1996, p. 53.
[170] H.J. Manning, R.A. Harvey, Xaar greyscale technology, in: Proc. IS&T's NIP15, 1999, p. 35.
[171] W. Zapka, R. Kaack, W. Voit, M. Schulz, M. Zimmermann, L. Levin, W. Ahlemeir, Large drop volumes from Xaar-type inkjet printheads, in: Proc. IS&T's NIP18, 2002, p. 161.
[172] B.V. Antohe, D.B. Wallace, Acoustic phenomena in a demand-mode piezoelectric inkjet printer, in: Proc. IS&T's NIP17, 2001, p. 885.
[173] H.F. Tiersten, Linear Piezoelectric Plate Vibrations, Plenum Press, New York, 1969.
[174] R. Holland, E.P. Eer Nisse, Design of Resonant Piezoelectric Devices, The M.I.T Press, Cambridge, MA, 1969.
[175] A.F. Ulitko, Theory of electromechanical energy conversion in nonuniformly deformable piezoeceramics, Sovjet Appl. Mech. (1977) 1055.
[176] M. McDonald, Crosstalk study of a high speed shear mode piezo inkjet printhead, in: Proc. IS&T's NIP15, 1999, p. 40.
[177] G. Beurer, J. Kretschmer, Function and performance of a shear mode piezo printhead, in: Proc. IS&T's NIP13, 1997, p. 621.
[178] J. Kretschmer, G. Beurer, Design parameters of a shear mode piezo printhead for a given resolution, in: Proc. IS&T's NIP13, 1997, p. 626.
[179] H. Tijdeman, On the propagation of sound waves in cylindrical tubes, J. Sound Vib. 39 (1975) 1.
[180] M. Beltman, P. van de Hoogt, R. Spiering, H. Tijdeman, Air loads on a rigid plate oscillating normal to a fixed surface, J. Sound Vib. 206 (1997) 217.
[181] W.M. Beltman, Viscothermal wave propagation including acousto-elastic interaction I Theory, J. Sound Vib. 227 (3) (1999) 555.
[182] W.M. Beltman, Viscothermal wave propagation including acousto-elastic interaction II Applications, J. Sound Vib. 227 (3) (1999) 587.
[183] J. Kergomard, M. Bruneau, A.M. Bruneau, Ph. Herzog, On the propagation constant of higher modes in a cylindrical waveguide, J. Sound Vib. 126 (1988) 178.
[184] M. Beltman, Viscothermal wave propagation including acousto-elastic interaction, Ph.D. Thesis, University of Twente, Enschede, 1998.
[185] M.J.H. Fox, P.N. Whitton, The damping of structural vibrations by thin gas films, J. Sound Vib. 73 (1980) 279.
[186] M. Bruneau, Ph. Herzog, J. Kergomard, J.D. Polack, General formulation of the dispersion equation in bounded visco-thermal fluid, Wave Motion 11 (1989) 441.
[187] L.C. Chow, R.J. Pinnington, Practical industrial method of increasing structural damping in machinery I Squeeze film damping with air, J. Sound Vib. 118 (1987) 123.
[188] L.C. Chow, R.J. Pinnington, Practical industrial method of increasing structural damping in machinery I Squeeze film damping with liquids, J. Sound Vib. 128 (1989) 333.
[189] T. Onsay, Effects of layer thickness on the vibration response of a plate-fluid layer system, J. Sound Vib. 162 (1993) 231.
[190] T. Basten, Noise reduction by viscothermal acousto elastic interaction in double wall panels, Ph.D. Thesis, University of Twente, Enschede, 2001.
[191] T.G.H. Basten, P.J.M. van der Hoogt, R.M.E.J. Spiering, H. Tijdeman, On the acousto-elastic behaviour of double-wall panels with viscothermal air layer, J. Sound Vib. 243 (4) (2001) 699.
[192] C. Karra, A. Akrout, L. Hammami, M. Haddar, Simulation of viscothermal losses on the acoustic behaviour of a thin fluid layer enclosed between two oscillating plates, Build. Acoust. 13 (2) (2006) 113.
[193] G. Plantier, M. Bruneau, Heat conduction effects on the acoustic response of a membrane separated by a very thin air film from a backing electrode, J. Acoustique 3 (1990) 243.
[194] M. Bruneau, A.M. Bruneau, P. Hamery, An improved approach to modelling the behaviour of thin fluid films trapped between a vibrating membrane and a backing wall surrounded by a reservoir at the periphery, Acoustica 1 (1993) 227.
[195] C. Karra, M. Ben Tahar, Effects of entropic wave in vibro-acoustic interaction between vibrating membrane and thin fluid layer, Flow Turb. & Comb. 61 (1) (1999) 179.
[196] J.B. Mehl, Acoustic resonance frequencies of deformed spherical resonators, J. Acoust. Soc. Am. 71 (1982) 1109.
[197] J.B. Mehl, Acoustic resonance frequencies of deformed spherical resonators II, J. Acoust. Soc. Am. 79 (1986) 278.
[198] M. Moldover, Gas filled spherical resonators: theory and experiment, J. Acoust. Soc. Am. 79 (1986) 253.
[199] H. Tillema, Noise reduction of rotating machinery by viscoelastic bearing supports, Ph.D. Thesis, University of Twente, Enschede, 2003.
[200] T. Veijola, M. Torowski, Compact damping models for laterally moving microstructures with gas-rarefaction effects, J. MEMS 10 (2) (2001) 263.

[201] T. Veijola, Compact model for squeezed film dampers with inertial and rarefied gas effects, J. Micromech. Microeng. 14 (7) (2004) 1109.
[202] T. Veijola, A two-port model for wave propagation along a long circular microchannel, Microfluidics Nanofluidics 3 (3) (2007) 359.
[203] S. Makarov, S. Ochmann, Non-linear and thermoviscous phenomena in acoustics part I, Acustica 83 (1997) 197.
[204] G.K. Batchelor, An Introduction to Fluid Dynamics, Cambridge University Press, 1970.
[205] M. Moser, Damping of structure born sound by the viscosity of a layer between two plates, Acustica 46 (1980) 210.
[206] N. Rott, Damped and thermally driven acoustic oscillations, J. Appl. Math. Phys. 20 (1969) 230.
[207] F. van der Eerden, Noise reduction with coupled prismatic tubes, Ph.D. Thesis, University of Twente, Enschede, 2000.
[208] B.V. Antohe, D.B. Wallace, Acoustic phenomena in a demand-mode piezoelectric inkjet printer, J. Imaging Sci. Technol. 46 (2002) 409.
[209] E. Manini, A. Scardovi, Experimental evaluation of reflections of acoustic waves in DOD systems, in: SPSE Proc. Adv. N.I.P Techn, 1982, p. 1092.
[210] T. Kitahara, Ink jet head with multi-layer piezoelectric actuator, in: Proc. IS&T's NIP11, 1995, p. 346.
[211] D.D. Darling, Frequency dependent fluidic inductance and resistance in inkjet passages, in: Proc. IS&T's NIP20, 2004, p. 877.
[212] M. Hannink, Acoustic resonators for the reduction of sound radiation and transmission, Ph.D. Thesis, University of Twente, Enschede, 2007.
[213] H. Fukumoto, H. Fukumoto, Y. Yokoyama, K. Endo, Y. Fujii, M. Takeda, Variable droplet size molten solder ejection tool for microelectronics packaging, in: Proc. IS&T's DF2006, 2006, p. 38.
[214] S. Sakai, Dynamics of Piezoelectric Inkjet Printing Systems, in: Proc. IS&T's NIP26, 2000, p. 15.
[215] J.F. Dijksman, Hydrodynamics of small tubular pumps, J. Fluid. Mech. 139 (1984) 173.
[216] F.T. Trouton, On the coefficient of viscous traction and its relation to that of viscosity, Proc. R. Soc. Lond. 77 (1906) 426.
[217] J.M. Cittadino, E. Mendes, A. Soucemarianadin, A tool for monitoring piezoelectric micro-pumps, in: Proc. IS&T's NIP21, 2005, p. 278.
[218] J.Q. Feng, A general fluid dynamic analysis of drop ejection in drop-on-demand ink jet devices, J. Imaging Sci. Technol. 46 (2002) 398.
[219] P.G. de Gennes, F. Brochard-Wyart, D. Quéré, Capillarity and Wetting Phenomena, Springer, Berlin, 2003.
[220] H.H. Chen, M.P. Brenner, The optimal faucet, Phys. Rev. Lett. 92 (2004) 166106.
[221] P. McGuinness, W. Drenckhan, D. Weaire, The optimal tap: three-dimensional nozzle design, J. Phys. D 38 (2005) 3382.
[222] A. Badea, C. Carasso, G. Panasenko, A model of a homogenized cavity corresponding to a multinozzle droplet generator for continuous inkjet printers, Num. Meth. PDE 14 (1998) 6.
[223] A. Badea, A. Capatina, C. Carasso, Optimization of a multinozzle inkjet printer, Comp. Methods Appl. Mech. Eng. 190 (2001) 18.
[224] K.F. Teng, A mathematical model of impulse jet mechanism, Math. Comp. Modeling 11 (1988) 751.
[225] K.F. Teng, R.W. Vest, Mathematical models of inkjet printing in thick-film hybrid microelectronics, Appl. Math. Modeling 12 (2) (1988) 182.
[226] P. Koltay, C. Moosmann, C. Litterst, W. Streule, R. Zengerle, Simulation of a micro dispenser using lumped models, Proc. MSM2002 1 (2002) 170.
[227] S.D. Howkins, C.A. Willis, H. Nishimura, Cross-talk reduction by smart delay firing, in: Proc. IS&T's NIP20, 2004, p. 845.
[228] M. McDonald, Continuous improvement: performance and reliability in shear mode piezo ink jet printing, in: Proc. IS&T's NIP17, 2001, p. 287.
[229] T.G. Duby, Performance improvements for commercial piezo printhead, in: Proc. IS&T's NIP17, 2001, p. 328.
[230] R.F. Burr, S.S. Berger, D.A. Tence, Overview of phase change piezoelectric ink jet fluids modeling and design, Proc. ASME 239 (1996) 545.
[231] W. Letendre, S. Halwawala, B. Smith, Jetting and imaging performance of the M-300/10 Jet Module, in: Proc. IS&T's NIP22, 2006, p. 83.
[232] J. Sumurel, Digital printing of bioinks, in: Proc. DF2006, 2006, p. 93.
[233] N. Noto, T. Torii, S. Suematsu, K. Kugai, A new compact high resolution solid ink print head and its application to a plate making printer, in: Proc. IS&T's NIP14, 1998, p. 50.
[234] J.F. Dijksman, Hydro-acoustics of piezoelectric driven ink-jet print heads, Flow Turb. Comb. 61 (1999) 211.
[235] S. Ishikura, M. Hibi, Acoustic analysis on oscillatory behaviors in piezoelectric inkjet printhead, in: Proc. IS&T's NIP22, 2006, p. 75.
[236] S. Ishikura, A. Matsumoto, Improvement in printing throughput for piezoelectric line inkjet printhead, in: Proc. IS&T's NIP23, 2007, p. 305.
[237] J. Kretschmer, C. Tille, I. Ederer, A drop-on-demand inkjet printhead for a wide range of applications, in: Proc. IS&T's NIP14, 1998, p. 31.
[238] S.C. Jung, H.S. Jang, J.H. Lee, B.S. Kim, K.G. Jang, A study on the improvement of the performance in injet head, in: Proc. IS&T's NIP15, 1999, p. 15.
[239] S.S. Berger, G. Recktenwald, Development of an improved model for piezo-electric driven ink jets, in: Proc. IS&'s NIP19, 2003, p. 323.
[240] A. Olsson, G. Stemme, E. Stemme, A valve-less planar fluid pump with two pump chambers, Sensors Actuators A 46–47 (1995) 549.
[241] R. Scardovelli, S. Zaleski, Direct numerical simulation of free-surface and interfacial flow, Ann. Rev. Fluid Mech. 31 (1999) 567.
[242] G. Tryggvason, B. Bunner, A. Esmaeeli, D. Juric, N. Al-Rawahi, W. Tauber, J. Han, S. Nas, Y.J. Jan, A front tracking method for the computations of multiphase flow, J. Comput. Phys. 169 (2001) 708.
[243] C.W. Hirt, J.L. Cook, T.D. Butler, A Lagrangian method fot calculating the dynamics of an incompressible fluid with free surface, J. Comput. Phys. 5 (1970) 103.
[244] C.W. Hirt, A.A. Amsden, J.L. Cook, An arbitrary Lagrangian–Eulerian computing method for all flow speeds, J. Comput. Phys. 14 (1974) 227.
[245] B.J. Ramaswamy, Numerical simulation of unsteady viscous free surface flow, J. Comput. Phys. 90 (1990) 396.
[246] E.D. Wilkes, S.D. Phillips, O.A. Basaran, Computational and experimental analysis of the dynamics of drop formation, Phys. Fluids 11 (1999) 3577.
[247] B. Ambravaneswaran, H.J. Subramani, S.D. Phillips, O.A. Basaran, Dripping-jetting transitions in a dripping faucet, Phys. Rev. Lett. 93 (3) (2004) 034501-1.
[248] M.S. Longuet-Higgins, E.D. Cokelet, The deformation of steep surface waves on water. I. A numerical method of computation, Phil. Trans. R. Soc. Lond. A 350 (1976) 1.
[249] M. Tjahjadi, H.A. Stone, J.M. Ottino, Satellite and subsatellite formation in capillary breakup, J. Fluid Mech. 243 (1992) 297.
[250] N.N. Mansour, T.S. Lundgren, Satellite formation in capillary jet breakup, Phys. Fluids A2 (1990) 1141.
[251] R.F. Day, E.J. Hinch, J.R. Lister, Self-similar capillary pinchoff of an inviscis liquid, Phys. Rev. Lett. 80 (1998) 704.
[252] R.M. Schulkes, The evolution and bifurcation of a pendant drop, J. Fluid Mech. 278 (1994) 83.
[253] D.F. Zhang, H.A. Stone, Drop formation in viscous flow at a vertically capillary tube, Phys. Fluids 9 (1997) 2234.
[254] W. von Ohnesorge, Die Bildung und die Auflösung flüssiger Strahlen, Z. Angew. Math. Mech. 16 (1936) 355.
[255] V. Bergeron, D. Bonn, J.Y. Martin, L. Vovelle, Impact and retraction of viscoelastic drops, Nature 405 (2000) 772.
[256] A. Haenlein, Über den zerfall eines flüssigkeitsstrahls, Forch. Geb. Ing. 2 (1931) 139.
[257] J. Eggers, Nonlinear dynamics and breakup of free-surface flows, Rev. Mod. Phys. 69 (1997) 865.
[258] D. Jang, D. Kim, J. Moon, Influence of fluid physical properties on inkjet printability, Langmuir 25 (2009) 2629.
[259] F.H. Harlow, J.E. Welch, Numerical calculation of time-dependent viscous incompressible flow, Phys. Fluids 8 (1965) 2182.
[260] J.E. Fromm, Numerical calculation of fluid dynamics of drop on demand jets, IBM J. Res. Dev. 28 (1984) 322.
[261] O.A. Basaran, Nonlinear oscillations of viscous liquid drops, J. Fluid Mech. 241 (1992) 169.
[262] X. Zhang, O.A. Basaran, An experimental study of dynamics of drop formation, Phys. Fluids 7 (1995) 1184.
[263] J.R. Richards, A.N. Beris, A.M. Lenhoff, Drop formation in liquid–liquid systems before and after jetting, Phys. Fluids 7 (11) (1995) 2617.
[264] J. Li, Y.Y. Renardy, M. Renardy, Numerical simulation of breakup of a viscous drop in simple shear flow with a volume-of-fluid method, Phys. Fluids 12 (2000) 269.
[265] J.L. Summers, H.M. Thompson, P.H. Gaskell, Flow structure and transfer jets in a contra-rotating rigid roll coating system, Theor. Comput. Fluid Dyn. 17 (3) (2004) 189.
[266] J.T. Yeh, A VOF-FEM and coupled inkjet simulation, in: Proc. ASME Fluid Eng. Div., 2001, p. 1.
[267] H.C. Wu, H.J. Lin, W.S. Hwang, A numerical study of the effect of operating parameters on drop formation in a squeeze mode inkjet device, Modeling and Sim. Mat. Sci. Eng. 13 (2005) 17.
[268] C.L. Chiu, J.Ch. Yang, C.H. Liu, J.P. Hu, Ch.C. Chang, The numerical study on size effects of the inkjet print head, in: Proc. IS&T's NIP17, 2001, p. 319.
[269] S. Osher, J.A. Sethian, Fronts propagating with curvature-dependent speed: algorithms based on Hamilton-Jacobi formulations, J. Comput. Phys. 79 (1988) 12.
[270] M. Sussman, P. Smereka, S.J. Osher, A level set approach to computing solutions to incompressible two-phase flow, J. Comput. Phys. 113 (1994) 146.

[271] S.J. Osher, R.P. Fedkiw, Level set methods: an overview and some recent results, J. Comput. Phys. 169 (2001) 463.
[272] J.A. Sethian, Evolution, implementation, and application of level set and fast marching methods for advancing fronts, J. Comput. Phys. 169 (2001) 503.
[273] M. Sussman, E.G. Pucket, A coupled level set and volume-of-fluid method for computing 3D and axisymmetric incompressible two-phase flows, J. Comput. Phys. 162 (2000) 301.
[274] J.D. Yu, S. Sakai, Piezo inkjet simulations using the finite difference level set method and equivalent circuit, in: Proc. IS&T's NIP19, 2003, p. 319.
[275] J.D. Yu, S. Sakai, J. Sethian, A coupled quadrilateral grid level set projection method applied to ink jet simulations, J. Comput. Phys. 206 (2005) 1.
[276] H.M.A. Wijshoff, Modeling the drop formation process in inkjet printheads, in: Flow3D News spring2007, 2007, p. 4. Flow3D is CFD software developed by Flow Science Inc., Santa Fe, New Mexico.
[277] B.D. Nichols, C.W. Hirt, Numerical simulations of BWR vent-clearing hydrodynamics, Nucl. Sci. Eng. 73 (1980) 196.
[278] C.W. Hirt, B.D. Nichols, Volume of Fluid (VOF) method for the dynamics of free boundaries, J. Comput. Phys. 39 (1981) 201.
[279] J. de Jong, H. Reinten, M. van den Berg, H. Wijshoff, M. Versluis, G. de Bruin, D. Lohse, Air entrapment in piezo-driven inkjet printheads, J. Acoust. Soc. Am. 120 (2006) 1257.
[280] X. Zhang, Dynamics of growth and breakup of pendant drops into air, J. Colloid Interface Sci. 212 (1999) 107.
[281] D.H. Michael, P.G. Williams, The equilibrium and stability of axi-symmetric pendant drops, Proc. R. Soc. Lond. A 351 (1976) 117.
[282] Chr. Clanet, J.C. Lasheras, Transition from dripping to jetting, J. Fluid. Mech. 383 (1999) 307.
[283] D.M. Henderson, W.G. Pritchard, L.B. Smolka, On the pinch-off of a pendant drop of viscous liquid, Phys. Fluids 11 (1997) 3188.
[284] E. Tyler, F. Watkin, Experiments with capillary jets, Phil. Mag. 14 (1932) 849.
[285] P. Martien, S.C. Pope, P.L. Scott, R.S. Shaw, The chaotic behavior of the leaky faucet, Phys. Lett. 110A (1985) 399.
[286] A. d'Innocenzo, L. Renna, Dripping faucet, Int. J. Theor. Phys 35 (1996) 941.
[287] M.C. Pugh, M.J. Shelley, Singularity formation in models of thin jets with surface tension, Comm. Pure Appl. Math. 51 (1998) 733.
[288] J. Lowengrub, L. Truskinovski, Quasi-compressible Cahn–Hilliard fluids and topological transitions, Proc. R. Soc. Lond. A 454 (1998) 2617.
[289] J. Eggers, Drop formation — an overview, Z. Angew. Math. Mech. 85 (6) (2005) 400.
[290] W.E. Ranz, Some experiments on orifice sprays, Can. J. Chem. Eng. 36 (1958) 175.
[291] H.A. Stone, B.J. Bentley, L.G. Leal, An experimental study of transient effects in the breakup of viscous drops, J. Fluid Mech. 173 (1986) 131.
[292] R. Clift, J.R. Grace, M.E. Weber, Bubbles, Drops, and Particles, Academic Press, New York, 1978.
[293] W.J. Heideger, M.W. Wright, Liquid extraction during drop formation: effect of formation time, AIChE J. 32 (1986) 1372.
[294] E.F. Goedde, M.C. Yuen, Experiments on liquid jet instability, J. Fluid Mech. 40 (1970) 495.
[295] A.U. Chen, P.K. Notz, O.A. Basaran, Computational and experimental analysis of pinch-off and scaling, Phys. Rev. Lett. 88 (2002) 174501.
[296] F. Lugli, F. Zerbetto, Atomistic simulation of drop-on-demand inkjet dynamics, J. Phys. Chem. C 112 (29)) (2008) 19616.
[297] H.M.A. Wijshoff, Drop formation mechanisms in piezo-acoustic inkjet, Proc. Nanotech2007 3 (2007) 448.
[298] T.A. Kowalewski, On the separation of droplets from a liquid jet, Fluid Dyn. Res. 17 (1996) 121.
[299] J.R. Lister, H.A. Stone, Capillary breakup of a viscous thread surrounded by another viscous fluid, Phys. Fluids 10 (1998) 2758.
[300] S.P. Lin, Breakup of Liquid Sheets and Jets, Cambridge University Press, 2003.
[301] O.B. Fawehinmi, P.H. Gaskell, P.K. Jimack, N. Kapur, H.M. Thompson, A combined experimental and computational fluid dynamics analysis of the dynamics of drop formation, Proc. ImechE 219C (2005) 1.
[302] J.U. Brackbill, D.B. Kothe, C. Zemach, A continuum method for modelling surface tension, J. Comput. Phys 100 (1992) 335.
[303] J. Eggers, T.F. Dupont, Drop formation in a one-dimensional approximation of the Navier–Stokes equation, J. Fluid Mech. 161 (1994) 205.
[304] D.T. Papageorgiou, On the breakup of viscous liquid threads, Phys. Fluids 7 (1995) 1529.
[305] O. Reynolds, On the theory of lubrication and its application to Mr. Beauchamp tower's experiments, including an experimental determination of the viscosity of olive oil, Phil. Trans. R. Soc. 177 (1886) 157.
[306] L.E. Cram, A numerical model of drop formation, in: J. Noye, C. Fletcher (Eds.), Computational Techniques and Applications, Elsevier, 1984.
[307] B. Ambravaneswaran, S.D. Phillips, O.A. Basaran, Theoretical analysis of a dripping faucet, Phys. Rev. Lett. 85 (2000) 5332.
[308] O.E. Yildrim, Q. Xu, O.A. Basaran, Analysis of the drop weight method, Phys. Fluids 17 (2000) 062107.
[309] N. Fuchikami, S. Ishioka, K. Kiyono, Simulation of a dripping faucet, J. Phys. Soc. Japan 68 (1999) 1185.
[310] P. Coullet, L. Mahadevan, C.S. Riera, Hydrodynamical models for the chaotic dripping faucet, J. Fluid Mech. 526 (2005) 1.
[311] H.J. Subramani, H.K. Yeoh, T. Suryo, Q. Xu, B. Abravaneswaran, O.A. Basaran, Simplicity and complexity in a dripping faucet, Phys. Fluids 18 (2006) 032106.
[312] F.D. Landau, E.M. Lifshitz, Fluid Mechanics, Pergamon, Oxford, 1984.
[313] S.E. Bechtel, M.G. Forest, K.J. Lin, Closure to all orders in 1-D models for slender viscoelastic free jets: an integrated theory for axisymmetric, torsionless flows, Stab. Appl. Anal. Cont. Media 2 (1992) 59.
[314] B. Ambravaneswaran, E.D. Wilkes, O.A. Basaran, Drop formation from a capillary tube: comparison of one-dimensional and two-dimensional analyses and occurrence of satellite drops, Phys. Fluids 14 (2002) 2606.
[315] P. Koltay, C. Moosmann, C. Litterst, W. Streule, B. Birkenmeier, R. Zengerle, Modeling free jet ejection on a system level — an approach for microfluidics, Proc. MSM2002 1 (2002) 112.
[316] D.Y. Shin, P. Grassia, B. Derby, Numerical and experimental comparisons of mass transport rate in a piezoelectric drop-on-demand inkjet print head, Int. J. Mat. Sci. 46 (2004) 181.
[317] D.Y. Shin, P. Grassia, B. Derby, Oscillatory incompressible fluid flow in a tapered tube with a free surface in an inkjet printhead, J. Fluids Eng. 127 (1) (2005) 98.
[318] R.E. Goldstein, A.I. Pesci, M.J. Shelley, Topology transitions and singularities in viscous flows, Phys. Rev. Lett. 70 (1993) 3043.
[319] P. Constantin, T.F. Dupont, R.E. Goldstein, L.P. Kadanoff, M.J. Shelley, S.M. Zhou, Droplet breakup in a model of the Hele–Shaw cell, Phys. Rev. E47 (1993) 4169.
[320] B. Lafaurie, C. Nardone, R. Scardovelli, S. Zaleski, G. Zanetti, Modeling merging and fragmentation in multiphase flow with SURFER, J. Comput. Phys. 113 (1994) 134.
[321] J. Eggers, Theory of drop formation, Phys. Fluids 7 (5) (1995) 941.
[322] J. Eggers, Breakup and coalescence of free surface flows, in: S. Yip (Ed.), Handbook of Materials Modeling, Springer, 2005.
[323] J. Eggers, E. Villermaux, Physics of liquid jets, Rep. Progr. Phys. 71 (2008) 036601.
[324] J.B. Keller, M.J. Miksis, Surface tension driven flows, SIAM J. Appl. Math. 43 (1983) 268.
[325] L. Ting, J.B. Keller, Slender jets and thin sheets with surface tension, SIAM J. Appl. Math. 50 (1990) 1533.
[326] I.M. Hutchings, G.D. Martin, S.D. Hoath, R.H. Morgan, Proc. IS&T's NIP22, 2006, p. 91.
[327] J. Eggers, Universal pinching of 3D axisymmetric free-surface flow, Phys. Rev. Lett. 71 (1993) 3458.
[328] M.P. Brenner, J.R. Lister, H.A. Stone, Pinching threads, singularities and the number 0.0304. . ., Phys. Fluids 8 (1996) 2827.
[329] D.H. Peregrine, G. Shoker, A. Symon, The bifurcation of liquid bridges, J. Fluid. Mech. 212 (1990) 25.
[330] J. Eggers, Singularities in droplet pinching with vanishing viscosity, SIAM J. Appl. Mech. 60 (2000) 1997.
[331] M.P. Brenner, J. Eggers, K. Joseph, S.R. Nagel, X.D. Shi, Breakdown of scaling in droplet fission at high Reynolds number, Phys. Fluids 9 (1997) 1573.
[332] Y.C. Chen, P.H. Steen, Dynamics of inviscid capillary breakup: collapse and pinch-off of a film bridge, J. Fluid Mech. 341 (1997) 245.
[333] P.K. Notz, A.U. Chen, O.A. Basaran, Satellite drops: unexpected dynamics and change of scaling during pinch-off, Phys. Fluid 13 (2001) 549.
[334] G. Barenblatt, Similarity, Self-Similarity and Intermediate Asymptotics, Cambridge University Press, 1996.
[335] A. Rothert, R. Richter, I. Rehberg, Transition from symmetric to asymmetric scaling function before drop pinch-off, Phys. Rev. Lett. 87 (2001) 084501.
[336] A. Rothert, R. Richter, I. Rehberg, Formation of a drop: viscosity dependence of three flow regimes, New J. Phys. 5 (2003) 59.
[337] P. Pierron, S. Alleman, A. Soucemarianadin, Dynamics of jetted liquid filaments, in: Proc. IS&T's NIP17, 2001, p. 308.

[338] B. Lopez, D. Vadillo, P. Pierron, A. Soucemarianadin, Transient phenomena during drop formation in DOD printing, in: Proc. IS&T's NIP18, 2002, p. 170.
[339] R.E. Grundy, Local similarity solutions for the initial-value problem in non-linear diffusion, IMA J. Appl. Math. 30 (1983) 209.
[340] A. Sierou, J. Lister, Self-similar recoil of inviscid drops, Phys. Fluids 16 (2004) 1379.
[341] I.N. Milosevic, E.K. Longmire, Pinch-off modes and satellite formation in liquid–liquid jet systems, Int. J. Multiphase Flow 28 (2002) 1853.
[342] G.I. Taylor, The dynamics of thin sheets of fluid III: disintegration of fluid sheets, Proc. R. Soc. Lond. A253 (1959) 313.
[343] P. Pierron, E. Auboussier, C. Schlemer, N. Galley, Influence of transducer control in dod printing, in: Proc. IS&T's NIP16, 2000, p. 56.
[344] M.P. Brenner, X.D. Shi, S.R. Nagel, Iterated instabilities during droplet fission, Phys. Rev. Lett. 73 (1994) 3391.
[345] X.D. Shi, M.P. Brenner, S.R. Nagel, A cascade of structure in a drop falling from a faucet, Science 265 (1994) 219.
[346] S. Kawano, Molecular dynamics of rupture phenomena in a liquid thread, Phys. Rev. E58 (1998) 4468.
[347] M. Moseler, U. Landman, Formation, stability, and breakup of nanojets, Science 289 (2000) 1165.
[348] J. Eggers, Dynamics of liquid nanojets, Phys. Rev. Lett. 89 (2002) 084502.
[349] Y. Hennequin, D.G.A.L. Aarts, J.H. van der Wiel, G. Wegdam, J. Eggers, H.N.W. Lekkerkerker, D. Bonn, Drop formation by thermal fluctuations at an ultralow surface tension, Phys. Rev. Lett. 97 (2006) 244503.
[350] H. Schlichting, Boundary layer theory, McGraw-Hill Book Company, New York, 1979.
[351] H.C. Lee, Boundary layer around a liquid jet, IBM J. Res. Dev. 21 (1977) 48.
[352] B. Beulen, J. de Jong, H. Reinten, M. van den Berg, H. Wijshoff, R. van Dongen, Flows on the nozzle plate of an inkjet printhead, Exp. Fluids 42 (2007) 217.
[353] D.B. Bogy, Drop formation in a circular liquid jet, Ann. Rev. Fluid Mech. 11 (1979) 207.
[354] D. Gonzales-Mendizabal, C. Olivera-Fuentes, J.M. Guzman, Hydrodynamics of laminar liquid jets. Experimental study and comarison with two models, Chem. Eng. Comm. 56 (1987) 117.
[355] K. Adachi, K. Tagashira, Y. Banda, H. Machida, N. Yoshioka, Steady laminar round jets pf a viscous liquid falling vertically in the atmosphere, AIChE J. 36 (1990) 738.
[356] J.R. Richards, A.N. Beris, A.M. Lenhoff, Steady laminar flow of liquid–liquid jets at high Reynolds numbers, Phys. Fluids A5 (1993) 1703.
[357] S. Chandrasekhar, Hydrodynamic and Hydromagnetic Stability, Dover, 1961.
[358] D.F. Rutland, G.J. Jameson, Theoretical prediction of the sizes of drops formed in the breakup of capillary jets, Chem. Eng. Sci. 25 (1970) 1689.
[359] X. Zhang, Dynamics of drop formation in viscous flows, Chem. Eng. Sci. 54 (1999) 1759.
[360] Y. Renardi, M. Renardi, PROST: a parabolic reconstruction of surface tension for the volume-of-fluid method, J. Comput. Phys. 183 (2002) 400.
[361] J.H. Hilbing, S.D. Heister, Droplet size control in liquid jet breakup, Phys. Fluids 8 (1996) 1574.
[362] K.C. Chaudhary, T. Maxworthy, The nonlinear capillary instability of a liquid jet. Part 3. Experiments on satellite drop formation and control, J. Fluid Mech. 96 (1980) 287.
[363] J.H. Xing, A. Boguslawsky, A. Soucemarianadin, P. Atten, P. Attané, Experimental investigation of capillary instability: results on jet stimulated by pressure modulations, Exp. Fluids 20 (1996) 302.
[364] S. Tomotika, Breaking up of a drop of viscous liquid immersed in another viscous fluid which is extending at a uniform rate, Proc. R. Soc. Lond. A 153 (1936) 302.
[365] H.A. Stone, Dynamics of drop deformation and breakup in viscous fluids, Ann. Rev. Fluid Mech. 26 (1994) 65.
[366] B.S. Cheong, T. Howes, Capillary jet instability under the influence of gravity, Chem. Eng. Sci. 59 (2004) 2145.
[367] B.S. Cheong, T. Howes, Effect of initial disturbance amplitude in gravity affected jet break-up, Chem. Eng. Sci. 60 (2005) 3715.
[368] E. Trinh, T.G. Wang, Large amplitude free and driven drop-shape oscillations: experimental observations, J. Fuid. Mech. 122 (1982) 315.
[369] J. Eggers, J.R. Lister, H.A. Stone, Coalescence of liquid drops, J. Fluid Mech. 401 (1999) 293.
[370] L. Duchemin, J. Eggers, C. Josserand, Inviscid coalescence of drops, J. Fluid Mech. 487 (2003) 167.
[371] N. Ashgriz, J.Y. Poo, Coalescence and separation in binary collisions of liquid drops, J. Fluid. Mech. 221 (1990) 183.
[372] H. Dong, W.W. Carr, J.F. Morris, An experimental study of drop-on-demand drop formation, Phys. Fluids 18 (2006) 072102.
[373] Q. Xu, O.A. Basaran, Computational analysis of drop-on-demand drop formation, Phys. Fluids 19 (2007) 102111.
[374] B. Barbet, P. Atten, A. Soucemarianadin, Capillary instability of a jet induced by surface tension modulations, in: Proc. IS&T's NIP13, 1997, p. 604.
[375] H.F. Bauer, Free liquid surface response induced by fluctuations of thermal Marangoni convection, AIAA J. 22 (1984) 421.
[376] F. Mashayek, N. Ashgriz, Nonlinear instability of liquid jets with thermocapillarity, J. Fluid Mech. 283 (1995) 97.
[377] N. Ashgriz, F. Mashayek, Temperal analysis of capillary jet breakup, J. Fluid Mech. 291 (1995) 163.
[378] E.P. Furlani, C.N. Delemetter, J.M. Chwalek, D.P. Trauernicht, Surface tension induced instability of viscous liquid jets, Proc. MSM2001 1 (2001) 186.
[379] E.P. Furlani, Temporal instability of viscous liquid microjets with spatially varying surface tension, J. Physics A 38 (2005) 263.
[380] E.P. Furlani, Thermal modulation and instability of Newtonian liquid microjets, Proc. Nanotech2005 1 (2005) 668.
[381] O.E. Yildrim, O.A. Basaran, Deformation and breakup of stretching bridges of Newtonian and shear-thinning liquids: comparison of one- and two-dimensional models, Chem. Eng. Sci. 56 (2001) 211.
[382] P. Coussot, F. Gaulard, Gravity flow instability of viscoplastic materials: the "ketchup drip", Phys. Rev. E 72 (2005) 031409.
[383] L.G. Fel, Y. Zimmels, Plateau instability of a liquid crystalline cylinder in a magnetic field, J. Colloid Interface Sci. 288 (2005) 553.
[384] R.E. Grisenti, J.P. Toennies, Cryogenic micro-jet source for orthotropic beams of ultra-large superfluid helium droplets, Phys. Rev. Lett. 90 (2003) 234501.
[385] M.E. Möbius, Clustering instability in a freely falling granular jet, Phys. Rev. E 74 (2006) 051304.
[386] B.J. de Gans, P.C. Duineveld, U.S. Schubert, Inkjet printing of polymers: state of the art and future developments, Adv. Mater. 16 (2004) 203.
[387] M. Goldin, J. Yerushalmi, R. Pfeffer, R. Shinnar, Breakup of a laminar capillary jet of a viscoelastic fluid, J. Fluid Mech. 38 (1969) 689.
[388] Y. Christanti, L.M. Walker, Effect of fluid relaxation time on jet breakup due to a forced disturbance of polymer solutions, J. Rheol. 47 (2002) 733.
[389] R.B. Bird, R.C. Armstrong, O. Hassager, Dynamics of Polymeric Liquids I. Fluid Mechanics II. Kinetic Theory, Wiley, New York, 1987.
[390] S.L. Goren, M. Gottlieb, Surface-tension-driven breakup of viscoelastic liquid threads, J. Fluid Mech. 120 (1982) 245.
[391] Y. Amarouchene, D. Bonn, J. Meunier, H. Kellay, Inhibition of a finite time singularity in droplet fission of polymeric fluids, Phys. Rev. Lett. 86 (2001) 3558.
[392] D. Xu, V. Sanchez-Romaguera, S. Barbosa, W. Travis, J.S. de Wit, P. Swan, S.G. Yeates, Inkjet printing of polymer solutions in the semi-dilute regime, in: Proc. IS&T's NIP23, 2007, p. 104.
[393] S. Hoath, G. Martin, T. Tuladhar, M. Mackley, I. Hutchings, Links between fluid rheology and drop-on-demand jetting and printability, in: Proc. IS&T's NIP24 and DF2008, 2008, p. 130.
[394] R.J. Furbank, J.F. Morris, Droplet formation from particulate suspensions, in: Proc. IS&T's NIP17, 2001, p. 304.
[395] R.J. Furbank, J.F. Morris, An experimental study of particle effects on drop formation, Phys. Fluids 16 (2004) 1777.
[396] W.T. Pimbley, H.C. Lee, Satellite droplet formation in a liquid jet, IBM J. Res. Dev. 21 (1977) 21.
[397] J.B. Keller, S.I. Rubinow, Y.O. Tu, Spatial instability of a jet, Phys. Fluids 16 (1973) 2052.
[398] W.T. Pimbley, Drop formation from a liquid jet: a linear one-dimensional analysis considered as a boundary value problem, IBM J. Res. Dev. 20 (1976) 148.
[399] M.C. Yuen, Non-linear capillary instability of a liquid jet, J. Fluid Mech. 33 (1968) 151.
[400] H.C. Lee, Drop formation in a liquid jet, IBM J. Res. Dev. 18 (1974) 364.
[401] R.M. Schulkes, The contraction of liquid filaments, J. Fluid Mech. 309 (1996) 277.
[402] P.K. Notz, O.A. Basaran, Dynamics and breakup of a contracting liquid filament, J. Fluid Mech. 512 (2004) 223.
[403] H. Dong, Drop on demand inkjet drop formation and depositions, Ph.D. Thesis, Georgia Institute of Technology, 2006.
[404] D.M. Henderson, H. Segur, L.B. Smolka, M. Wadati, The motion of a falling liquid filament, Phys. Fluids 12 (2000) 550.
[405] H.M.A. Wijshoff, Manipulating drop formation in piezo acoustic inkjet, in: Proc. IS&T's NIP22, 2006, p. 79.

[406] M. Kanaya, MACH for pigment ink, in: Proc. IS&T's NIP19, 2003, p. 280.
[407] D.D. Darling, Driving waveforms to reduce voltage requirements of inkjets, in: Proc. IS&T's NIP20, 2004, p. 851.
[408] M. McDonald, New advances in piezoelectric carbon printhead technology, in: Proc. IS&T's NIP24 and DF2008, 2008, p. 117.
[409] M. Usui, et al., The development of pigment ink for plain paper, in: Proc. IS&T's NIP18, 2002, p. 369.
[410] M.B. Groot Wassink, Enabling higher fetting frequencies for inkjet printheads using Iterative Learning Control, in: Proc. IS&T's NIP 21, 2005, p. 273.
[411] R.L. Adams, The printing technology of the Tektronix Phaser340, in: Proc. IS&T's NIP11, 1995, p. 280.
[412] R.L. Adams, The printing technology of the Tektronix Phaser340, J. Imaging Sci. Technol. 40 (1996) 383.
[413] A.U. Chen, O. Basaran, A new method for significantly reducing drop radius without reducing nozzle radius in drop-on-demand drop production, Phys. Fluids 14 (2002) L1.
[414] Chr. Rensch, Creation of small microdrops, MicroFab Technical note, October, 2006.
[415] C. Huh, L.E. Scriven, Hydrodynamic model of steady movement of a solid/liquid/fluid contact line, J. Colloid Interface Sci. 35 (1971) 85.
[416] L. Pisman, Y. Pomeau, Disjoining potential and spreading of thin liquid layers in the diffuse-interface model coupled to hydrodynamics, Phys. Rev. E 62 (2000) 2480.
[417] C. Poulard, A.A. Cazabat, Spontaneous spreading of nematic liquid crystals, Langmuir 21 (2005) 6270.
[418] E. Stemme, G. Stemme, A valveless diffuser/nozzle-based fluid pump, Sensors Actuators A39 (1993) 159.
[419] J. de Jong, H. Reinten, H. Wijshoff, M. van den Berg, K. Delescen, R. van Dongen, F. Mugele, M. Versluis, D. Lohse, Marangoni flow on an inkjet nozzle plate, Appl. Phys. Lett. 91 (2007) 204102.
[420] A. Oron, S.H. Davis, S.G. Bankoff, Long-scale evolution of thin liquid films, Rev. Mod. Phys. 69 (3) (1997) 931.
[421] P.G. de Gennes, Wetting: statics and dynamics, Rev. Mod. Phys. 57 (3) (1985) 827.
[422] I. Yildrim, Surface free energie characterization of powders, Ph.D. Thesis, Virginia State University, 2001.
[423] C. Bauer, S. Dietrich, Wetting films on chemically heterogeneous substrates, Phys. Rev. E 60 (1999) 6919.
[424] A. Moosavi, M. Rauscher, S. Dietrich, Motion of nanodroplets near edges and wedges, Phys. Rev. Lett. 97 (2006) 236101.
[425] A. Moosavi, A. Rauscher, S. Dietrich, Motion of nanodroplets near chemical heterogeneities, Langmuir 24 (2008) 734.
[426] P. Swain, R. Lipowsky, Contact angle on heterogeneous surfaces: a new look at Cassie and Wenzel's laws, Langmuir 14 (1998) 6772.
[427] J. Bico, U. Thiele, D. Quéré, Wetting on textured surfaces, Colloids Surf. A 206 (2002) 41.
[428] F.F. Joanny, P.G. de Gennes, Model for contact angle hysteresis, J. Chem. Phys. 11 (1984) 552.
[429] A. Cazabat, M.A.C. Stuart, Dynamics of wetting-effects of surface roughness, J. Phys. Chem. 90 (1986) 5845.
[430] H. Kusumaatmaja, J.M. Yeomans, Modeling contact angle hysteresis on chemically patterned and superhydrophobic surfaces, Langmuir 23 (2007) 6019.
[431] N.A. Patankar, On the modeling of hydrophobic contact angles on rough surfaces, Langmuir 19 (2003) 1249.
[432] X.B. Zhou, J.Th.M. de Housson, Influence of surface roughness on the contact angle, J. Mater. Res. 10 (1995) 1984.
[433] J. Bico, C. Marzolin, D. Quéré, Pearl drops, Europhys. Lett. 47 (1999) 220.
[434] A. Marmur, Wetting on real surfaces, J. Imaging Sci. Technol. 44 (2000) 406.
[435] G. Reiter, Dewetting of thin polymer films, Phys. Rev. Lett. 68 (1992) 75.
[436] K. Jacobs, S. Herminghaus, K.R. Mecke, Thin liquid polymer film rupture via defects, Langmuir 14 (1998) 965.
[437] R. Konnur, K. Kargupta, A. Sharma, Instability and morphology of thin liquid films on chemically heterogeneous substrates, Phys. Rev. Lett. 84 (2000) 931.
[438] K. Kargupta, A. Sharma, Templating of thin films induced by dewetting on patterned surfaces, Phys. Rev. Lett. 86 (2001) 4536.
[439] E. Ruckenstein, R. Jain, Spontaneous rupture of thin films, J. Chem. Soc. Faraday Trans. II 70 (1974) 132.
[440] M. Williams, S. Davis, Nonlinear theory of film rupture, J. Colloid Interface Sci. 90 (1982) 220.
[441] A. Sharma, G. Reiter, Instability of thin polymer films on coated substrates: rupture, dewetting, and drop formation, J. Colloid Interface Sci. 178 (1996) 383.
[442] R. Seemann, S. Herminghaus, K. Jacobs, Dewetting patterns and molecular forces: a reconciliation, Phys. Rev. Lett. 86 (2001) 5534.
[443] M.J. Lighthill, Waves in Fluids, Cambridge University Press, 1978.
[444] B.R. Lutz, J. Chen, D.T. Schwartz, Microfluidics without microfabrication, Proc. Natl. Ac. Sci. 100 (2003) 4395.
[445] P. Marmottant, S. Hilgenfeldt, Controlled vesicle deformation and lysis by single oscillating bubbles, Nature 423 (2003) 153.
[446] T.M. Squires, S.R. Quake, Microfluidics: Fluid physics at nanoliter scale, Rev. Mod. Phys. 77 (3) (2005) 977.
[447] D.T. Wasan, A.D. Nikolov, H. Brenner, Droplets speeding on surfaces, Science 291 (2001) 605.
[448] J.H. Snoeijer, G. Delon, M. Fermigier, B. Andreotti, Avoided critical behavior in dynamically forced wetting, Phys. Rev. Lett. 96 (2006) 174504.
[449] P.G. Simpkins, V.J. Kuck, On air entrainment in coatings, J. Colloid Interface Sci. 263 (2003) 562.
[450] C. Duez, C. Ybert, C. Clanet, L. Bocquet, Making a splash with water repellency, Nature Phys. 3 (2007) 180.
[451] T.D. Blake, K.J. Ruschak, A maximum speed of wetting, Nature 282 (1979) 489.
[452] R.V. Sedev, J.G. Petrov, The critical condition for transition from steady wetting to film entrainment, Colloids Surf. 53 (1991) 147.
[453] T. Podgorski, J.M. Flesselles, L. Limat, Corners, cusps, and pearls in running drops, Phys. Rev. Lett. 87 (2001) 036102.
[454] L. Leger, J. Joanny, Liquid spreading, Rep. Progr. Phys. 55 (1992) 431.
[455] T.D. Blake, Y.D. Shikhmurzaev, Dynamic wetting by liquids of different viscosity, J. Colloid Interface Sci. 253 (2002) 196.
[456] J. Eggers, R. Evans, Comment on dynamic wetting by liquids of different viscosity, J. Colloid Interface Sci. 280 (2004) 537.
[457] Y.D. Shikhmurzaev, T.D. Blake, Response to the comment by J. Eggers and R. Evans, J. Colloid Interface Sci. 280 (2004) 539.
[458] P.A. Thompson, M.O. Robbins, Simulations of contact line motion — slip and the dynamic contact angle, Phys. Rev. Lett. 63 (1989) 766.
[459] M.J. de Ruijter, T.D. Blake, J. de Coninck, Dynamic wetting studied by molecular modeling simulations of droplet spreading, Langmuir 15 (1999) 7836.
[460] O.V. Voinov, Hydrodynamics of wetting, Fluid Dynamics 11 (1976) 714.
[461] V.M. Starov, V.V. Kalinin, J.D. Chen, Spreading of liquid drops over solid substrates, Adv. Colloid Interface Sci. 50 (1994) 187.
[462] S. Middleman, Modeling Axisymmetric Flow, Academic Press, 1995.
[463] L.M. Hocking, A moving fluid interface on a rough surface, J. Fluid Mech. 76 (1976) 801.
[464] F.T. Dodge, The spreading of liquid droplets on solid surfaces, J. Colloid Interface Sci. 121 (1988) 154.
[465] J.L. Barrat, L. Bocquet, Large slip effect at a nonwetting fluid-solid interface, Phys. Rev. Lett. 82 (1999) 4671.
[466] C. Cottin-Bizonne, B. Cross, A. Steinberger, E. Charlaix, Boundary slip on smooth hydrophobic surfaces: intrinsic effets and possible artifacts, Phys. Rev. Lett. 94 (2005) 056102.
[467] J. Lyklema, Fundamentals of Interface and Colloid Science vol. III: Liquid–Fluid Interfaces, Academic Press, 2000.
[468] A.A. Darhuber, S.M. Troian, Principles of microfluidic actuation by modulation of surface stresses, Ann. Rev. Fluid Mech. 37 (2005) 425.
[469] O.E. Jensen, J.B. Grotberg, Insoluble surfactant spreading on a thin viscous film: shock evolution and film rupture, J. Fluid Mech. 240 (1992) 59.
[470] O.E. Jensen, J.B. Grotberg, The spreading of heat or soluble surfactant on a thin liquid film, Phys. Fluids A5 (1993) 58.
[471] O.K. Matar, Nonlinear evolution of thin free viscous films in the presence of soluble surfactant, Phys. Fluids 14 (2002) 4216.
[472] L.Y. Yeo, O.K. Matar, E.S.P. Ortiz, G.F. Hewitt, The dynamics of Marangoni-driven local film drainage between two drops, J. Colloid Interface Sci. 241 (2001) 233.
[473] W.B. Hardy, The spreading of fluids on glass, Phil. Mag. 38 (1919) 49.
[474] F. Heslot, N. Fraysse, A.M. Cazabat, Molecular layering in the spreading of wetting liquid drops, Nature 338 (1989) 640.
[475] M.P. Valignat, G. Oshanin, S. Villette, A.M. Cazabat, M. Moreau, Molecular weight dependence of spreading rates of ultrathin polymeric films, Phys. Rev. Lett. 80 (1998) 5377.
[476] A.A. Darhuber, W.W. Reisner, S.M. Troian, Dynamics of capillary spreading along hydrophilic microstripes, Phys. Rev. 64 (2001) 031603.

[477] A.A. Darhuber, J.M. Davis, W.W. Reisner, S.M. Troian, Thermocapillary actuation of liquid flow on chemically patterned surfaces, Phys. Fluids 15 (2003) 1295.
[478] J.D. Brock, I.M. Cohen, I.P. Ivanov, H.P. Le, J. Roy, Oscillations of an air bubble in an ink jet, J. Imaging Sci. Technol. 10 (1984) 127.
[479] N.P. Hine, Deaeration system for a high-performance drop-on- demand ink jet, J. Imaging Technol. 17 (1991) 223.
[480] L. Liggieri, F. Ravera, A. Passerone, Drop formation instabilities induced by entrapped gas bubbles, J. Colloid Interface Sci. 140 (1990) 436.
[481] M.S. Plesset, A. Prosperetti, Bubble dynamics and cavitation, Ann. Rev. Fluid Mech. 9 (1977) 145.
[482] T.G. Leighton, The Acoustic Bubble, Academic Press, London, 1994.
[483] R. Jeurissen, J. de Jong, H. Reinten, M. van den Berg, H. Wijshoff, M. Versluis, D. Lohse, The effect of an entrained air bubble on the acoustics of an ink channel, J. Acoust. Soc. Am. 123 (2008) 2496.
[484] J. de Jong, M. Versluis, G. de Bruin, D. Lohse, H. Reinten, M. van den Berg, H. Wijshoff, N. de Jong, Acoustical and optical characterization of air entrapment in piezo-driven inkjet printheads, Proc. IEEE-IUS 2 (2005) 1270.
[485] J. de Jong, R. Jeurissen, H. Borel, M. van den Berg, H. Wijshoff, H. Reinten, M. Versluis, A. Prosperetti, D. Lohse, Entrapped air bubbles in piezo-driven inkjet printing: their effect on the droplet velocity, Phys. Fluids 18 (2006) 121511.
[486] D. Lohse, J. de Jong, M. Versluis, M. van den Berg, H. Wijshoff, H. Reinten, Disturbing bubbles in piezo-acoustic printing, in: Proc. 6th EFMC, 2006, p. 369.
[487] A. Prosperetti, Y. Hao, Modelling of spherical gas bubble oscillations, Phil. Trans. R. Soc. Lond. A 357 (1999) 203.
[488] Y. Hao, A. Prosperetti, The effect of viscosity on the spherical stability of oscillating gas bubbles, Phys. Fluids 11 (1999) 1309.
[489] Y. Hao, A. Prosperetti, The dynamics of vapor bubbles in acoustic pressure fields, Phys. Fluids 11 (1999) 2008.
[490] C.E. Brennen, Cavitation and Bubble Dynamics, Oxford University Press, 1995.
[491] S. Hilgenfeldt, D. Lohse, M.P. Brenner, Phase diagrams for sonoluminiscescing bubbles, Phys. Fluids 8 (1996) 2808.
[492] S. Hilgenfeldt, M.P. Brenner, S. Grossmann, D. Lohse, Analysis of Rayleigh–Plesset dynamics for sonoluminescing bubbles, J. Fluid Mech. 365 (1998) 171.
[493] S. Hilgenfeldt, D. Lohse, Predictions for upscaling sonoluminescence, Phys. Rev. Lett. 82 (1999) 1086.
[494] J.R. Blake, M.C. Hooton, P.B. Robinson, R.P. Tong, Collapsing cavities, toroidal bubbles and jet impact, Phil. Trans. R. Soc. Lond. A 355 (1997) 537.
[495] R.P. Tong, W.P. Schiffers, S.J. Shaw, J.R. Blake, D.C. Emmony, The role of splashing in the collapse of a laser-generated cavity near a rigid boundary, J. Fluid Mech. 380 (1999) 339.
[496] M.P. Brenner, S. Hilgenfeldt, D. Lohse, Single-bubble sonoluminescense, Rev. Mod. Physics 74 (2002) 425.
[497] B.C. Khoo, E. Klaseboer, K.C. Hung, A collapsing bubble-induced micro-pump using the jetting effect, Senors Actuators 118 (2004) 152.
[498] K.S.F. Lew, E. Klaseboer, B.C. Khoo, A collapsing bubble-induced micropump: an experimental study, Sensors Actuators A 133 (2007) 161–172.
[499] R.J. Dijkink, J.P. van der Dennen, C.D. Ohl, A Prosperetti, The 'acoustic scallop': a bubble-powered actuator, J. Micromech. Microeng. 16 (2006) 1653.
[500] T.G. Leighton, D.G. Ramble, A.D. Phelps, C.L. Morfey, P.P. Harris, Acoustic detection of gas bubbles in a pipe, Acustica 82 (1988) 801.
[501] B. Krasovitskia, E. Kimmel, Gas bubble pulsation in a semiconfined space subjected to ultrasound, J. Acoust. Soc. Am. 109 (2001) 891.
[502] P. Zhong, Y. Zhou, S. Zhu, Dynamics of bubble oscillation in constrained media and mechanisms of vessel rupture in SWL, Ultrasound in Med. & Biol. 27 (2001) 119134.
[503] J. Cui, M. Hamilton, P. Wilson, E. Zabolotskaya, Bubble pulsations between parallel plates, J. Acoust. Soc. Am. 119 (2006) 2067.
[504] E. Ory, H. Yuan, A. Prosperetti, S. Popinet, S. Zaleski, Growth and collapse of a vapor bubble in a narrow tube, Phys. Fluids 12 (2000) 1268.
[505] E. Sassaroli, K. Hynynen, Forced linear oscillations of microbubbles in blood capillaries, J. Acoust. Soc. Am. 115 (2004) 3235.
[506] S. Qin, K.W. Ferrara, Acoustic response of compliable microvessels containing ultrasound contrast agents, Phys. Med. Biol. 51 (2006) 5065.
[507] S. Qin, K.W. Ferrara, The natural frequency of oscillation of ultrasound contrast agents in microvessels, Ultrasound in Med. & Biol. 33 (2007) 1140.
[508] C.F. Caskey, S.M. Stieger, S. Qin, P.A. Dayton, K.W. Ferrara, Direct observations of ultrasound microbubble contrast agent interaction with the microvessel wall, J. Acoust. Soc. Am. 122 (2007) 1191.
[509] H.N. Oguz, A. Prosperetti, The natural frequency of oscillation of gas bubbles in tubes, J. Acoust. Soc. Am. 103 (1998) 3301.
[510] X. Geng, H. Yuan, H.N. Oguz, A. Prosperetti, The oscillation of gas bubbles in tubes: Experimental results, J. Acoust. Soc. Am. 106 (1999) 674.
[511] A. Prosperetti, The thermal behavior of oscillating gas bubbles, J. Fluid Mech. 222 (1991) 587.
[512] X.M. Chen, A. Prosperetti, Thermal processes in the oscillations of gas bubbles in tubes, J. Acoust. Soc. Am. 104 (1998) 1389.
[513] A. Prosperetti, L.A. Crum, K.W. Commander, Nonlinear bubble dynamics, J. Acoust. Soc. Am. 83 (1988) 502.
[514] R. Jeurissen, J. de Jong, H. Reinten, M. van den Berg, H. Wijshoff, M. Versluis, D. Lohse, Effect of an entrained air bubble on the acoustics of an ink channel, J. Acoust. Soc. Am. 123 (2008) 2496.
[515] R. Jeurissen, J. de Jong, H. Borel, M. Versluis, M. van den Berg, H. Wijshoff, H. Reinten, A. Prosperetti, D. Lohse, Sound absorption of bubbles in inkjet-printer microchannels, in: Proc. 6th EFMC, 2006, p. 340.
[516] J. Rensen, D. Bosman, J. Magnaudet, C.D. Ohl, A. Prosperetti, R. Toegel, R, M. Versluis, D. Lohse, Spiraling bubbles: how acoustic and hydrodynamic forces compete, Phys. Rev. Lett. 86 (2001) 4819.
[517] T.G. Leighton, A.J. Walton, M.J.W. Pickworth, Primary Bjerknes forces, Eur. J. Phys. 11 (1990) 47.
[518] L.A. Crum, Bjerknes Forces on Bubbles Om a Stationary Sound Field, Elsevier Academic Press, 2004.
[519] J. Magnaudet, D. Legendre, The viscous drag force on a spherical bubble with a time-dependent radius, Phys. Fluids 10 (1998) 550.
[520] J. Magnaudet, I. Eames, The motion of high-Reynolds-number bubbles in inhomogeneous flows, Ann. Rev. Fluid Mech. 32 (2000) 659.
[521] P.K. Kundu, I.M. Cohen, Fluid Mechanics, Elsevier Academic Press, 2004.
[522] D. Legendre, J. Magnaudet, The lift force on a spherical bubble in a viscous linear shear flow, J. Fluid Mech. 368 (1998) 81.
[523] J. Magnaudet, D. Legendre, Some aspects of the lift force on a spherical bubble, Appl. Sci. Res. 58 (1998) 441.
[524] R. Toegel, S. Luther, D. Lohse, Viscosity destabilizing sonoluminescing bubbles, Phys. Rev. Lett. 96 (2006) 114301.
[525] H.N. Oguz, A. Prosperetti, Dynamics of bubble growth and detachment from a needle, J. Fluid Mech. 257 (1993) 111.
[526] A. Prosperetti, H.N. Oguz, Physalis: a new method for the numerical simulation of disperse systems; potential flow of spheres, J. Comput. Phys. 167 (2001) 196.
[527] S. Takagi, H.N. Oguz, Z. Zhang, A. Prosperetti, Physalis: a new method of particle simulation part II: two-dimensional Navier–Stokes flow around cylinders, J. Comput. Phys. 187 (2003) 371.
[528] R. Bergmann, M. Stijnman, M. Sandtke, D. van der Meer, A. Prosperetti, D. Lohse, Giant bubble collapse, Phys. Rev. Lett. 96 (2006) 154505.
[529] R. Jeurissen, Bubbles in inkjet printheads. Analytical and numerical models, Ph.D. Thesis, University of Twente, 2009.
[530] M.M. Fyrillas, A.J. Szeri, Dissolution or growth of soluble spherical oscillating bubbles, J. Fluid Mech. 277 (1994) 381.
[531] E.E. Michaelis, Hydrodynamic force and heat/mass transfer from particles, bubbles, and drops — The Freeman Scholar Lecture, J. Fluid Eng. 125 (2003) 209.
[532] M.P. Brenner, D. Lohse, T.F. Dupont, Bubble shape oscillations and the onset of sonoluminescence, Phys. Rev. Lett. 75 (1995) 954.
[533] R. Toegel, D. Lohse, Phase diagrams for sonoluminescing bubbles: a comparison between experiment and theory, J. Chem. Phys. 118 (2003) 1863.
[534] J.R. Womersley, Method for the calculation of velocity, rate of flow and viscous drag in arteries when the pressure gradient is known, J. Physiol. 127 (1955) 553.
[535] R. Jeurissen, A. van der Bos, H. Reinten, M. van den Berg, H. Wijshoff, J. de Jong, M. Versluis, D. Lohse, Acoustic measurement of bubble size in an inkjet printhead, J. Acoust. Soc. Am. 126 (2009) 2184.
[536] W. Zapka, M. Crankshaw, W. Voit, J. Brünahl, U. Herrmann, G. Münchow, Increased inkjet printing frequency from offset channel printheads, in: Proc. IS&T's NIP19, 2003, p. 272.